FIRAT UNIVERSITY
GRADUATE SCHOOL OF NATURAL AND APPLIED SCIENCES
T Ü R K İ Y E

CONTROL AND ANALYSIS OF A THREE PHASE INDUCTION MOTOR BY USING STM32

Lana Majeed MOHAMMED

Master's Thesis

DEPARTMENT OF ELECTRICAL AND ELECTRONICS ENGINEERING
Division of Electrical Machines

AUGUST 2021

FIRAT UNIVERSITY
GRADUATE SCHOOL OF NATURAL AND APPLIED SCIENCES
TÜRKİYE

Department of Electrical and Electronics Engineering

Master's Thesis

CONTROL AND ANALYSIS OF A THREE PHASE INDUCTION MOTOR BY USING STM32

Author
Lana Majeed MOHAMMED

Supervisor
Prof. Dr. Hasan KÜRÜM

AUGUST 2021
ELAZIG

FIRAT UNIVERSITY
GRADUATE SCHOOL OF NATURAL AND APPLIED SCIENCES
TÜRKİYE

Department of Electrical and Electronics Engineering

Master's Thesis

Title:	Control and Analysis of a Three Phase Induction Motor by Using STM32
Author:	Lana Majeed MOHAMMED
Submission Date:	08 July 2021
Defense Date:	17 August 2021

THESIS APPROVAL

This thesis, which was prepared according to the thesis writing rules of the Graduate School of Natural and Applied Sciences, Fırat University, was evaluated by the committee members who have signed the following signatures and was unanimously approved after the defense exam made open to the academic audience.

		Signature
Supervisor:	Prof. Dr. Hasan KÜRÜM Firat University, Faculty of Engineering	Approved
Chair:	Doç. Dr. Ahmet ORHAN Firat University, Faculty of Engineering	Approved
Member:	Dr. Öğr. Üyesi Zeki OMAÇ Munzur University, Faculty of Engineering	Approved

This thesis was approved by the Administrative Board of the Graduate School on

.... / .... / 20 ....

Signature

Associated Prof. Dr. Kürşat Esat ALYAMAÇ
Director of the Graduate School

DECLARATION

I hereby declare that I wrote this Master's Thesis titled “Control and Analysis of a Three Phase Induction Motor by Using STM32” in consistent with the thesis writing guide of the Graduate School of Natural and Applied Sciences, Firat University. I also declare that all information in it is correct, that I acted according to scientific ethics in producing and presenting the findings, cited all the references I used, express all institutions or organizations or persons who supported the thesis financially. I have never used the data and information I provide here in order to get a degree in any way.

17 August 2021

Lana Majeed MOHAMMED

PREFACE

This thesis presents an implementation of an Indirect Field Orientation Control (IFOC) strategies to control the operation induction motor (IM). due to this motor extensively used in numerous application ranging from industries to home due to its Robustness, reliability.

First, I thank God for his protection and ability to get the job done. Then I would like to thank everyone who has contributed in one way or another to the completion of this Research.

I would like to thank my supervisor, Prof. Dr. HASAN KÜRÜM, for his compassion, kind support, great knowledge, confidence, directions, and thorough guidance throughout my research work. His advice was invaluable throughout my research. I profited from his advice at many stages of the work, especially when exploring new ideas. His upbeat attitude and believe in my research both inspired and reassured me. His meticulous editing greatly aided in the completion of this study.

I would like to thank all of my teachers for their help throughout the procedure, both in keeping me calm and in trying to put the pieces back together. I cannot list all of your names here, but you are always on my mind. I will be eternally grateful for your generosity.

Last but not least, I want to show my thankfulness to my parents (Mr. Majeed Mohammed Majeed and Mrs. Almas Hamagharib Qadr) for their love, encouragement, prayers, and support throughout my life. Thanks for providing me the courage to reach for the stars and pursue my dreams.

Lana Majeed MOHAMMED
ELAZIG, 2021

TABLE OF CONTENTS

ABSTRACT

Control and Analysis of a Three Phase Induction Motor by Using STM32

Lana Majeed MOHAMMED

Master's Thesis

FIRAT UNIVERSITY
Graduate School of Natural and Applied Sciences

Department of Electrical and Electronics Engineering

August 2021, Page: xviii + 120

Three-phase induction motors are the essential machines for high power applications where high efficiency, high reliability, and robust construction are required. Controlling the speed of the induction motor is one of the most important targets for most applications, especially in electric cars. However, in medium and high power applications, to control the speed of the induction machine, the current must be controlled instantaneously to prevent the motor from damage during the transient condition while the motor starts up or the sudden changes of the load. Therefore, the IFOC approach is recently used to control the speed of three-phase induction machines. In this method, the currents and the voltages are controlled instantaneously to keep the speed of the motor constant and provide safe operations.

In this thesis, 0.25 kW three-phase induction motor modeled by MATLAB / SIMULINK and simulated in Direct-On-Line (DOL) condition after that for applying Indirect Field Orienteion Control (IFOC) method a three PI controller needed for current, flux and speed loop also they designed a cording to a motor’s parameter that found them in Laboratory and calculated by hand after that the motor controlled by IFOC with adding some extra point to increasing the performance of system like lookup table for more protecting the motor from high voltage and also filed weakening designed.

In the practical part inverter, rectifier, and sensor boards designed using proteus platform then the open-loop test is done by using 0.25 kW three-phase IM, Rectifier board, Inverter board, STM32F103C8 microcontroller and tested them using the Space Vecor Pulse Width Modulation (SVPWM) signals that designed by the microcontroller. Then for closed-loop control is done using 0.25 kW three-phase IM , Rectifier board , Inverter board ,sensor board, STM32F103C8 microcontroller) and IFOC method implemented.

Keywords: Induction Motor , Field Orientation Control , STM32, SVPWM ,MATLBA/SIMULINK

ÖZET

ÜÇ FAZLI ENDÜKSİYON MOTORUNUN STM32 İLE KONTROLÜ VE ANALİZİ

Lana Majeed MOHAMMED

Yüksek Lisans Tezi

FIRAT ÜNİVERSİTESİ
Fen Bilimleri Enstitüsü

Elektrik Elektronik Mühendisliği Anabilim Dalı

Ağustos 2021, Sayfa: xviii + 120

Üç fazlı asenkron motorlar, yüksek verim, yüksek güvenilirlik, yüksek güçlü ve sağlam yapının ihtiyaç duyulduğu uygulamalar için en uygun makinelerdir. Asenkron motorun hızının kontrol edilmesi, uygulamaların çoğu için en önemli amaçlardan biridir. Orta ve yüksek güçlü uygulamalarda, asenkron makinenin hızını kontrol etmek için, motorun çalışması sırasındaki geçici durum veya yükteki ani değişiklikler sırasında motorun hasar görmesini önlemek için akımın anlık olarak kontrol edilmesi gerekir. Bu çalışmada, üç fazlı asenkron makinelerin hızını kontrol etmek için indirek vektör kontrol (IFOC) yaklaşımı kullanılmaktadır. Bu yöntemde motorun hızını sabit tutmak ve güvenli çalışmasını sağlamak için akımlar ve gerilimler anlık olarak kontrol edildi.

Bu tezde ilkin 0.25 kw üç fazlı bir asenkron motor IFOC çalışması için MATLAB / SIMULINK modeli gerçekleştirildi ve teorik sonuçlar alındı. Modeli gerçekleştirilen asenkron motorun, güç ve sürücü kartı gerçekleştirilerek açık ve kapalı çevrim kontrolü yapılarak deneysel sonuçlar alındı. Kontrol için ihtiyaç duyulan tetikleme sinyalleri STM32 kullanıldı, kontrol kodları C programlama dili ile yazıldı.

Güç ve tetikleme devreleri Protues platformu kullanılarak tasarlandı ve fiziksel üretimleri gerçekleştirildi. Güç devresinde üç fazlı bir köprü doğrultucu, IGBT'den oluşan evirici ve tetikleme sinyal üreticisinden oluşmaktadır. Tetikleme sinyallerini üretmek için STM32F103C8 mikro kontrolör ve ayrıca motor konum bilgisi almak için bir enkoder kullanıldı.

Deneysel çalışmalar 0.25 kw gücünde bir üç fazlı asenkron motor kullanılarak, açık ve kapalı çevrim kontrollerinin doğru çalışıp çalışmadığı deneysel olarak test edildi. Elde edilen sonuçlar ile teorik ve deneysel çalışmaların doğruluğu gösterildi.

Anahtar Kelimeler: Asenkron Motor , Alan Yönlendirme Kontrolü , STM32, SVPWM ,MATLBA/SIMULINK

LIST OF FIGURES

Page

LIST OF TABLES

LIST OF APPENDICES

Page

SYMBOLS AND ABBREVIATIONS

Symbols

n_{sync}	: Synchrouns speed
f_e	: power source frequency
P	: Number of Pole
n_{slip}	: Slip Speed
n_m	: Mechanical Speed
S	: Slip
E_r	: Voltage in Rotor
E_{r0}	: voltage at locked-rotor conditions
f_r	: Frequency of rotor
X_r	: Reactance of rotor
ω_r	: rotor angular velocity
L_r	: rotor inductance
X_{r0}	: blocked-rotor reactance
I_r	: rotor phase (rms) current
R_r	: rotor coil resistance
$Z_{r.eq}$	: The equivalent rotor impedance
r_s	: stator coil resistance
L_{ls}	: stator leakage inductance
L_m	: magnetizing inductance
I_s	: stator phase (rms) current
V_s	: stator phase voltage vector
L_{lr}	: rotor leakage inductance
P_g	: air gap power
P_m	: Mechanical power
P_{cu}	: copper loss
$P_{cu,s}$	: Stator copper loss
$P_{cu,r}$	: Rotor copper loss
P_h	: hysteresis loss
ω_s	: slip anguler velosity
P_e	: eddy current losses
Φ	: flux
$P_{s,core}$	: stator core loss
$P_{r,core}$	: rotor core loss
P_{str}	: stray loss
ω_r	: rotor anguler velosity
T_e	: Electromagatic torque
λ^s_{abcs}	: stator flux in stationary frame(abc)
L_{abcs}	: stator inductance(abc)
i^s_{abcs}	: stator current in stationary frame(abc)
λ_{as}	: a-phase flux in a stator
λ_{bs}	: b-phase flux in a stator
λ_{cs}	: c-phase flux in a stator

i_{as} : a-phase current in a stator
i_{bs} : b-phase current in a stator
i_{cs} : c-phase current in a stator
θ_r : rotor angle
L_{ms} : magnetizing inductance in a stationary frame
i_{ar}^r : a-phase current in a rotor in rotor frame
i_{br}^r : b-phase current in a rotor in rotor frame
i_{cr}^r : c-phase current in a rotor in rotor frame
i_{abcr}^r : rotor current in rotor frame(abc)
λ_{abcr}^r : rotor flux linkage in rotor frame(abc)
L_{abcr} : rotor inductance(abc)
λ_{ar}^r : a-phase flux rotor in rotor frame
λ_{br}^r : b-phase flux rotor in rotor frame
λ_{cr}^r : c-phase flux rotor in rotor frame
λ_{dq0s}^s : stator flux in stationary frame(dq)
i_{dqs}^s : stator current in stationary frame(dq)
λ_{ds}^s : flux of stator in stationary frame – d axis
λ_{qs}^s : flux of stator in stationary frame – q axis
i_{dqr}^r : current of rotor in rotor frame (dq)
λ_{dqr}^r : flux of rotor in rotor frame (dq)
θ_e : angle of the synchronous frame
λ_{dqs}^e : flux of stator in synchronous frame(dq)
λ_{dqr}^e flux of rotor in synchronous frame(dq)
i_{dqs}^e : current of stator in synchronous frame(dq)
i_{dqr}^e : current of rotor in synchronous frame(dq)
λ_{ds}^e : flux of stator in synchronous frame – d axis
λ_{dr}^e : flux of rotor in synchronous frame – d axis
i_{ds}^e : current of stator in synchronous frame – d axis
i_{dr}^e : current of rotor in synchronous frame – d axis
λ_{qs}^e : flux of stator in synchronous frame – q axis
λ_{qr}^e : flux of rotor in synchronous frame – q axis
i_{qs}^e : current of stator in synchronous frame – q axis
i_{qr}^e : current of rotor in synchronous frame – q axis
σ : leakage factors
V_{abcs}^s : voltage of stator in stationary frame(abc)
V_{abcr}^r : voltage of rotor in rotor frame(abc)
i_{abcs}^s : current of stator in stationary frame(abc)
V_{dqs}^s : voltage of stator in stationary frame(dq)
V_{dqr}^r : voltage of rotor in rotor frame(dq)
V_{dqr}^s : voltage of rotor in stationary frame(dq)
i_{dqr}^s : current of rotor in stationary frame(dq)
λ_{dqr}^s : flux of rotor in stationary frame(dq)
i_{dr}^s : current of rotor in stationary frame – d axis
λ_{dr}^s : flux of rotor in stationary frame – d axis

λ_{qr}^{s} : flux of rotor in stationary frame – q axis
i_{qr}^{s} : current of rotor in stationary frame – q axis
v_{ds}^{s} : voltage of stator in stationary frame – d axis
v_{qs}^{s} : voltage of stator in stationary frame – q axis
V_{dqs}^{e} : voltage of stator in synchronous frame (dq)
ω_{sl} : slip anguler velosity
τ_{s} : stator time constant
τ_{r} : rotor time constant
V_{dqs}^{g} : voltage of stator- generalized(dq)
i_{dqs}^{g} : current of stator - generalized(dq)
λ_{dqr}^{g} : flux of rotor - generalized(dq)
λ_{f} : field flux
i_{f} : field current
i_{a} : armature current
θ_{f} : field angle
θ_{sl} : slip angle
I_{α} : alpha current
I_{β} : beta current
i_{d} : current in d axis
i_{q} : current in q axis
V_{sd} : voltage in d axis
V_{sq} : voltage in q axis
v_{α} : alpha voltage
v_{β} : beta voltage
v_{a} : voltage phase - a
v_{b} : voltage phase -b
v_{c} : voltage phase -c
ω_{n} : Natural frequency
ε : Damping factor
i_{sd}^{*} : rated current d axis
i_{sq}^{*} : rated current q axis
i_{mrd} : magnatatization current
L_{o} : Magnetizing inductance
V_{ab} : phase voltage phase a and phase b
V_{bc} : phase voltage phase b and phase c
V_{ca} : phase voltage phase c and phase a
V_{dc} : direct current voltage

Abbreviations

EV : Electric Vehicle
DC : Direct current
AC : Alternating current
IM : Induction Motor
IC : Integrated Circuit

PMSM : Permanent Magnet Synchronous Motor
DSP : Digital Signal Processor
CPU : Central Processing Unit
MPU : Micro Processor Unit
MCU : Micro Controller Unit
VFD : Variable Frequency Drive
DOL : Direct On Line
DTC : Direct Torque Control
FOC : Field-Oriented Control
DFOC : Direct Field Oriented Control
IFOC : Indirect Field Oriented Control
IRFOC : Indirect Rotor Field Oriented Control
MMF : Magneto Motive Force
PI : Proportional Integral
PWM : Pulse Width Modulation
SVPWM : Space Vector Pulse Width Modulation
SPWM : Sinusoidal Pulse Width Modulation
MHD : Magneto Hydro Dynamic
THD : Total Harmonic Distortion
VSI : Voltage Source Inverter
CSI : Current Source Inverter
IGBT : Insulated-Gate Bipolar Transistor
ADC : Analog to Digital Converter
DAC : Digital to Analogue Converter
DMA : Direct Memory Access
MOI : Moment of Inertia
VCIMD : Vector Control Induction Motor Deive

1. INTRODUCTION

Because of their robustness, cheapness, high speed operation and less maintenance requirements, the induction motors (IM) are the most common type of electromechanical drive in industrial, commercial and residential applications. To reach the best efficiency of induction motor drive (IMD), many new techniques of control have been developed in the last few years. In general, induction motor can be controlled by both open and closed loop control techniques. These are also known as scalar and field orientation control (FOC) schemes. FOC aims to control the rotor flux and torque of the motor by estimating the speed and voltage. This estimation can be either directly done through measurements or indirectly through calculations [1,29].

FOC method takes into consideration both successive steady-states and real mathematical equations that describe the motor itself. The control thus obtained has a better dynamic for torque variations in a wider speed range. FOC approach needs more computational power than a standard V/f control scheme. This need can be overcome by the use of Digital Signal processors. As a result, FOC provides the advantages of full motor torque capability at low speed, better dynamic behavior, higher efficiency for each operation point in a wide speed range, decoupled control of torque and flux, short term overload capability, and four quadrant operation [31].

1.1. The importance of the IM and it is type

An IM is comparable to a polyphase converter with a free-spinning secondary winding. The electromagnetic induction produces the torque. Induction is determined by the speed slip across the rotor and the stator field. As a consequence, an IM can operate without being directly connected to the rotor. Thus, there is no need for brushes and commutators. The IM thus requires low maintenance, and also, it is mechanically robust vibration and shock. IMs are also made of cheap ordinary materials such as iron, copper and aluminium. In addition, The grid lines can also be used to drive IMs. They are used extensively in manufacturing and household appliances; Pumps, cranes, elevators, coolers, traction drives, etc. In fact, 90 per cent of industrial engines are IMs[33]. Among all other AC competitors, IMs have the most proven technology [2]. We have two kinds of IMs in general. The first is a three-phase IM, whereas the second is a single-phase IM [37].To get the single-phase IM started, several approaches are utilized. Because mechanical techniques are impractical, the motor is momentarily started by turning it into a two-phase motor. The Auxiliary method utilized to start the motor distinguishes single-phase IMs. They are organised as follows: Permanent-split capacitor motor, Shaded-pole motor, Capacitor-start capacitor-run motor, Split-phase motor, Capacitor-start motor [37].

Three-phase IM rotors are classified into two types:

A rotor squirrel cage, also known as a rotor cage: The three-phase IM rotor in the squirrel cage is tubular in shape and has slots around its perimeter. The slots are not formed in order, but are somewhat skewed. Skewing avoids stator and rotor teeth from becoming magnetically locked, allowing for quieter and smoother motor operation. The squirrel cage rotor is composed of copper bars, brass, or aluminium, . These aluminium, brass, or copper bars are referred as rotor conductors, and they are installed in the slots on the the perimeter of the rotor . The rotor conductors are significantly reduced by the end rings, which are composed of copper or aluminium. These rotor conductors are mechanically fastened to the end ring, resulting in a full closed circuit that mimics a cage, thus the phrase "squirrel cage IM." The squirrel cage rotor's winding is generated symmetrically. Because the bars are continually underutilised , the rotor resistance is quite low due to the end rings, and external resistance not to be utilised because the bars are continuously shorted. The nonattendance of a slip ring and brushes improves and stabilises the Squirrel cage's three-phase IM construction, making it a commonly employed three-phase IM. These motors offer the benefit of being able to change the number of pole pairs at any time. [36,37]

Slip ring or wound three-phase IM: slip-ring rotors are employed in motors that employ this rotor kind. This three-phase IM's rotor has the same number of poles as the stator but fewer slots and spins per cycle than the stronger conductor. The rotor, like the stator, frequently has star or delta windings. The rotor includes the number of slots, and inside these slots, rotor winding is placed. The three terminals are connected via a star connector. The three-phase slip ring IM, as the name implies, is made up of slip rings that are linked to a similar shaft as the rotor ring. External resistance may be easily linked via the brushes and Slip rings, resulting in enhanced speed control and three-phase IM starting torque. The brushes are utilized to transmit electricity from the rotor's winding. These brushes are also linked to three-phase star resistors. The rotor first joins the resistance and is gradually detached as the rotor gains speed. Whereas the machine is running, the slip ring is lowered by inserting a metal collar that links all slip rings altogether and removes the brushes. This lessens brush wear and tear. It is less often used than an IM in a squirrel cage attributed to the prevalence of sliding rings and brushes in the rotor. It has a cylindrical laminated core and is wound in three stages, much like the stator. The rotor winding is evenly dispersed and generally star-connected in the slots. The open ends of the rotor winding are removed and connected. On the rotor shaft are three insulated slip rings, with one brush sitting on each slip ring. The three brushes are coupled to a three-phase rheostat with a star connection. The external resistors are added to the rotor circuit at the commencement to provide a high starting torque. As the resistance is reduced progressively to zero,The machine works at full load. The external resistors are only needed during the initialization process. Whenever the motor reaches regular pace, the three brushes short-circuit, causing the wound rotor to behave similarly to a squirrel cage rotor [37,35].

1.2. Description of Vector control algorithm with IM

There are two main steps in designing an electrical drives control system.

In order to analyze and evaluate the system, the driving mechanism must first be converted into a mathematical model.As external disruptions happen, the imposed machine reaction is obtained by an optimal regulator.

IM control has two basic directions.[4]

Analogue: The system parameter (mainly rotor speed) directly calculated by closed loops, compared to the parameters.

Digital: Estimation of system parameters (without calculating rotor speed) in sensorless control schemes [45].

By applying the following methodologies, the parameter estimation can be carried out[4].

- The algorithm for calculating slip frequency.
- Utilizing a state equation to estimate the speed.
- Depending on slot space harmonic voltages, an estimate is made.
- Mechanism of flux estimation and flux vector control .
- Torque and flux may be controlled directly.
- The sensorless speed control method relies on observers.
- Responsive systems as a model.
- Techniques for Kalman filtering.
- Sensorless control with parameter modification is possible.
- Sensorless control method dependent on neural networks.
- Sensorless control dependent on fuzzy logic.

IM control methods classified based on the controlled signal [4].

The advancement of the motor and its driving system has aided in the ongoing advancement of electric vehicles. Because the motor and its drive system are the foundation of electric cars, motor control is a critical component in their production [18]. Controlling an IM is difficult because both the magnitude and phase of the stator quantities must be regulated to provide decoupled control of the stator phase current's torque and flux making constituents [3].Various Control techniques are used in the business. (For example, the scalar technique (V/f), field-oriented control (FOC), direct torque control (DTC), and so on.) [36]. IMs may be regulated in a variety of ways. The most basic approaches rely on modifying the structure of the stator windings. The so-called wye-delta switch, for example, may be employed to simply reduce the starting current. Another form of switch simulates a gear change by altering the pole previously mentioned, i.e. adjusting the stator's magnetic pole count

In contemporary ASDs, nevertheless, the stator voltage and current are under control. In a steady state, they are characterised by their amplitude and frequency. Because these are the altered parameters, the control method is referred to as a scalar control system. A sudden shift in magnitude or frequency can have unfavourable transitory consequences, such as a typically steady motor torque disruption. Consequently, this does not apply to low-performance ASDs such as blowers, fans, or pumps.The motor speed is frequently adjusted using an open-loop system, which eliminates the need for a speed sensor (Despite the fact that current sensors are commonly utilised in overcurrent protection circuits). Vector control approaches are helpful in high-performance drive systems in which one of the control parameters is the torque produced by the motor. Vector control systems are more difficult to understand than scalar control systems. Voltage and current sensors are frequently utilized, and speed and angle sensors might also be essential for the ASD to function at its peak. Nowadays, almost all electric motor control systems have relied on some sort of integrated digital circuit, including digital signal processors (DSPs), microcontrollers, or microcomputersor[34,5].

Vector control: The amplitude and frequency of the voltage, current, and flux connection space vectors, as well as their instantaneous position, are regulated by the system state relations. FOC and direct time control are the most often utilised vector control techniques (DTC).

The steady-state effectiveness of an inverter-fed IM's drives is identical to that of an independently stimulated dc motor. However, as compared to DC machines, an IM with simple control has a relatively sluggish dynamic output[6]. This disadvantage has limited the usage of IM drives in high-performance industries like reversed sheet rolling mills and several machine tool drives. Therefore, the domain-oriented control of AC machines has been established, allowing the AC motor to be operated in the same way as an independently stimulated DC motor. The fundamental goal of field oriented control is to maximize performance while regulating torque and speed. In the independently stimulated DC motor, the MMF created by the field current and the MMF given by the armature current are spatially quadratures. As a result, there is no magnetic connection between the field and armature circuits. As a result, the armature current may be adjusted independently, and torque can be controlled more quickly while maintaining constant field flux. On AC machines, torque is also created as a result of the interplay of current and flux. In an IM, however, because power is only provided to the stator, the current required to create flux and the current required to produce torque are not readily detachable. As a result, the fundamental principle underlying field-oriented control is to isolate the mechanisms of the stator current is charge of flux generation and torque. Inverter control accomplishes field-oriented control in alternating current machines by changing the amplitude, frequency, and phase of the stator current. Because motor control is accomplished by regulating the current amplitude and phase angle, this control method is known as a field-oriented control system[7].

Takahashi pioneered direct torque control in Japan in 1984, while Dopenbrock pioneered it in Germany in 1985. Today, this control system is regarded as one of the most advanced AC Drive control technology in the world. This is a straightforward control method that eliminates the need for coordination transformation, PI regulators, modulators, and location encoders for pulse duration. By selecting proper switching kinds for the inverter, this technique leads to direct and independent control of motor torque and flux. Primary motor inputs, such as stator voltages and currents, are used to compute electromagnetic torque and stator flux. The inverter's voltage vector is appropriately designed to minimise torque and flux errors within the hysteresis bands. This control method has advantages such as quicker torque response in transient operations and higher steady-state efficiency[4].

1.3. STM32 Microcontrollers

A microcontroller is an integrated circuit (IC) component that controls other parts of an electronic system, often through a memory, microprocessor unit (MPU), and certain peripherals. These devices are intended for use in integrated systems that require computing power as well as agile, delicate interaction with digital, analogue, or electromechanical elements. The most popular term for this type of integrated circuit is "microcontroller," although the acronym "MCU" is often used alternatively since it stands for "microcontroller unit." You may also encounter "µC" (where the Greek letter mu substitutes "micro") on occasion. "Microcontroller" is a good name since it emphasizes the distinguishing features of this item class. The word "micro" denotes smallness, while the phrase "controller" denotes an improved capacity to execute control duties. This functionality is the consequence of integrating a digital processor and digital memory with extra hardware especially intended to assist the microcontroller in interacting with other components.

The STM32 series of 32-bit microcontrollers centred on the Arm ® Cortex ®-M CPU is intended to provide MCU users with unprecedented levels of flexibility. It provides devices that combine very high performance, real-time abilities, digital signal processing, low-power / low-voltage operation, and connection while retaining complete integrating and growth simplicity. Founded on an industry-standard core, the unrivalled variety of STM32 microcontrollers comes with a large selection of tools and software to help project creation, making this family of devices appropriate for both small projects and end-to-end platforms[8].

1.4. Literature Review

In 2007 L. Sbita and M. Ben Hamed wrote a paper that an internal model IM speed controller is designed and developed for a system of scalar IM drives. An identification approach relying on the recursive least square algorithm is effectively implemented in this project to categorize the parameters of the drive system's stated mathematical model. The experimental findings obtained with a 1 KW IM drive system show that the suggested speed controller has high efficiency and effectiveness across the full speed ranges and under a wide variety of loads. The suggested method has a stable structure and a basic and straightforward design, distinguishing it from previous techniques. Owing to the drawbacks of speed sensorless, a simple speed estimator dependent on the creation of the controller signal on the one hand and the monitoring of artificial neural networks on the other and torque modulation may be the focus of future study effort[9].

In 2008, Nasser Hashernnia and Behzad Asaei published a study in which the benefits of each motor and the one that is most suited for usage in electric vehicle (EV) applications are researched and compared to other electric motors. DC, switching reluctance, permanent magnet synchronous, induction, and brushless DC motors are the five primary types of electric motors investigated. While IM technology is more progressed than others, it is thought that brushless DC and permanent magnet motors are better suited for EV applications. These motors would produce less power, use less energy, and have a higher power-to-volume ratio. The decreasing cost of permanent magnet materials, as well as the increasing efficiency of permanent magnet and brushless DC motors, make them increasingly desirable for EV applications [2].

Radu Bojoi, Paolo Guglielmi, and Gian-Mario Pellegrino released a paper in 2008. This paper mentions an SDRFOC system for use in low-cost three-phase IM drives. A Sensorless closed-loop rotor flux observer was utilized to estimate rotor flux. The observer is relatively straightforward to conduct using low-cost fixed-point DSP controllers, making it an intriguing alternative to substitute the traditional open-loop control of V/Hz. The observer's efficacy is supported by the outcomes of the experiments acquired for a low-cost vacuum pump drive and laboratory test equipment[10].

Huiying Liu, Jun Tian, Yuxian Gai, and Shaoping Huang published a paper in 2010 titled. Motors need to preserve energy in the face of energy hard realities. This study presents PMSM as a high-quality, energy-saving generator. It exposes to the high-power PMSM an intelligent control scheme from the controller to the inner algorithm, comprising both the hardware and software aspects of the whole servo system. The vector control approach is developed, and the idea of coordinate transfer is presented by building the mathematical model of PMSM in multiple reference systems. Furthermore, the study reveals that the parameters in the d and q axes are decoupled, the torque control characteristics are linear, and when the vector control approach is employed, the output torque is constant, and the velocity spectrum is broad. Finally, the IGBT transistor and the

IR2214 chips were used to build a standard electrical circuit for use. Utilize the benefits of the STM32 MCU, which, according to the logical theory and usual algorithm we used, is suited for electrical machine control to get optimal outcomes[11].

In 2011 Zhi Shang wrote a thesis about FOC has the highest steady efficiency and the highest speed following function. Conventional DTC and sensorless DTC achieve improved dynamic output. No matter the conventional or Senseless DTC in the DTC family. The torque is controlled by a hysteresis controller, DTC, so that a better torque output is seen with less variability[12].

In 2012 ALNASIR, Z.A. and ALMARHOON A.H. wrote an article about An IM model developed and measurable, controllable, and stable. Simulink sub-models were then developed for various DTC scheme components. On a 6kW induction unit, the suggested DTC model was tested and evaluated. The simulation results have demonstrated very high accuracy in independent control of flux and torque. However, due to some slight difference in the stator flux, a substantial starting up stator current is induced. Further work is therefore needed to limit the start-up stator current to protect the equipment of the system and power electronics[13].

Nirupama Patra authored an MSc thesis in 2013 on how to direct torque control is one of the finest controllers recommended for all IM drives. This enables decoupled motor stator flux control as well as electromagnetic torque control. Because it does not require a pulse width modulator or coordinate conversions, this IM control strategy is simple to execute than other vector control approaches, according to the study. Unwanted torque and current ripple, on the other hand, are introduced [4].

In 2014 Zeina Bitar and Samih Al Jabi wrote the research. This research involves researching the performance of an electric car IM and field-oriented control, an electronic inverter used to drive this IM. After a transient time that does not exceed 0.4 s in all loading cases of the car, the IM reaches a steady state with constant rotation speed. This confirms the suitability of the IM to be used in an electric car. When applying various load torques, the maximum phase current is 200 A, which is less than the nominal current. The IM current is rising proportionally to the value of the slope angle. An IM can change its state and run when the rotating speed is decreased until stopped during running, as the absorbed induction generator current became negative. In all the running cases suggested for the car, the action of the verified IM is very acceptable, promoting its use in a car produced in Syria[14].

Azman bin mat Hussin completed his MSc Thesis in 2014, introducing a Direct Torque Control (DTC) approach for regulating IM operation. The aim is to determine how efficient the torque and flux are. Torque regulation of an IM base has been developed in this thesis using a DTC method and a thorough analysis. Direct torque control was the first technique to regulate the real motor control variable for torque and flux. This approach improved the precision and speed of torque control, high dynamic speed response, and motor control. The DTC theory, the switching table, and the choosing of the torque and flux hysteresis band amplitudes are covered in this paper. DTC's simple dynamic efficiency is discussed. The output involves when the motor starts and when the nominal value of the motor starts. Simulation using a flexible simulation kit, MATLAB/SIMULINK, has demonstrated the quality of this control system. In addition, the researcher offers simulation data linked to the theoretical elements discussed in the study. The findings show that the suggested direct torque control can regulate the IM's functioning[15].

B. Srinu Naik released research in 2014. It is critical to regulating the IM since it is the most frequent motor used in industrial motor control systems. As a result, a well-established IM drive that is simple, durable, low cost, and low maintenance may perform the needed purpose. Several writers have published research papers on IM vector control methods. Moreover, it is clear from the examination of vector control approaches that the indirect vector control technique has surpassed the direct vector control technique in popularity. Therefore, the approach followed for more work is the indirect vector control strategy[16].

In 2015 Amit Kumar, Tejavathu Ramesh wrote an article about (Direct Field Oriented Control of IM Drive).

This work introduces direct field-oriented control of an IM drive, and the outcome is enhanced by utilizing a field-oriented control scheme over the scalar control system under transient and steady-state situations. The model is simulated in the Matlab/Simulink framework, and the simulation outcomes are provided under different operating circumstances, such as no-load, forward load, varied load torques, speed reversal, and abrupt change in speed conditions[17].

In 2015 Divyesh J Vaghela and Himanshu N Chaudhari published a paper that explores design parameters, performance parameters, and Permanent Magnet Synchronous Motor (PMSM) drive mathematical modelling. The Field Orientation Control (FOC) technique is being used for PMSM speed control. For the control algorithm, the hysteresis control method is used to provide constant torque operation on the load side. The PMSM drive aims to control the speed with constant torque operation over an extensive velocity range. The results of the simulation show that there is a strong dynamic response to the speed and current controller. In the MATLAB Simulink framework, simulation was performed. The simulation consists of all practical components and mathematical equations that allow different control schemes to measure current and voltage. The hardware circuit is implemented using the STM32F processor and uses MATLAB Simulink and hardware results to examine the result [18].

IFOC is the most powerful approach in current-source inverter fed IM driving, according to Zhen Guo, Jiasheng Zhang, Zhenchuan Sun, and Changming Zheng. The simulation framework of the IM model is created in the rotor flux system. Rotor flux observers are created and implemented in MATLAB utilizing stator currents and speed. The IM's transient response study in various operating conditions simulation findings demonstrates that the control system has high dynamic performance and accuracy[19].

In 2017 Chuanwei Zhang and Nuoting Wang published a paper. The main focus of this article is the control system for electrical machinery and the design of the control system for electrical machinery. The motor control system employs a dual closed-loop control system for the internal current loop and an exterior velocity loop. In this article, the AC IM is chosen as the study object, and the AC IM mathematical model is constructed, which includes the flux equation, motion equation, voltage equation, and torque equation. The simulation model of the AC IM is described in Matlab / Simulink, the simulation outputs are assessed, and the motor control system's accuracy is confirmed. The three-phase asynchronous motor PID control algorithm is tested [20].

Mr. Ankit Agrawal, Mr. Rakesh Singh Lodhi, and Dr. Pragya Nema published a paper in 2018 on the modelling and simulation of the two-level inverter scalar control & vector control approach for IM driving. THD and speed-torque features of a three-phase squirrel cage IM were studied to tackle the rise in lower order harmonics. This article compares scalar control versus vector control approaches for a three-phase IM using Matlab / Simulink. A scalar & vector control inverter comparison and performance is utilized in the motor to control speed, current, and torque. The Matlab simulation environment is utilized to mimic both scalar and vector control for the IM drive. The torque ripple is reduced, and so the harmonics of the lower order are reduced. The results of scalar and vector to level inverter simulations indicate constant velocity, constant torque, and variable velocity variable torque. Compared to a scalar, the two-level inverter applications provide greater power quality due to decreased harmonic material [21].

In 2019 Mirza Abdul Waris Begh and Hans-Georg Herzog studied on A comparison of the two vector control methods was proposed in this paper: FOC and DTC for an IM and a PMSM, and an effort was made to compare the pros and cons of both methods for the same machine. Due to the balance of merits of the two systems, it is very hard to state the superiority of one scheme over the other explicitly. Based on the discussion and the findings provided, one can nevertheless conclude that the two control systems provide comparable performance in terms of torque control in their basic configuration. In summary, it can be seen that both methods have good performance with faster dynamics of torque in the case of DTC and better steady-state behaviour in the case of FOC. In addition, PMSM has the advantage of lightweight and smaller drives with the same power level. In particular applications, both IMs and PMSMs are used and have a respectable market share. However, it should be noted that the lower inductance of the PMSM causes higher torque ripples with DTC compared to an IM, and lower sampling times must be used to decrease the ripple to an acceptable level. In short, based on the requirement of a particular application, one control method may be more appropriate than the other. With the use of different technologies, both FOC and DTC can be improved to deliver better, improved and comparable performance [22].

In 2019, K. A. M. Annuar, M. R. M. Sapiee, Rozilawati M. Nor, M. S. M. Azali, M.B.N. Shah, and Sahazati Md. Rozali released a study describing how, in the constant V/f control technique, the stator resistance and leakage inductance decreases are expected to be minimal particularly at high speed and low load. In other words, because the back emf is quite big at fast speeds, voltage dips may be ignored. Constant V/f, continuous Eg/f, and thus constant air-gap flow are anticipated by keeping constant V/f. This assumption, nevertheless, is incorrect at low speeds because a substantial voltage drop develops across the stator's impedance. This ag is no longer approximated by terminal voltage, V. MATLAB Simulink is used to simulate the open-loop constant V/f. At low speeds, the drive's quality is demonstrated to degrade. The use of voltage surge to improve performance is displayed and explained [23].

Susmitha Suresh and Rajeevan P. P. wrote a paper in 2020 that offers novel direct torque control (DTC) methods for IM (IM) drives premised on the idea of voltage vectors in virtual space. In the first approach proposed in this work, six virtual voltage space vectors are employed to realize a DTC with a constant switching frequency. The second approach employs both abstract voltage space vectors and actual voltage space vectors to realize a twelve-vector DTC to decrease torque ripple. The number of vectors in the third system is raised to 18 by employing 12 space vectors for virtual voltage and six real vectors. The fourth approach applies the notion of virtual vectors to dual inverters fed by open-end winding IM drives in order to reduce common-mode voltage across windings with a greater number of vectors. The neighbouring three-phase, two-level inverter voltage space vectors are switched at a consistent frequency to produce virtual voltage space vectors. These DTC schemes, like the standard DTC scheme, are basic because they lack coordinated and real-time calculations. These DTC methods have been tested experimentally on an IM driven by two-level voltage source inverters in both transient and steady-state operating circumstances. A digital signal processor (TMS320F28335) is utilized to perform the control system [24].

In 2020 Wang Qinglong, Yu Changzhou and Yang Shuying wrote a paper. In this paper, the asynchronous motor system is generated from the synchronous rotating coordinate system and the indirect orientation of the rotor flux vector control system is supplied, and a simulation system collection centred on MATLAB / Simulink and a set of asynchronous platform tests are presented, based on the detailed capacities of the electric car asynchronous motor drive system. The simulation and experimental findings demonstrate that the system has a good dynamic and steady-state control influence [25].

In 2020 Shivam Yadav and Anshul Kumar Mishra wrote an article about Space vector pulse width modulation (SVPWM), and sinusoidal pulse width modulation is the most commonly used techniques for improving power efficiency harmonic reduction (SPWM). A model with two control techniques (SPWM, SVPWM) for indirect FOC IM drive was modelled and simulated. The detailed comparative study of efficiency (steady-state) and torque Ripples are carried out at different drive phases in this model. For this setup, the comparative analysis has been studied theoretically and clarified by simulation performance[26].

A comparative analysis of direct field-oriented control (DFOC) and indirect field-oriented control (IFOC) is presented in this work by Sanjay Kumar Kakodia and Dr Giribabu Dynamina in 2020. At low speeds, the steady-state quality is better but the dynamic responsiveness is low speed management of IM drives is one of the hardest challenges. Vector control results in a neater steady-state and transient reaction. Vector control necessitates knowledge of the rotor angle. Hall sensors or adaptive scheme estimates are used to detect the rotor's angle. However, mounting sensors in the system shaft is complex and costly. The efficiency of IM's DFOC and IFOC supplied by the multi-level inverter is tested in high and low-speed operations, correspondingly. The IFOC is suited for low-speed efficiency, but the DFOC is appropriate for running at rated speeds. The usefulness of DFOC and IFOC is evaluated employing the MATLAB/Simulink framework [27].

1.5. Motivation and Problem

In this study, induction machines are used. Driver devices using induction machines excel with advantages such as being cheap compared to other machines, not requiring maintenance and easy to repair in the event of any failure. The downside of the IM is that the torque and speed cannot be controlled independently. Therefore, complex, interconnected equations in speed control algorithms need to be solved. There are many methods for speed control of IMs. We can classify them as dynamic and static control methods. Static control methods are easy to implement, but performance is worse than dynamic control methods.

1.6. Direction of work

As static control methods of the induction machine, control can be shown by V/f (scalar control). Vector control will be used as the IM's dynamic control technique. The vector control method is the best driver system in terms of dynamic behaviour characteristics. The vector control method's main premise is dependent on the separation of machine current into q-d components, which create torque and flux, and independent control of these components, as previously indicated. The system is the best driver in relation to torque-speed characteristics. Speed control in the vector control method is very good. High power and efficiency can be used in drive mechanisms, the drive system that shows the closest operation to the dynamic characteristics of the DC machine in fast, responsive drive mechanisms. The generated torque depends on a single current component.

Although dynamic control methods have many advantages, it requires very fast processors in practical applications according to static control methods. Therefore, in this study, IM control will be encoded using a processor from the STM32 series. STM32 is a family of 32-bit microcontroller integrated circuit by STMicroelectronics.

1.7. Thesis Structure

The outline of the thesis will be presented in the section. Each chapter will be introduced shortly.

2. Analysis and mathmatical modelling of three-phase IM: we will introduce mathematical modelling of IM in detail

3. Material and Method: All of the elements and Softwares described will be used in experimental work and all their parameters. The most important things in this thesis are the type of control that use, so we will describe FOC method and the two main types of it which is Indirect Field Oriented Control and Direct Field Oriented Control; then, we introduce how IFOC is working with an IM.

4. Modelling of three phase IM: In this chapter all of the equations that descussed in chapter two will use for designing a model of IM and Control system of it.

5.Experimental Work: experimental work will introduce.

6. Results and Discussion: Finally, in this chapter, we will introduce the results of the expermental work and result of control system.

7. Conclusion: Here in general we will talk about the main points that we will notice from working on this thesis.

2. Analysis and Mathematical Modelling of Three Phase IM

An induction motor of a 3-phase squirrel cage is the focus of the thesis. It is motor's rotor is made out of aluminum bars that are short-circuited with linking both of them to the two side rings, allowing the rotor to create its own induction current and magnetic field. As a result, the AC induction motor is a reliable, durable, and low-cost option for electric motors [37,10]. Figure 2.1 depicts the structure of a squirrel cage induction motor. A revolving stator flux is produced in an induction generator by electric currents feeding from three phase ends and flowing through the stator windings. The speed control of this magnetic field is calculated as the quantity of poles of the induction motor multiplied by the frequency of the source of power [4].

$$n_{sync} = \frac{120 f_e}{p} \tag{2.1}$$

In this equation, n_{sync} stands for the synchronous speed in rotations per minute, f_e stands for the power source frequency aslo, p stands for the number of poles.

Because the rotor bars are short-circuited, the revolving magnetic field from the stator induces a voltage, which results in a huge circulating current. After that, the rotating magnetic field engages with the generated rotor current. A tangential electromagnetic current is exerted upon rotor bars as a result of Lorentz's equation, and the total force upon every rotor bar creates a torque, which finally pushes the rotor in the line of the spinning field[28].

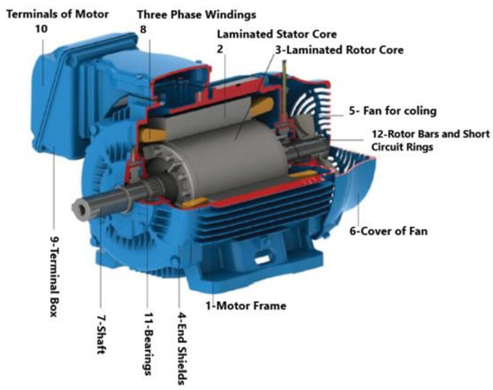

Figure 2.1. Cross section of a squirrel cage induction motor

The rotor is still very much in resting position whenever the rotating magnetic field is produced for its first time. In order to maintain the revolving stator flux, the rotor would move quickly. The revolving field does not slice the rotor bars as well as it used to, so the voltage in the rotor bars drops as the rotor speed rises. The rotor bars would no more be broken by the field when the rotor speed matches the flux speed, and the rotor will begin to decelerate [10]. The rotor speed would never match the synchronous speed, which is the reason that induction motors are known as asynchronous motors. The slip rapidity is recognized as the speed differential of both the stator and rotor:

$$n_{slip} = n_{sync} - n_m \tag{2.2}$$

A slip ratio can also be defined as follows

$$s = \frac{n_{sync} - n_m}{n_{sync}} \tag{2.3}$$

It's worth noting that, $s = 0$ if the rotor rotates with synchronous speediness in case of the rotor comes to a complete stop, $s = 1$.

2.1. IM Equivalent circuit

An IM is a three-phase transformer with a unique design. On the cylindrical core structure of IMs there are both primary and secondary windings. Figure 2.2 showing different between IM and transformer. However, there are a few differences between the IMs [29].

1. IM cores have a cylindrical shape, whereas transformer cores are of the E-I type.
2. In comparison to transformers, there is an air gap in IMs.
3. In contrast to transformer windings, which are concentric, IM windings are scattered over the air gap.
4. In comparison to transformers, the IM has a secondary winding and it will be always shorter.
5. Rotation of the IM auxiliary core and winding is permitted.

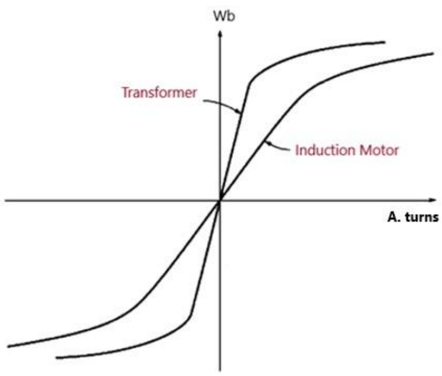

Figure 2.2. The magnetization curve of an induction motor with Transformer

A voltage is generated in the rotor windings once load is connected to the stator windings in an induction motor. The higher the absolute speed here in between the magnetic fields of both rotor and stator, the higher the frequency and rotor voltage will be. When the rotor is motionless, known as the locked-rotor or blocked-rotor condition, the maximum relative motion is created in the rotor, resulting in the highest voltage and rotor frequency. In case of having the same velocity of both the rotor spins with the stator magnetic field, there will be no comparative drive and both the voltage and frequency are the lowest (0 V and 0 Hz). At any velocity between these immoderations, the voltage amplitude and frequency created in the rotor is immediately changing with the rotor slip. As a result, if E_{r0} is the magnitude of the induced rotor voltage at locked-rotor conditions, the amplitude of the applied voltage at that slip is expressed by the formula [37].

$$E_r = sE_{r0} \tag{2.4}$$

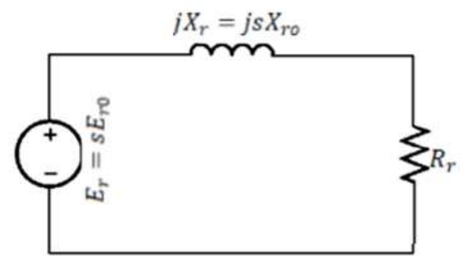

Figure 2.3. Rotor model of an induction motor

And also the formula would provide the frequency of the induced voltage at any slip.

$$f_r = sf_e \tag{2.5}$$

In a rotor with both resistance and reactance, this voltage is generated. The rotor resistance R_r is stable (save for the skin effect) and unaffected by slip, but the reactance of rotor is further multifaceted. The induction motor rotor capacity, as well as the voltage frequency and current in the rotor, determine its reactance. The rotor reactance is determined below with a rotor inductance of L_r.

$$X_r = \omega_r L_r = 2\pi f_r L_r \tag{2.6}$$

$$X_r = 2\pi f_e L_r = s(2\pi f_e L_r) = sX_{r0} \tag{2.7}$$

In which the blocked-rotor reactance is X_{r0}.

The rotor equivalent circuit that results can be seen in Figure 2.3.

The rotor current flow is calculated as

$$I_r = \frac{E_r}{R_r + jX_r} \tag{2.8}$$

$$I_r = \frac{E_r}{R_r + jsX_{r0}} \tag{2.9}$$

$$I_r = \frac{E_{r0}}{\frac{R_r}{s} + jX_{r0}} \tag{2.10}$$

It is feasible to view all of the rotor effects generated by changing rotor movement as being produced by a changing impedance fed with electricity from a stable voltage source E_{r0}, as shown in the final equation of I_r.Figure 2.4 show the Rotor equivalent circuit with a slip effects concentrated in resistor R_r . From this perspective, the analogous rotor impedance is

$$Z_{r.eq} = \frac{R_r}{s} + jX_{r0} \tag{2.11}$$

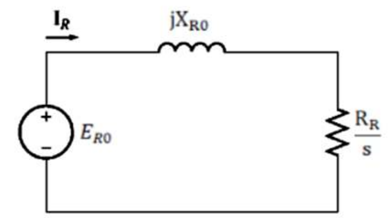

Figure 2.4. Rotor equivalent circuit with a slip effects concentrated in resistor R_r

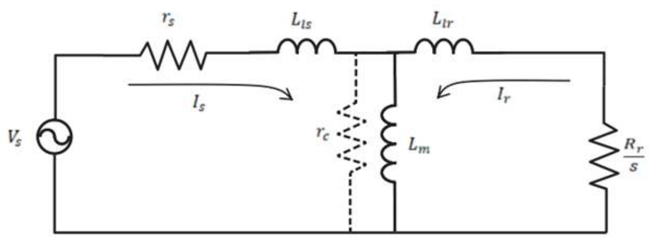

Figure 2.5. The induction motor's final per-phase equivalent circuit

Figure 2.5 show the IM dynamics are characterized by using the T-equivalent circuit.

$$(r_s + j\omega_e L_{ls})I_s + j\omega_e L_m(I_s + I_r) = V_s \tag{2.12}$$

$$\left(\frac{r_r}{s} + j\omega_e L_{lr}\right) I_r + j\omega_e L_m(I_s + I_r) = 0 \tag{2.13}$$

P_g is the power transferred to the rotor (or air-gap power) is shown by.

$$P_g = 3I_r^2 \frac{R_r}{s} \qquad 2.14)$$

The entire amount of electrical energy transferred to mechanical energy is:

$$P_m = P_g - P_{cu} = 3I_r^2 R_r(\frac{1-s}{s}) \tag{2.15}$$

2.2. Loss from IMs

Basic frequency lost and harmonic damages are the two types of losses. Copper losses in, core losses (eddy current and hysteresis), the rotor and stator, Abandoned losses, and motorized losses make up the basic frequency losses (windage and friction)[30].

In the stator, the copper loss is computed as follows:

$$P_{cu,s} = 3I_s^2 R_s \tag{2.16}$$

The copper loss in the rotor is estimated as follows:

$$P_{cu,r} = 3I_r^2 R_r \tag{2.17}$$

For an accurate copper losses analysis, both the temperature and the influence of the winding's skin effect would be required. The resistances of both the rotor and stator are computed connected by an adaptive motor structure analyzer to avoid this[27,31].

Changes in the steel laminations magnetization result in a loss of energy. Eddy currents and hysteresis contribute to losses. In a sinusoidal flux supply, the eddy and hysteresis current losses can be calculated using Steinmetz formulas for core losses.

$$P_h = K_h \Phi^2 \omega_s \tag{2.18}$$

$$P_e = K_e \Phi^2 \omega_s^2 \tag{2.19}$$

Therefore, the equation of the stator core loss defined as:

$$P_{s,core} = K_{s,h} \Phi^2 \omega_s + K_{s,e} \Phi^2 \omega_s^2 \tag{2.20}$$

The rotor and stator core loss are both the same, however it is measured in slip frequency rather than stator frequency.

$$P_{r,core} = K_{r,h} \Phi^2 (s\omega_s) + K_{r,e} \Phi^2 (s\omega_s)^2 \tag{2.21}$$

The rotor central loss is ignored in comparison to the stator central loss since a minimal slip is required to work the induction motor. Also, the motor's overall core loss defined as:

$$P_{core} \approx P_{s,core} = (K_h \omega_s + K_e \omega_s^2)\, \Phi^2 \tag{2.22}$$

The stray loss is the small part of the overall losses that is not covered by the combination of all rotor and stator copper loss, central loss, abrasion and windage losses. The stray loss could indeed be approximated by assuming that it is equal to the rotor current difference and so could be regarded as better resistance.Resistance (P_{str}) in the stator branch represents it, and it is defined: [27].

$$P_{str} = C_{str}\omega^2 I_r^2 \tag{2.23}$$

In which the C_{str} is constant.

The stray loss is performed by considering overall losses and deducting the combination of windage and abrasion, core rotor and sator loss from these losses, as per IEEE 112B standard test process for induction motors (indirect measurement). [27,20]

The resistances of both rotor and sator rise with rising the motor temprature. The temperature of the stator could be calculated easily, however the rotor temperature is more difficult to determine. Also, the thermal model of the motor must be known in order to calculate the temperature precisely. The skin effect may be neglected in stator winding, however it dominates in squirrel cage rotor bars. The skin effect owing to the central frequency could be omitted in an inverter-fed machine, however for harmonic frequencies, the rotor nearly seems immobile, and so essentially it is the rotor in which all the stator harmonic currents pass, resulting in a dominant skin effect.

It's possible to assess stator and rotor resistances electronically than it is to measure temperature and understand the motor mechanical engineering data sheets. We'll go over how to use the adaptive motor parameter observer to estimate stator and rotor resistances later [27,37].

2.3. Curve of Torque-Speed

Because both the torque of an induction motor and the rotor current are equivalent, the rotor current must be computed to obtain torque.

$$T = \frac{P_m}{\omega_r} = 3|I_r^2|\frac{(1-s)r_r}{s\omega_r} \tag{2.24}$$

The equivalent circuit for an induction motor is frequently adjusted to make calculations easier, as seen in Figure 2.6 With the source, the magnetizing inductance Lm is transferred to the power supply.

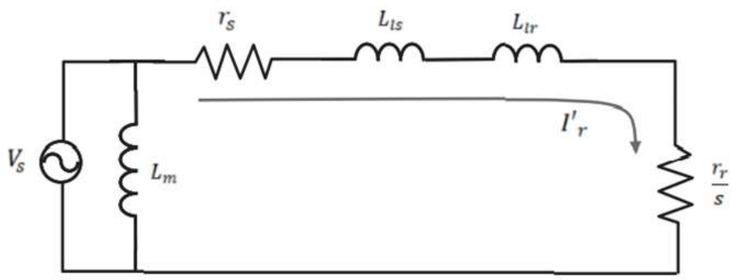

Figure 2.6. Induction motor equivalent circuit with modifications

The voltage descent across the stator's seepage current and confrontation is assumed to be modest. The leakage current is substantially smaller than the magnetizing inductance.Figure 2.6 showing the IM modification equivalent circuit. Induction motors have a leakage reactance $j\omega_e\ L_{ls}$ that is roughly 5% fewer than the magnetizing reactance $j\omega_e\ L_m$.I'_r stands for the rotor current in the modified circuit is intended as

$$|I'_r| = \frac{|V_s|}{\sqrt{(r_r+\frac{r_r}{s})^2+\omega_e^2(L_{ls}+L_{lr})^2}} \tag{2.25}$$

The explanation of the slip determins that $\frac{P}{2\omega_e} = \frac{1-s}{\omega_r}$. Henceforward, the electro-magnetic torque is premeditated like the following.

$$T_e = \frac{P}{2}\frac{3r_r}{s\omega_e}\frac{|V_s|^2}{(r_s+\frac{r_r}{s})^2+\omega_e^2(L_{ls}+L_{lr})^2} \tag{2.26}$$

As for minor slip like $s \approx 0$, torque calculation is approached as

$$T_e \approx \frac{P}{2}\frac{3r_r}{\omega_e s}\frac{|V_s|^2}{\left(\frac{r_r}{s}\right)^2} \approx \frac{3P|V_s|^2}{2\omega_e r_r}s \tag{2.27}$$

The torque is linear in s in a tiny slip zone. As a result, at s = 0, the torque curve will be shown in a straight line. However, when s =1, is approximated in such a way that [33].

$$T_e = \frac{P}{2}\frac{3r_r}{s\omega_e}\frac{|V_s|^2}{(r_s+r_r)^2+\omega_e^2(L_{ls}+L_{lr})^2} \tag{2.28}$$

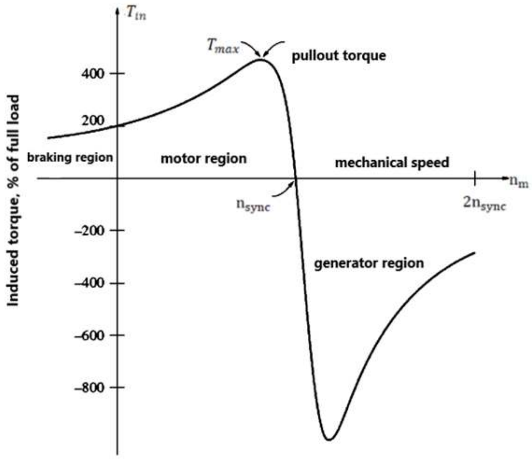

Figure 2.7. Curve of Torque-Speed Characteristic

From figure 2.7 can see the diffrent between motor region and generator region.In this thesis we worked just in motor region.

2.4. IMs Starting

With turning on an induction motor immediately from the supply, it has ability to ingests 5–7 times its maximum current load and yields only 1.5–2.5 times the maximum torque load. The great beginning current can lead to a substantial power loss, which might also obstruct with the functioning of additional apparatus along the same track. Therfore, beginning induction motors with larger rankings (usually above 25kW) straight from the basics source is not recommended. The following sections cover the different starting procedures for induction motors of the Squirrel Cage type[32].

2.4.1. Direct-On-Line Starters

Small 3-phase type of induction motors could be operated on-line directly, that implies the motor is run straight by the assessed source. Though, as stated earlier, the initial current would be quite great, typically (5 – 7) times the rated current. It's expected that the beginning torque would be (1.5 t- 2.5) times the complete torque load. A Direct-On-Line Starter (DOL) starter, typically comprises of a contactor and motor defense devices including a circuit breaker, might be castoff to begin induction motors immediately working. A DOL starter is containing a coil-operated contactor that could be regulated by push buttons for start and finish.The contactor is electrified when the begin button is pushed, and it simultaneously connects all 3 phases of the motor to the source. To terminate the motor, the stopping switch disanimate the contactor and disengages all three components. A DOL starter is naturally included in motors rated underneath 5kW to avoid massive power loss in the source line caused by heavy initial current.

2.4.2. Squirral Cage Motors Starting

In squirrel cage motors, the beginning overload power is limited by lowering the stator voltage. For squirrel cage induction motor starting, these processes are typically referred to as decreased voltage methods. The approaches used for this are as follows: Using Core Resistors: The aim is to lower certain voltage and send it to the stator at a lower voltage. Assume a 50% reduction in the beginning voltage. The beginning current is then lowered by the very same amount as per Ohm's law (V=I/Z). The beginning torque of an induction motor of 3-phase is roughly equal to the difference of the functional voltage, according to the torque formula. That is to say, if there is an applied desired voltage of 50%, the foundation torque would only be 25% of the classic voltage value. This process is frequently used to begin tiny induction motors smoothly. For motors that have high launching torque needs, using primary resistors as a starting technique is not advised. The resistors are usually chosen such that the motor can get 70% of the rated voltage. Maximum resistance is linked with the stator winding in series when the motor starts, and it slowly reduces when the motor accelerates. As the motor achieves the desired speed, the resistances are disengaged in the circuit, and the stages of the stator are wired up to the source lines straight.

Auto-Transformers : It also has another name which is Auto-starters. They can be utilized with squirrel cage motors that are either connected in star shape or delta shape connection. It's fundamentally a step down transformer of a 3-phase with several inputs that permit users to begin the motor at (50, 65, or 80 percent) of streak voltage, respectively.Whenever this kind of transformer is ongoing, the power flow from the source line has continuously been relative to the transformation ratio fewer than that of the motor current. If an engine is operated on a 65 percent tap, for instance, both the applied current and voltage to the motor is 65 percent of the line voltage beginning value, though the line current is 65 percent of 65 percent (for instance 42 percent). Transformer activity is responsible for the change between motor currents and line. An auto-internal starter's connections are depicted in the illustration. The adjustment is in the "start" position whenever the motor starts, and a diminished voltage (selected by a tap) is supplied around the stator. The auto-transformer is routinely detached from the circuit by itself whenever the motor grasps an exact rate, perhaps around 80 percent of its motor voltage, and the button is fixed to "run." Air-break is an example of (small motors) or oil-immersed (big motors) alterations are used to convert the circuit from begin to operation. With delay circuits on an autostarter, also there are safeguards for no-voltage and overloading. This strategy is employed in motors that are built with a delta linked stator. It is to be known that the stator winding is associated in star shape for starting but in delta shape for operating at regular speed using a two-way switch.Whenever the stator winding is associated in star shape, the voltage across all the motor phases are lowered by a feature of 1/(sqrt. 3) related to when the stator winding is connected in delta. The beginning torque for a delta connected winding would be 1/3 that of a delta shape connection winding. Therfore, a star-delta starter is comparable to an automatic-transformer with a proportion of 1/(sqrt. 3) or a voltage reduction of 58 percent[33].

2.5. Mathmatical Modelling of Flux Linkage in IM

Different induction motor voltage models are transformed in both the synchronous and stationary reference frames. The concept of constructing induction motor dynamic models is strongly reliant on coordinate transformations. Because the rotor velocity differs from the synchronous speed, the procter is a little more involved. Field oriented control is based on a dynamic model in an equivalent circuit. [33]

The voltage model is obtained by taking the time gradient of the flux linkage. The flux linkage formulas for the stator and rotor are first given in the frame of reference, later on plotted into the frame of synchronous. Both stator and rotor currents stimulate the stator flux. The stator flux created by the stator current in a homogeneous air gap device is equivalent to $\boldsymbol{\lambda}_{abcs}^{s} = \mathbf{L}_{abcs}\mathbf{i}_{abcs}^{s}$

$$\begin{bmatrix}\lambda_{as}\\ \lambda_{bs}\\ \lambda_{cs}\end{bmatrix} = \begin{bmatrix} L_{ls}+L_{ms} & -\frac{1}{2}L_{ms} & -\frac{1}{2}L_{ms} \\ -\frac{1}{2}L_{ms} & L_{ls}+L_{ms} & -\frac{1}{2}L_{ms} \\ -\frac{1}{2}L_{ms} & -\frac{1}{2}L_{ms} & L_{ls}+L_{ms}\end{bmatrix}\begin{bmatrix}i_{as}\\ i_{bs}\\ i_{cs}\end{bmatrix} \tag{2.29}$$

The linkage variations with the rotor angle, θ_r because the coil of rotor is stabled upon the surface. Precisely, the a-phase flux is labeled like $\lambda_{as}^{s} = L_{ms}\cos\theta_r i_{ar}^{r}$, the flux connecting spreads the all-out when θ_r= 0. Also, lets say $\theta_r = \pi/2$ the flux is zero. it is known that the value of b and c phase windings are $2\pi/3$ and $4\pi/3$ separately in stage, the stator flux donated by the current of rotor defined as

$$L_{ms}\begin{bmatrix} \cos\theta_r & \cos(\theta_r+\frac{2\pi}{3}) & \cos(\theta_r-\frac{2\pi}{3}) \\ \cos(\theta_r-\frac{2\pi}{3}) & \cos\theta_r & \cos(\theta_r+\frac{2\pi}{3}) \\ \cos(\theta_r+\frac{2\pi}{3}) & \cos(\theta_r-\frac{2\pi}{3}) & \cos\theta_r \end{bmatrix}\begin{bmatrix}i_{ar}^{r}\\ i_{br}^{r}\\ c_{cr}^{r}\end{bmatrix} \tag{2.30}$$

Joining $\mathbf{L}_{abcs}\mathbf{i}_{abcs}^{s}$ with $\mathbf{M}(\theta_r)\mathbf{i}_{abcr}^{r}$, a whole appearance of the stator flux assembly is found

$$\boldsymbol{\lambda}_{abcs}^{s} = \mathbf{L}_{abcs}\mathbf{i}_{abcs}^{s} + \mathbf{M}(\theta_r)\mathbf{i}_{abcr}^{r}. \tag{2.31}$$

Likewise, the rotor flux connection understood by the frame of rotor is assumed to be:

$$\boldsymbol{\lambda}^{r}_{abcr} = \mathbf{M}(-\theta_r)\mathbf{i}^{s}_{abcs} + \mathbf{L}_{abcr}\mathbf{i}^{r}_{abcr} \tag{2.32}$$

Where

$$\boldsymbol{\lambda}^{r}_{abcr} = \begin{bmatrix} \lambda^{r}_{ar} \\ \lambda^{r}_{br} \\ \lambda^{r}_{cr} \end{bmatrix} \text{and } \mathbf{L}_{abcr} = \begin{bmatrix} L_{lr} + L_{ms} & -\frac{1}{2}L_{ms} & -\frac{1}{2}L_{ms} \\ -\frac{1}{2}L_{ms} & L_{lr} + L_{ms} & -\frac{1}{2}L_{ms} \\ -\frac{1}{2}L_{ms} & -\frac{1}{2}L_{ms} & L_{lr} + L_{ms} \end{bmatrix}$$

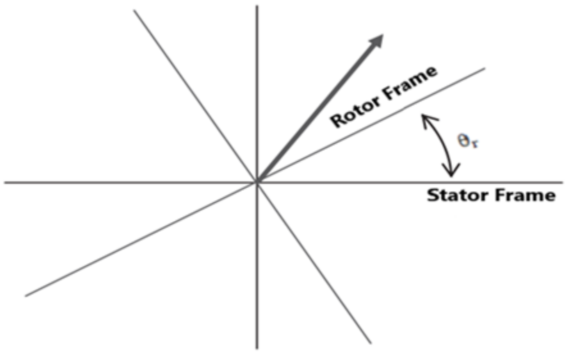

Figure 2.8. Both Rotor and Stator Frame

From figure 2.8 the different between rotor frame and stator frame by θ_r showed.

Currently, for transformation into dq stationary frame we multiplying T(0) by $\boldsymbol{\lambda}^{s}_{abcs}$:

$$\boldsymbol{\lambda}^{s}_{dq0s} = \mathbf{T}(0)\boldsymbol{\lambda}^{s}_{abcs} = \mathbf{T}(0)\mathbf{L}_{abcs}[\mathbf{T}^{-1}(0)\mathbf{T}(0)]\mathbf{i}^{s}_{abcs} = \mathbf{T}(0)\mathbf{L}_{abc}\mathbf{T}^{-1}(0)\mathbf{i}^{s}_{dqs} \tag{2.33}$$

In which

$$\boldsymbol{\lambda}^{s}_{dq0s} = \begin{bmatrix} \lambda^{s}_{ds} \\ \lambda^{s}_{qs} \\ \lambda_0 \end{bmatrix} \qquad \mathbf{L}_{dq0} = \begin{bmatrix} L_{ls} + \frac{3}{2}L_m & 0 & 0 \\ 0 & L_{ls} + \frac{3}{2}L_m & 0 \\ 0 & 0 & L_{ls} + \frac{3}{2}L_m \end{bmatrix}$$

In the balanced 3- phase system, in the frame of dq the thir vector component is zero. The rotor current input, $\mathbf{M}(\theta_r)\mathbf{i}^{r}_{abcr}$ with stator flux as well desires to be plotted into the same motionless frame. In calculating the transformation, an impose tariffs is more efficient. Whenever the 3rd module of a 3-phase vector is neglected, a complex integer can be used to identify it

$$\boldsymbol{\lambda}_{dq0s}^{s} = \begin{bmatrix} \lambda_{ds}^{s} \\ \lambda_{qs}^{s} \\ \lambda_{0} \end{bmatrix} \quad \Longleftrightarrow \quad \boldsymbol{\lambda}_{dqs}^{s} = \lambda_{ds}^{s} + j\lambda_{qs}^{s} = \frac{2}{3}[\lambda_{as}^{s} + e^{j\frac{2\pi}{3}}\lambda_{bs}^{s} + e^{j\frac{4\pi}{3}}\lambda_{cs}^{s}] \tag{2.34}$$

Rather than calculating it with T(0), the plotting regulation previously is exploited. The alteration in the stator portion was previously exposed ; $\boldsymbol{\lambda}_{dq}^{s} = \mathbf{L}_{s}\mathbf{i}_{dq}^{s}$, in which $L_s = \frac{3}{2}L_{ms} + L_{ls}$ the rotor coil input is malformed

$$\mathbf{M}(\theta_r)\mathbf{i}_{abcr}^{r} \Longleftrightarrow \frac{2}{3}L_{ms}[\cos\theta_r i_{ar} + \cos(\theta_r + 2\pi/3)i_{br} + \cos(\theta_r - 2\pi/3)i_{cr}$$
$$+ e^{j\frac{2\pi}{3}}\{\cos(\theta_r - 2\pi/3)i_{ar} + \cos\theta_r i_{br} + \cos(\theta_r + 2\pi/3)i_{cr}\}$$
$$+ e^{-j\frac{2\pi}{3}}\{\cos(\theta_r + 2\pi/3)i_{ar} + \cos(\theta_r - 2\pi/3)i_{br} + \cos\theta_r i_{cr}\}]$$

$$= \frac{2}{3}\frac{1}{2}L_{ms}\Big[\left(e^{j\theta_r} + e^{-j\theta_r}\right)i_{ar} + \left(e^{j(\theta_r+\frac{2}{3}\pi)} + e^{-j(\theta_r+\frac{2}{3}\pi)}\right)i_{br} + \left(e^{j(\theta_r-\frac{2}{3}\pi)} + e^{-j(\theta_r-\frac{2}{3}\pi)}\right)i_{cr}$$
$$+ \left(e^{j\theta_r} + e^{-j(\theta_r-\frac{4}{3}\pi)}\right)i_{ar} + \left(e^{j(\theta_r+\frac{2}{3}\pi)} + e^{-j(\theta_r-\frac{2}{3}\pi)}\right)i_{br} + \left(e^{j(\theta_r+\frac{4}{3}\pi)} + e^{-j\theta_r}\right)i_{cr}$$
$$+ \left(e^{j\theta_r} + e^{-j(\theta_r+\frac{4}{3}\pi)}\right)i_{ar} + \left(e^{j(\theta_r-\frac{4}{3}\pi)} + e^{-j\theta_r}\right)i_{br} + \left(e^{j(\theta_r-\frac{2}{3}\pi)} + e^{-j(\theta_r+\frac{2}{3}\pi)}\right)i_{cr}\Big]$$

$$= \frac{1}{2}L_{ms}\frac{2}{3}\left[3e^{j\theta_r}i_{ar} + 3e^{j(\theta_r+\frac{2}{3}\pi)}i_{br} + 3e^{j(\theta_r-\frac{2}{3}\pi)}i_{cr}\right]$$

$$= \left(\frac{3}{2}L_{ms}\right)e^{j\theta_r}\frac{2}{3}\left[i_{ar} + e^{j\frac{2}{3}\pi}i_{br} + e^{-j\frac{2}{3}\pi}i_{cr}\right] = \mathbf{L}_m e^{j\theta_r}\mathbf{i}_{dqr}^{r} \tag{2.35}$$

which $L_m \equiv \frac{3}{2}L_{ms}$ we gain the stator flux in the stationary frame by :

$$\boldsymbol{\lambda}_{dqs}^{s} = \mathbf{L}_s\mathbf{i}_{dqs}^{s} + \mathbf{L}_m e^{j\theta_r}\mathbf{i}_{dqr}^{r} \tag{2.36}$$

The rotor flux calculation with orientation to the frame of rotor is shown by:

$$\boldsymbol{\lambda}_{dqr}^{r} = \mathbf{L}_m e^{-j\theta_r}\mathbf{i}_{dqs}^{s} + \mathbf{L}_r i_{dqr}^{r} \tag{2.37}$$

Where $L_r = \frac{3}{2}L_{ms} + L_{lr}$Meanwhile the frame of rotor is referenced on $e^{j\theta_r}$the stator current is realized overdue from θ_rConsequently $e^{-j\theta_r}$ is calculated to i_{dqs}^{s}.

A frame of synchronous reference is a rotating mount that revolves simultaneously rate as the electrical angular velocity,ω_e .It is the stator and rotor flux's (angular) speed. At time t, the synchronous frame's d-axis angle is represented by θ_e.

$$\theta_e = \int_0^t \omega_e dt = \omega_e t$$

ω_e stands for the electrical speed. letter, 'e' is castoff to designate a mutable in the frame of synchronous. The symbol was first initiated from the expression,‘exciting’.

Remember in IMs $\omega_e \neq \frac{P}{2}\omega_r$ while it is identical in synchronous apparatuses. Subsequently the frame of synchronous is θ_e fast from the motionless frame, and a vector could be signified with a lesser angle. Thus, its vector is gotten from calculating the motionless vector to $e^{-j\theta_e}$. Likewise, it is essential to calculate the rotor vector frame by $e^{-j(\theta_e-\theta r)}$. Exactly

$$\boldsymbol{\lambda}_{dqs}^{e} = e^{-j\theta_e}\boldsymbol{\lambda}_{dqs}^{s} \tag{2.38}$$

$$\boldsymbol{\lambda}_{dqr}^{e} = e^{-j(\theta_e-\theta r)}\boldsymbol{\lambda}_{dqr}^{r} \tag{2.39}$$

From the dissimilar frames flux angles understood, and they are portrayed in Figure 2.9 Remember that

$$\boldsymbol{\lambda}_{dqs}^{e} = L_{ls}\mathbf{i}_{dqs}^{e} + L_m\left(\mathbf{i}_{dqs}^{e} + \mathbf{i}_{dqr}^{e}\right) = L_s\mathbf{i}_{dqs}^{e} + L_m\mathbf{i}_{dqr}^{e} \tag{2.40}$$

$$\boldsymbol{\lambda}_{dqr}^{e} = L_{lr}\mathbf{i}_{dqr}^{e} + L_m\left(\mathbf{i}_{dqs}^{e} + \mathbf{i}_{dqr}^{e}\right) = L_r\mathbf{i}_{dqs}^{e} + L_m\mathbf{i}_{dqr}^{e} \tag{2.41}$$

In the meantime $L_s = L_{ls} + L_m$ and $L_r = L_{lr} + L_m$ The same formulas are shown in the matrix form

$$\begin{bmatrix}\lambda_{ds}^{e}\\ \lambda_{dr}^{e}\end{bmatrix} = \begin{bmatrix}L_s & L_m\\ L_m & L_r\end{bmatrix}\begin{bmatrix}i_{ds}^{e}\\ i_{dr}^{e}\end{bmatrix} \tag{2.42}$$

$$\begin{bmatrix}\lambda_{qs}^{e}\\ \lambda_{qr}^{e}\end{bmatrix} = \begin{bmatrix}L_s & L_m\\ L_m & L_r\end{bmatrix}\begin{bmatrix}i_{qs}^{e}\\ i_{qr}^{e}\end{bmatrix} \tag{2.43}$$

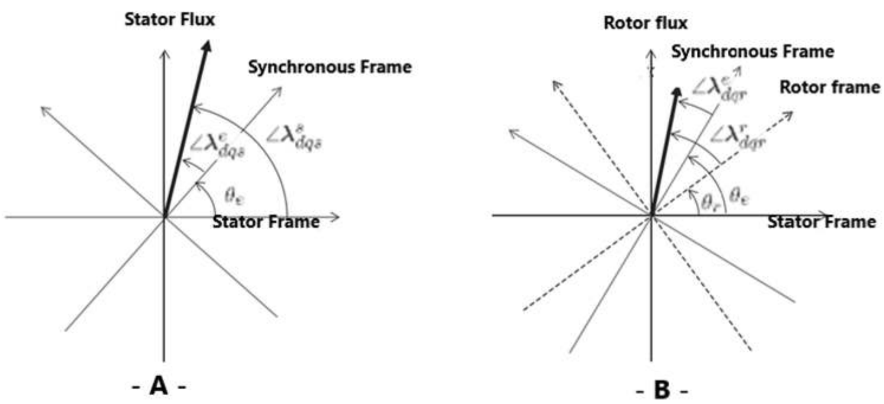

Figure 2.9. (a) From the stationary frame (stator), and (b) from the rotor frame

Transformation into the synchronous frame also explained this in figure 2.9. Flux to current relatives are showed in figure 2.10 Using the matrix inversion, following can be attained [33].

$$\begin{bmatrix} i_{ds}^{e} \\ i_{dr}^{e} \end{bmatrix} = \frac{1}{\sigma L_s L_r} \begin{bmatrix} \mathrm{L_r} & -\mathrm{L_m} \\ -\mathrm{L_m} & \mathrm{L_s} \end{bmatrix} \begin{bmatrix} \lambda_{\mathrm{ds}}^{\mathrm{e}} \\ \lambda_{\mathrm{dr}}^{\mathrm{e}} \end{bmatrix} \tag{2.44}$$

$$\begin{bmatrix} i_{qs}^{e} \\ i_{qr}^{e} \end{bmatrix} = \frac{1}{\sigma L_s L_r} \begin{bmatrix} \mathrm{L_r} & -\mathrm{L_m} \\ -\mathrm{L_m} & \mathrm{L_s} \end{bmatrix} \begin{bmatrix} \lambda_{qs}^{e} \\ \lambda_{qr}^{e} \end{bmatrix} \tag{2.45}$$

Where

$$\sigma = 1 - \frac{\mathrm{L_m^2}}{\mathrm{L_r L_s}}$$

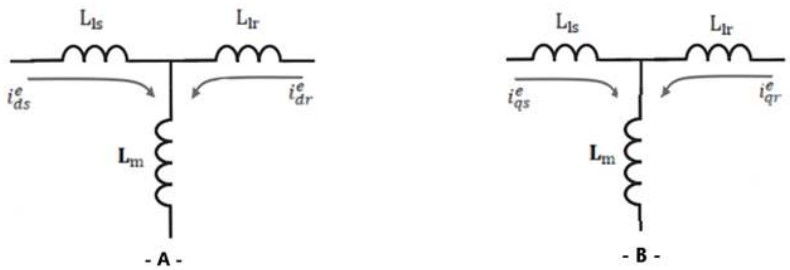

Figure 2.10. The flux to current relationship in the frame of synchronous is: (a) The d-axis; (b) The q-axis

In table 2.1 we can see all of equationes in diffrent frames.

Table 2.1. The flux calculations are shortened in

Frame	Stator Flux	Rotor Flux
abc	(Stationary frame) $\boldsymbol{\lambda}_{\mathrm{abcs}}^{\mathrm{s}} = \mathbf{L}_{\mathrm{abcs}}\mathbf{i}_{\mathrm{abcs}}^{\mathrm{s}} + \mathbf{M}(\theta_{\mathrm{r}})\mathbf{i}_{\mathrm{abcr}}^{\mathrm{r}}$	(Rotor frame) $\boldsymbol{\lambda}_{\mathrm{abcr}}^{\mathrm{r}} = \mathbf{M}(-\theta_{\mathrm{r}})\mathbf{i}_{\mathrm{abcs}}^{\mathrm{s}} + \mathbf{L}_{\mathrm{abcr}}\mathbf{i}_{\mathrm{abcr}}^{\mathrm{r}}$
dq	(Stationary frame) $\boldsymbol{\lambda}_{\mathrm{dqs}}^{\mathrm{s}} = \mathbf{L}_{\mathrm{s}}\mathbf{i}_{\mathrm{dqs}}^{\mathrm{s}} + \mathbf{L}_{\mathrm{m}}e^{j\theta_{\mathrm{r}}}\mathbf{i}_{\mathrm{dqr}}^{\mathrm{r}}$	(Rotor frame) $\boldsymbol{\lambda}_{\mathrm{dqr}}^{\mathrm{r}} = \mathbf{L}_{\mathrm{m}}e^{-j\theta_{\mathrm{r}}}\mathbf{i}_{\mathrm{dqs}}^{\mathrm{s}} + \mathbf{L}_{\mathrm{r}}\mathrm{i}_{\mathrm{dqr}}^{\mathrm{r}}$
dq	(Synchronous frame) $\boldsymbol{\lambda}_{\mathrm{dqs}}^{\mathrm{e}} = \mathrm{L_{ls}}\mathbf{i}_{\mathrm{dqs}}^{\mathrm{e}} + \mathrm{L_m}\left(\mathbf{i}_{\mathrm{dqs}}^{\mathrm{e}} + \mathbf{i}_{\mathrm{dqr}}^{\mathrm{e}}\right)$ $= \mathrm{L_s}\mathbf{i}_{\mathrm{dqs}}^{\mathrm{e}} + \mathrm{L_m}\mathbf{i}_{\mathrm{dqr}}^{\mathrm{e}}$	(Synchronous frame) $\boldsymbol{\lambda}_{\mathrm{dqr}}^{\mathrm{e}} = \mathrm{L_{lr}}\mathbf{i}_{\mathrm{dqr}}^{\mathrm{e}} + \mathrm{L_m}\left(\mathbf{i}_{\mathrm{dqs}}^{\mathrm{e}} + \mathbf{i}_{\mathrm{dqr}}^{\mathrm{e}}\right)$ $= \mathrm{L_s}\mathbf{i}_{\mathrm{dqs}}^{\mathrm{e}} + \mathrm{L_m}\mathbf{i}_{\mathrm{dqr}}^{\mathrm{e}}$

2.6. Mathmatical Modelling of Voltage in IM

Let P=d/dt voltage formulas for both the stator and rotor are shown below.

$$\mathbf{V}^{s}_{abcs} = r_s \mathbf{i}^{s}_{abcs} + P\boldsymbol{\lambda}^{s}_{abcs} \tag{2.46}$$

$$\mathbf{V}^{r}_{abcr} = r_r \mathbf{i}^{r}_{abcr} + P\boldsymbol{\lambda}^{r}_{abcr} \tag{2.47}$$

It's worth noting the formula for rotor is stated with having the frame of rotor in mind, while the formula for stator is prepared with having the frame of stationary in mind. We get the voltage formulas in the dq stationary and rotor frames by smearing T(0) to the sides in both way and eliminating the dimension[33].

$$\mathbf{V}^{s}_{dqs} = r_s \mathbf{i}^{s}_{dqs} + P\boldsymbol{\lambda}^{s}_{dqs} \tag{2.48}$$

$$\mathbf{V}^{r}_{dqr} = r_r \mathbf{i}^{r}_{dqr} + P\boldsymbol{\lambda}^{r}_{dqr} \tag{2.49}$$

The rotor equation must be transformed because the stator voltage formula is now in the stationary frame. It is possible to accomplish this by multiplying $e^{j\theta_r}$ on both sides :

$$\mathbf{V}^{s}_{dqr} = e^{j\theta_r}\mathbf{V}^{r}_{dqr} = r_s e^{j\theta_r}\mathbf{i}^{r}_{dqr} + e^{j\theta_r}\mathbf{P}\left[e^{-j\theta_r}e^{j\theta_r}\boldsymbol{\lambda}^{r}_{dqr}\right] = r_r\mathbf{i}^{s}_{dqr} + \mathbf{P}(-j\omega_r)\boldsymbol{\lambda}^{s}_{dqr} \tag{2.50}$$

The operator, '$\mathbf{p}$' and an operand, $e^{-j\theta_r}$do not shuttle, for instance, $\mathbf{P}e^{-j\theta_r} = e^{-j\theta_r}\mathbf{P}$ as θ_r is a function of t. Consequently, a performance of introducing the character $1 = e^{j\theta_r}e^{-j\theta_r}$ desires to be exploited.

As in the squirrel cage, when the secondary circuit is lessned IM, $\mathbf{V}^{r}_{dqr} = \boldsymbol{V}^{s}_{dqr} = 0$ Therefore, the rotor formulas are assumed componentwise as

$$0 = r_s\mathbf{i}^{s}_{dr} + P\boldsymbol{\lambda}^{s}_{dr} + \omega_r\boldsymbol{\lambda}^{s}_{qr} \tag{2.51}$$

$$0 = r_s\mathbf{i}^{s}_{qr} + P\boldsymbol{\lambda}^{s}_{qr} + \omega_r\boldsymbol{\lambda}^{s}_{dr} \tag{2.52}$$

In the stationary frame there is an IM model:

$$\begin{bmatrix} v^{s}_{ds} \\ v^{s}_{qs} \\ 0 \\ 0 \end{bmatrix} = \begin{bmatrix} r_s + pL_s & 0 & pL_m & 0 \\ 0 & r_s + pL_s & 0 & pL_m \\ pL_m & -\omega_r L_m & r_s + pL_s & -\omega_r L_m \\ -\omega_r L_m & pL_m & -\omega_r L_m & r_s + pL_s \end{bmatrix} \begin{bmatrix} i^{s}_{ds} \\ i^{s}_{qs} \\ i^{s}_{dr} \\ i^{s}_{qr} \end{bmatrix} \tag{2.53}$$

Similarly, this model could be described in ordinary differential form

$$p\begin{bmatrix} i^s_{dqs} \\ i^s_{dqr} \end{bmatrix} = \frac{1}{\sigma L_s L_r}\begin{bmatrix} L_r I & -L_m I \\ -L_m I & L_r I \end{bmatrix}\left(\begin{bmatrix} r_s I & O \\ -\omega_r L_m J & -\omega_r L_r J \end{bmatrix}\begin{bmatrix} i^s_{dqs} \\ i^s_{dqr} \end{bmatrix} + \begin{bmatrix} V^s_{dqs} \\ 0 \end{bmatrix}\right) \tag{2.54}$$

where

$$I = \begin{bmatrix} 1 & 0 \\ 0 & 1 \end{bmatrix} \quad J = \begin{bmatrix} 0 & -1 \\ 1 & 0 \end{bmatrix} \quad \text{and} \quad O = \begin{bmatrix} 0 & 0 \\ 0 & 0 \end{bmatrix}$$

In the motionless frame, from calculating both $e^{-j\theta_e}$ with V^s_{dqs}, there is a fresh depiction V^e_{dqs} in the frame of synchronous, i.e.,

$$V^e_{dqs} = r_s i^e_{dqs} + e^{-j\theta_e}\, p\left[e^{j\theta_e} e^{-j\theta_e}\, \lambda^s_{dqs}\right] = r_s i^e_{dqs} + p\lambda^e_{dqs} + j\omega_e \lambda^e_{dqs} \tag{2.55}$$

Like what we did in the preceding alteration, the extra term, $j\omega_e\lambda^e_{dqs}$ seems in the frame of synchronous reference. It is recognized by means of the speediness voltage, and named the coupling voltage. Let $V^e_{dqs} = v^e_{ds} + jv^e_{qs}$ and $\lambda^e_{dqs} = \lambda^e_{ds} + j\lambda^e_{qs}$ therefore the following can be obtained:

$$v^e_{ds} = r_s i^e_{ds} + p\lambda^e_{ds} - \omega_e \lambda^e_{qs} \tag{2.56}$$

$$v^e_{qs} = r_s i^e_{qs} + p\lambda^e_{qs} - \omega_e \lambda^e_{ds} \tag{2.57}$$

The rotor voltage formula could be distorted similarly. However, the transforming angle is $\theta_e - \theta_r$ the formula turn out to be like

$$v^e_{dqr} = r_r i^e_{dqr} + p\lambda^e_{dqr} + j(\omega_e - \omega_r)\lambda^e_{dqr} \tag{2.58}$$

Componentwise, it can be equal to

$$0 = r_r i^e_{dr} + p\lambda^e_{dr} - j(\omega_e - \omega_r)\lambda^e_{qr} \tag{2.59}$$

$$0 = r_r i^e_{qr} + p\lambda^e_{qr} + j(\omega_e - \omega_r)\lambda^e_{dr} \tag{2.60}$$

in the synchronous frame the equivalent circuits could be shown in figure 2.11

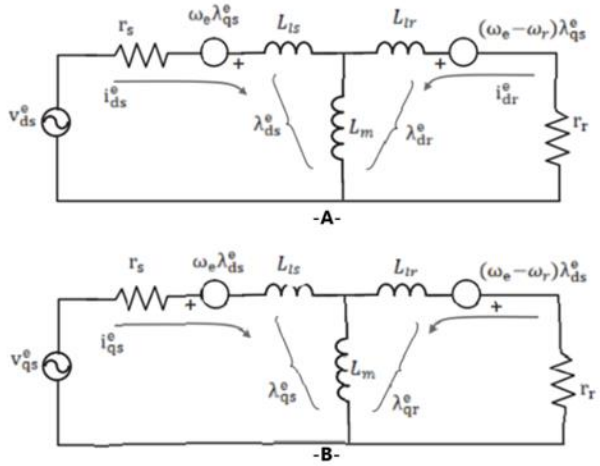

Figure 2.11. (a) d-axis also (b) q-axis are the equivalent circuits for IM in the synchronous frame.

The IM model can also be expressed using simply the current variables:

$$\begin{bmatrix} v_{ds}^e \\ v_{qs}^e \\ 0 \\ 0 \end{bmatrix} = \begin{bmatrix} r_s + pL_s & -\omega_e L_s & pL_m & -\omega_e L_m \\ \omega_e L_s & r_s + pL_s & \omega_e L_m & pL_m \\ pL_m & -\omega_{sl} L_m & r_s + pL_s & -\omega_{sl} L_r \\ -\omega_{sl} L_m & pL_m & \omega_{sl} L_r & r_s + pL_r \end{bmatrix} \begin{bmatrix} i_{ds}^e \\ i_{qs}^e \\ i_{dr}^e \\ i_{qr}^e \end{bmatrix} \tag{2.61}$$

2.7. IM Dynamic Models

With changing the state variables, numerous dynamic prototypes emerge. The below simplified concept serves as the starting point. However, as the model includes both flux and current variables, the variables are redundant:

$$V_{dqs}^e = r_s i_{dqs}^e + \frac{d\lambda_{dqs}^e}{dt} + j\omega_e \lambda_{dqs}^e \tag{2.62}$$

$$0 = r_r i_{dqr}^e + \frac{d\lambda_{dqr}^e}{dt} + j(\omega_e - \omega_r)\lambda_{dqr}^e \tag{2.63}$$

The formulas should be transformed in the form of a partial differential equation to mathematically resolve IM dynamics or build a state viewer (ODE).

2.7.1. Current Variable with ODE Model

With the existing variables, an IM model can be drived in ODE procedure in this subsection.

$$pi_{dr}^e = -\frac{1}{L_r}(L_m p i_{ds}^e - \omega_{sl} L_m i_{qs}^e + r_r i_{dr}^e - \omega_{sl} L_r i_{qr}) \tag{2.64}$$

Substituting (2.64) into the first line of (2.61), then we can get

$$\sigma L_s p i_{ds}^e = -r_s i_{ds}^e + \left(\omega_e L_s - \omega_{sl}\frac{L_m^2}{L_r}\right) i_{qs}^e + \frac{L_m}{L_r} r_r i_{dr}^e + L_m(\omega_e - \omega_{sl}) i_{qr}$$

Remember that

$$\frac{\omega_e}{\sigma} - \frac{L_m^2}{\sigma L_s L_r}\omega_{sl} = \omega_e + \omega_r \frac{L_m^2}{\sigma L_s L_r} = \omega_e + \omega_r \frac{1-\sigma}{\sigma} \tag{2.65}$$

Then

$$p i_{ds}^e = -\frac{r_s}{\sigma L_s} i_{ds}^e + \left(\omega_e + \omega_r \frac{1-\sigma}{\sigma}\right) i_{qs}^e + \frac{L_m}{\sigma L_s}\frac{r_r}{L_r} i_{dr}^e + \frac{L_m}{\sigma L_s}\omega_r i_{qr}$$

Like the old ones, terminologies for $p i_{qs}^e$, $p i_{dr}^e$, and $p i_{qr}^e$ could be consequent. Short the outcome, we canget a model of IM dynamic in the ODE procedure:

$$\frac{d}{dt}\begin{bmatrix} i_{ds}^e \\ i_{qs}^e \\ i_{dr}^e \\ i_{qr}^e \end{bmatrix} = \begin{bmatrix} -\frac{r_s}{\sigma L_s} & \omega_e + \omega_r \frac{1-\sigma}{\sigma} & \frac{L_m r_s}{\sigma L_s L_r} & \omega_r \frac{L_m}{\sigma L_s} \\ -\omega_e - \omega_r \frac{1-\sigma}{\sigma} & -\frac{r_s}{\sigma L_s} & -\omega_r \frac{L_m}{\sigma L_s} & \frac{L_m r_r}{\sigma L_s L_r} \\ \frac{L_m r_s}{\sigma L_r L_s} & -\omega_r \frac{L_m}{\sigma L_r} & -\frac{r_r}{\sigma L_r} & \omega_e - \frac{\omega_r}{\sigma} \\ \omega_r \frac{L_m}{\sigma L_r} & \frac{L_m r_s}{\sigma L_r L_s} & -\omega_e + \frac{\omega_r}{\sigma} & -\frac{r_r}{\sigma L_r} \end{bmatrix} \begin{bmatrix} i_{ds}^e \\ i_{qs}^e \\ i_{dr}^e \\ i_{qr}^e \end{bmatrix}$$

$$+ \begin{bmatrix} \frac{1}{\sigma L_s} & 0 \\ 0 & \frac{1}{\sigma L_s} \\ -\frac{L_m}{\sigma L_r L_s} & 0 \\ 0 & -\frac{L_m}{\sigma L_r L_s} \end{bmatrix} \begin{bmatrix} v_{ds}^e \\ v_{qs}^e \end{bmatrix} \tag{2.66}$$

Another expression would be

$$\frac{d}{dt}\begin{bmatrix} i_{dqs}^e \\ i_{dqr}^e \end{bmatrix} = \begin{bmatrix} -\frac{r_s}{\sigma L_s}\mathbf{I}\left(\omega_e + \omega_r \frac{1-\sigma}{\sigma}\right)\mathbf{J} & \frac{L_m}{\sigma L_s}\left(\frac{1}{\tau_r}\mathbf{I} - \omega_r \mathbf{J}\right) \\ \frac{L_m}{\sigma L_r}\left(\frac{r_s}{L_s}\mathbf{I} + \omega_r \mathbf{J}\right) & -\frac{1}{\sigma \tau_r}\mathbf{I} - \left(\omega_e - \frac{\omega_r}{\sigma}\right)\mathbf{J} \end{bmatrix}$$

$$\begin{bmatrix} i_{dqs}^e \\ i_{dqs}^e \end{bmatrix} + \begin{bmatrix} \frac{1}{\sigma L_s} I \\ -\frac{L_m}{\sigma L_r L_s} I \end{bmatrix} V_{dqs}^e \tag{2.67}$$

In which $\tau_r = L_r / r_r$ is rotor time constant.

The one ODE model shown above can be resulting further methodically: The IM dynamics (2.61) is :

$$p\begin{bmatrix} L_s\mathbf{I} & L_m\mathbf{I} \\ L_m\mathbf{I} & L_r\mathbf{I} \end{bmatrix}\begin{bmatrix} i_{dqs}^e \\ i_{dqr}^e \end{bmatrix} = \begin{bmatrix} -r_s\mathbf{I}-\omega_e\mathbf{J} & -L_m\mathbf{J} \\ -L_m\mathbf{J} & -r_r\mathbf{I}-\omega_{sl}\mathbf{J} \end{bmatrix}\begin{bmatrix} i_{dqs}^e \\ i_{dqr}^e \end{bmatrix} + \begin{bmatrix} V_{dqs}^e \\ 0 \end{bmatrix} \tag{2.68}$$

Remember that

$$\begin{bmatrix} L_s\mathbf{I} & \omega_e L_m\mathbf{I} \\ \omega_e L_m\mathbf{I} & L_r\mathbf{I} \end{bmatrix}^{-1} = \frac{1}{L_s L_r \sigma}\begin{bmatrix} L_r\mathbf{I} & -L_m\mathbf{I} \\ -L_m\mathbf{I} & L_s\mathbf{I} \end{bmatrix} \tag{2.69}$$

Both sides of (2.68), the model (2.67) should be multiplyed by (2.69)

2.7.2. Current-Flux Variables with IM ODE Model

Here, it is more preferable to use flux like the rotor variable for the field leaning regulator that follows. Also, using $[\mathbf{i}_{dqs}^{e\ T}, \boldsymbol{\lambda}_{dqr}^{e\ T}]^T$ as the stator variable is preferable too.

$$\begin{bmatrix} \boldsymbol{i}_{dqs}^e \\ \boldsymbol{i}_{dqr}^e \end{bmatrix} = \begin{bmatrix} \mathbf{I} & \mathbf{O} \\ -\frac{L_m}{L_r}\mathbf{I} & \frac{1}{L_r}\mathbf{I} \end{bmatrix}\begin{bmatrix} \boldsymbol{i}_{dqs}^e \\ \boldsymbol{\lambda}_{dqr}^e \end{bmatrix} \tag{2.70}$$

Substituting (2.70) into (2.61), this will be gotten

$$\begin{bmatrix} V_{dqs}^e \\ 0 \end{bmatrix} = \begin{bmatrix} (r_s+pL_s)\mathbf{I}+\omega_e L_s\mathbf{J} & pL_m\mathbf{I}+\omega_e L_m\mathbf{J} \\ pL_m\mathbf{I}+\omega_{sl}L_m\mathbf{J} & (r_r+pL_r)\mathbf{I}+\omega_e L_r\mathbf{J} \end{bmatrix}\begin{bmatrix} \mathbf{I} & \mathbf{O} \\ -\frac{L_m}{L_r}\mathbf{I} & \frac{1}{L_r}\mathbf{I} \end{bmatrix}\begin{bmatrix} \mathbf{i}_{dqs}^e \\ \boldsymbol{\lambda}_{dqr}^e \end{bmatrix} =$$

$$\begin{bmatrix} (r_s+p\sigma L_s)\mathbf{I}+\omega_e\sigma L_s\mathbf{J} & p\frac{L_m}{L_r}\mathbf{I}+\omega_e\frac{L_m}{L_r}\mathbf{J} \\ -\frac{r_r L_m}{L_r}\mathbf{I} & \left(\frac{r_r}{L_r}+p\right)\mathbf{I}+\omega_{sl}\mathbf{J} \end{bmatrix}\begin{bmatrix} \mathbf{i}_{dqs}^e \\ \boldsymbol{\lambda}_{dqr}^e \end{bmatrix} \tag{2.71}$$

We get the terms by collecting them using the differential operator on the left hand side.

$$\begin{bmatrix} \sigma L_s\mathbf{I} & \frac{L_m}{L_r}\mathbf{I} \\ \mathbf{O} & \mathbf{I} \end{bmatrix} p\begin{bmatrix} \mathbf{i}_{dqs}^e \\ \boldsymbol{\lambda}_{dqr}^e \end{bmatrix} = \begin{bmatrix} V_{dqs}^e \\ 0 \end{bmatrix} - \begin{bmatrix} r_s\mathbf{I}+\omega_e\sigma L_s\mathbf{J} & \omega_e\frac{L_m}{L_r}\mathbf{J} \\ -\frac{r_r L_m}{L_r}\mathbf{I} & \left(\frac{r_r}{L_r}\right)\mathbf{I}+\omega_{sl}\mathbf{J} \end{bmatrix}\begin{bmatrix} \mathbf{i}_{dqs}^e \\ \boldsymbol{\lambda}_{dqr}^e \end{bmatrix} \tag{2.72}$$

We use the underlying assumption to get the matrix inverse to the left side of equation (2.52)

$$\begin{bmatrix} A & B \\ O & C \end{bmatrix}^{-1} = \begin{bmatrix} A^{-1} & -A^{-1}BC^{-1} \\ O & C^{-1} \end{bmatrix}$$

In which , $O \in \Re^{n\times n}$ equals to a zero matrix and $A,C \in \Re^{n\times n}$ are invertible .

Now,

$$\begin{bmatrix} \sigma L_s \mathbf{I} & \frac{L_m}{L_r}\mathbf{I} \\ \mathbf{0} & \mathbf{I} \end{bmatrix}^{-1} = \begin{bmatrix} \frac{1}{\sigma L_s}\mathbf{I} & -\frac{L_m}{\sigma L_r L_s}\mathbf{I} \\ \mathbf{0} & \mathbf{I} \end{bmatrix} \tag{2.73}$$

Applying (2.73) to (2.72), this will be gotten

$$\frac{d}{dt}\begin{bmatrix} \mathbf{i}_{dqs}^{e} \\ \boldsymbol{\lambda}_{dqr}^{e} \end{bmatrix} = \begin{bmatrix} -\left(\frac{1}{\sigma\tau_s}+\frac{1-\sigma}{\sigma\tau_r}\right)\mathbf{I}-\omega_e\mathbf{J} & \frac{L_m}{\sigma L_r L_s}\left(\frac{1}{\tau_r}\mathbf{I}-\omega_r\mathbf{J}\right) \\ \frac{L_m}{\tau_r}\mathbf{I} & -\frac{1}{\tau_r}\mathbf{I}-\omega_{sl}\mathbf{J} \end{bmatrix} \begin{bmatrix} \mathbf{i}_{dqs}^{e} \\ \boldsymbol{\lambda}_{dqr}^{e} \end{bmatrix} + \frac{1}{\sigma L_s}\begin{bmatrix} V_{dqs}^{e} \\ 0 \end{bmatrix} \tag{2.74}$$

Or

$$\frac{d}{dt}\begin{bmatrix} i_{ds}^{e} \\ i_{qs}^{e} \\ \lambda_{dr}^{e} \\ \lambda_{qr}^{e} \end{bmatrix} = \begin{bmatrix} -\frac{1}{\sigma\tau_s}-\frac{(1-\sigma)}{\sigma\tau_r} & \omega_e & \frac{L_m}{\sigma\tau_r L_r L_s} & \frac{\omega_r L_m}{\sigma L_r L_s} \\ -\omega_e & -\frac{1}{\sigma\tau_s}-\frac{(1-\sigma)}{\sigma\tau_r} & -\frac{\omega_r L_m}{\sigma L_r L_s} & \frac{L_m}{\sigma\tau_r L_r L_s} \\ \frac{L_m}{\tau_r} & 0 & -\frac{1}{\tau_r} & \omega_{sl} \\ 0 & \frac{L_m}{\tau_r} & -\omega_{sl} & -\frac{1}{\tau_r} \end{bmatrix} \begin{bmatrix} i_{ds}^{e} \\ i_{qs}^{e} \\ \lambda_{dr}^{e} \\ \lambda_{qr}^{e} \end{bmatrix} + \frac{1}{\sigma L_s}\begin{bmatrix} v_{ds}^{e} \\ v_{qs}^{e} \\ 0 \\ 0 \end{bmatrix} \tag{2.75}$$

$\tau_s = L_s/r_s$ The motionless frame ODE prototypical in current-flux variables is gotten by (2.54) equation from replacing $\omega_e = 0$ Then, ω_{sl} must be replaced by $\omega_e - \omega_r = -\omega_r$ Thus, there is a motionless model that has been gotten like:

$$\frac{d}{dt}\begin{bmatrix} \mathbf{i}_{dqs}^{e} \\ \boldsymbol{\lambda}_{dqr}^{e} \end{bmatrix} = \begin{bmatrix} -\left(\frac{1}{\sigma\tau_s}+\frac{1-\sigma}{\sigma\tau_r}\right)\mathbf{I}-\omega_e\mathbf{J} & \frac{L_m}{\sigma L_r L_s}\left(\frac{1}{\tau_r}\mathbf{I}-\omega_r\mathbf{J}\right) \\ \frac{L_m}{\tau_r}\mathbf{I} & -\frac{1}{\tau_r}\mathbf{I}-\omega_{sl}\mathbf{J} \end{bmatrix} \begin{bmatrix} \mathbf{i}_{dqs}^{e} \\ \boldsymbol{\lambda}_{dqr}^{e} \end{bmatrix} + \frac{1}{\sigma L_s}\begin{bmatrix} V_{dqs}^{e} \\ 0 \end{bmatrix} \tag{2.76}$$

Associating (2.74) with (2.76), the IM dynamics could be comprehensive self-sufficiently of the frame like:

$$\frac{d}{dt}\begin{bmatrix} \mathbf{i}_{dqs}^{g} \\ \boldsymbol{\lambda}_{dqr}^{g} \end{bmatrix} = \begin{bmatrix} -\left(\frac{r_s}{\sigma L_s}+\frac{1-\sigma}{\sigma\tau_r}\right)\mathbf{I} & \frac{L_m}{\sigma L_r L_s}\frac{1}{\tau_r}\mathbf{I} \\ \frac{L_m}{\tau_r}\mathbf{I} & -\frac{1}{\tau_r}\mathbf{I} \end{bmatrix} \begin{bmatrix} \mathbf{i}_{dqs}^{g} \\ \boldsymbol{\lambda}_{dqr}^{g} \end{bmatrix} - \omega_A \begin{bmatrix} \mathbf{J} & \frac{L_m}{\sigma L_r L_s}\mathbf{J} \\ 0 & 0 \end{bmatrix} \begin{bmatrix} \mathbf{i}_{dqs}^{g} \\ \boldsymbol{\lambda}_{dqr}^{g} \end{bmatrix} +$$
$$\omega_B \begin{bmatrix} 0 & -\frac{L_m}{\sigma L_r L_s}\mathbf{J} \\ 0 & 0 \end{bmatrix} \begin{bmatrix} \mathbf{i}_{dqs}^{g} \\ \boldsymbol{\lambda}_{dqr}^{g} \end{bmatrix} + \frac{1}{\sigma L_s}\begin{bmatrix} V_{dqs}^{g} \\ 0 \end{bmatrix} \tag{2.77}$$

ω_A and ω_B could be subjective standards since they content the restraint, $\omega_A - \omega_B = \omega_r$ The formula develops the frame of synchronous IM prototypical with $\omega_A = \omega_e$ and $\omega_B = \omega_{sl}$ Also, a motionless IM model consequences with $\omega_A = 0$ and $\omega_B = -\omega_{sl}$ Beforehand, Also the dynamic formulas were resulting founded on two pole engine. overall, ω_r shall be traded by $\frac{P}{2}\omega_r$,and the slip need to be demarcated as $\omega_{sl} = \omega_e - \frac{P}{2}\omega_r$ [33]. General IM dynamic formulas are shortened in table 2.2.

Table 2.2. P-Pole IM dynamic formulas

Frame	Equations
Stationary	$\begin{bmatrix}\mathbf{V}_{dqs}^{s}\\0\end{bmatrix}=\begin{bmatrix}(r_s+L_s p)\mathbf{I} & pL_m\mathbf{I}\\ pI+\frac{P}{2}\omega_r L_m\mathbf{J} & (r_s+L_s p)\mathbf{I}+\frac{P}{2}\omega_r L_r\mathbf{J}\end{bmatrix}\begin{bmatrix}\mathbf{i}_{dqs}^{s}\\ \mathbf{i}_{dqr}^{s}\end{bmatrix}$
Synchronous	$\begin{bmatrix}\mathbf{V}_{dqs}^{s}\\0\end{bmatrix}=\begin{bmatrix}(r_s+L_s p)\mathbf{I}+\omega_e L_s\boldsymbol{J} & pL_m\mathbf{I}+\omega_e L_m\boldsymbol{J}\\ pI+\frac{P}{2}\omega_{sl} L_m\mathbf{J} & (r_s+L_s p)\mathbf{I}+\frac{P}{2}\omega_{sl} L_r\mathbf{J}\end{bmatrix}\begin{bmatrix}\mathbf{i}_{dqs}^{s}\\ \mathbf{i}_{dqr}^{s}\end{bmatrix}$
(Stationary) ODE with current variables	$\frac{d}{dt}\begin{bmatrix}\mathbf{i}_{dqs}^{s}\\ \mathbf{i}_{dqr}^{s}\end{bmatrix}=\begin{bmatrix}-\frac{r_s}{\sigma L_s}\mathbf{I}-\frac{P}{2}\omega_r\frac{1-\sigma}{\sigma}\mathbf{J} & \frac{L_m}{\sigma L_s}\left(\frac{1}{\tau_r}\mathbf{I}-\frac{P}{2}\omega_r\mathbf{J}\right)\\ \frac{L_m}{\sigma L_r}\left(\frac{r_s}{L_s}\mathbf{I}+\frac{P}{2}\omega_r\mathbf{J}\right) & -\frac{1}{\sigma}\left(\frac{1}{\tau_r}\mathbf{I}-\frac{P}{2}\omega_r\boldsymbol{J}\right)\end{bmatrix}\begin{bmatrix}\mathrm{i}_{dqs}^{s}\\ \mathrm{i}_{dqr}^{s}\end{bmatrix}$ $+\begin{bmatrix}\frac{1}{\sigma L_s}\mathbf{I}\\ -\frac{L_m}{\sigma L_r L_s}\mathbf{I}\end{bmatrix}\mathbf{V}_{dqs}^{s}$
(Synchronous) ODE with current variables	$\frac{d}{dt}\begin{bmatrix}\mathrm{i}_{dqs}^{e}\\ \mathrm{i}_{dqr}^{e}\end{bmatrix}=\begin{bmatrix}-\frac{r_s}{\sigma L_s}\mathbf{I}\left(\omega_e+\frac{P}{2}\omega_r\frac{1-\sigma}{\sigma}\right)\mathbf{J} & \frac{L_m}{\sigma L_s}\left(\frac{1}{\tau_r}\mathbf{I}-\frac{P}{2}\omega_r\mathbf{J}\right)\\ \frac{L_m}{\sigma L_r}\left(\frac{r_s}{L_s}\mathbf{I}+\frac{P}{2}\omega_r\mathbf{J}\right) & -\frac{1}{\sigma\tau_r}\mathbf{I}-\left(\omega_e-\frac{p\omega_r}{2\sigma}\right)\mathbf{J}\end{bmatrix}$ $\begin{bmatrix}\mathrm{i}_{dqs}^{e}\\ \mathrm{i}_{dqr}^{e}\end{bmatrix}+\begin{bmatrix}\frac{1}{\sigma L_s}\mathbf{I}\\ -\frac{L_m}{\sigma L_r L_s}\mathbf{I}\end{bmatrix}\mathbf{V}_{dqs}^{e}$
(Stationary) ODE with current-flux variables	$\frac{d}{dt}\begin{bmatrix}\mathbf{i}_{dqs}^{s}\\ \boldsymbol{\lambda}_{dqr}^{s}\end{bmatrix}=\begin{bmatrix}-\left(\frac{r_s}{\sigma L_s}+\frac{1-\sigma}{\sigma\tau_r}\right)\mathbf{I} & \frac{L_m}{\sigma L_r L_s}\left(\frac{1}{\tau_r}\mathbf{I}-\omega_r\mathbf{J}\right)\\ \frac{L_m}{\tau_r}\mathbf{I} & -\frac{1}{\tau_r}\mathbf{I}-\omega_r\mathbf{J}\end{bmatrix}\begin{bmatrix}\mathbf{i}_{dqs}^{s}\\ \boldsymbol{\lambda}_{dqr}^{s}\end{bmatrix}$ $+\frac{1}{\sigma L_s}\begin{bmatrix}V_{dqs}^{s}\\0\end{bmatrix}$
(Synchronous) ODE with current-flux variables	$\frac{d}{dt}\begin{bmatrix}\mathbf{i}_{dqs}^{e}\\ \boldsymbol{\lambda}_{dqr}^{e}\end{bmatrix}=\begin{bmatrix}-\left(\frac{r_s}{\sigma L_s}+\frac{1-\sigma}{\sigma\tau_r}\right)\mathbf{I}-\omega_e\mathbf{J} & \frac{L_m}{\sigma L_r L_s}\left(\frac{1}{\tau_r}\mathbf{I}-\omega_r\mathbf{J}\right)\\ \frac{L_m}{\tau_r}\mathbf{I} & -\frac{1}{\tau_r}\mathbf{I}-\omega_{sl}\mathbf{J}\end{bmatrix}\begin{bmatrix}\mathbf{i}_{dqs}^{e}\\ \boldsymbol{\lambda}_{dqr}^{e}\end{bmatrix}$ $+\frac{1}{\sigma L_s}\begin{bmatrix}V_{dqs}^{e}\\0\end{bmatrix}$

3. MATERIAL AND METHOD

In this Chapter implementing In-direct Rotor Field Oriented Control (IRFOC) , method for IM will introduce and the equipment that used in this thesis will discuss.

3.1. Material of Work

As mentioned before, the purpose of this research is to control three-phase induction motor by IFOC method. The following equipment is the equipment that used:

- Three-Phase Induction motor: 0.25 kW, 2 pole three-phase IM from ABB is used as showed in figure.3.1

Figure 3.1. 0.25 kW three-phase IM

- STM32F103C8 Microcontroller: The STM32F103xx medium-density performance line family includes the high-performance ARM® Cortex®-M3 32-bit RISC core running at 72 MHz, high-speed integrated memories (Flash memory up to 128 Kbytes and SRAM up to 20 Kbytes), and a comprehensive set of boosted I/Os and peripherals linked to two APB buses. All devices include two 12-bit ADCs, three general-purpose 16-bit timers, one PWM timer, and conventional and sophisticated communication connections such as up to two I^2Cs and SPIs, three USARTs, a USB, and a CAN. The devices are powered by a 2.0 to 3.6 V DC source. They are offered in two temperature ranges: –40 to +85 °C and –40 to +105 °C increased temperature range. A broad range of power-saving modes enables the development of low-power systems. The STM32F103xx medium-density capability line family contains devices in six distinct package variants ranging in size from 36 to 100 pins. Separate configurations of peripherals are offered dependent on the device selected; the explanation below provides an insight of the whole range of peripherals offered in this family. Because of these characteristics, the STM32F103xx medium-density performance line microcontroller family is useful for a broad range of situations of systems like application control, motor drives, medical and portable equipment , GPS systems, PC and gaming peripherals, applications in industry , inverters, PLCs, printers, alarm systems, scanners, HVACs, and video intercoms[41].Figure 3.2 showing STM32F103C8 microcontroller.

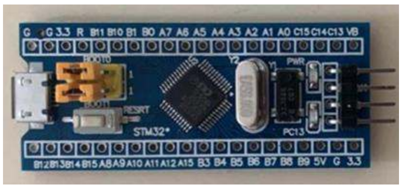

Figure 3.2. STM32F103C8 Microcontroller

- ST LINK/V2: The ST-LINK/V2 is an STM8 and STM32 microcontroller in-circuit programmer and debugger.And it is showing in fig3.3. To connect with any STM8 or STM32 microcontroller placed on an interface board, the single-wire interface module (SWIM) and JTAG/serial wire debugging (SWD) interfaces are utilized. In addition to the same capabilities as the ST-LINK/V2, the ST-LINK/V2-ISOL provides digital isolation among the PC and the specific application board. It is also capable of withstanding voltages of up to 1000 V_{rms}. STM8 applications connect with the ST Visual Develop (STVD-STM8) or ST Visual Programmer (STVP-STM8) software, as well as third-party combined production environments through the USB full-speed interface. STM32 programs connect with the STM32CubeMX software tool or third party combined development environments through the USB full-speed interface.[41]

Figure 3.3. ST LINK/V2 Mini St Programmer USB STM8 STM32

- Component for designing Inverter Board

IGBTs: An insulated-gate bipolar transistor (IGBT) is a three-terminal power semiconductor device that is characteristically seen as an electronic switch. As technology progressed, it evolved to integrate highly efficiently with quick switching. It comprises four consecutive layers (P–N–P–N) regulated by a metal–oxide–semiconductor (MOS) gate arrangement. Even though the IGBT has the same topological structure as a thermistor with a "MOS" gate (MOS-gate thermistor), the thermistor action is repressed, and that only the transistor action is allowed across the entire device's operating range variable-frequency drives (VFDs), electric automobiles, trains, variable-speed freezers, lamp ballasts, arc-welding equipment, and air conditioners all utilize it in switching power supply[34].Figure 3.4 show the symbol ig IGBT.

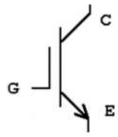

Figure 3.4. IGBT schematic symbol

The IGBTs that used in this work is n-channel, and it starts working from 7.2 Volt.

Optocoupler: An optoisolator (likewise recognized as a photocoupler, optical isolator or optocoupler) is an electronic component that takes advantage of the light to transmit electrical signals across two isolated circuits. Opto-isolators keep high voltages from damaging the signal-receiving system. Opto-isolators on the market can tolerate input-to-output voltages of up to 10 kV and voltage transients of up to 25 kV/s. An optoisolator is a device that combines an LED with a phototransistor in a single opaque box. LED-photodiode, LED-LASCR, and lamp-photoresistor pairings are some instances of source-sensor configurations. Opto-isolators are often used to transmit digital (on-off) signals, although certain techniques let its used with analog signals too.The Optocoupler used in this thesis is HCPL-3120 and it is show in figure 3.5.

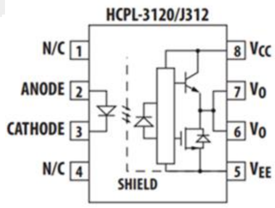

Figure 3.5. Schematic of HCPL-3120

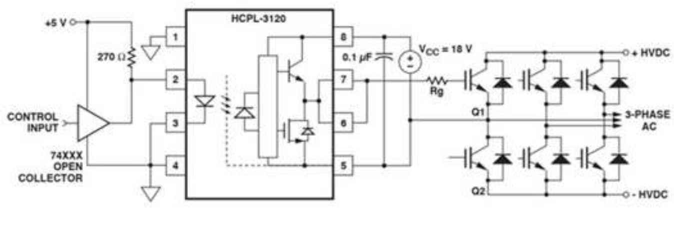

Figure 3.6. The circuit diagram of IGBTs and optocoupler

In figure 3.6 we can see the circuit diagram of IGBTs connection with optocoupler.

Buffer IC (7432): OR gates are fundamental logic gates that are featured in TTL and CMOS logic families. The 4071 is a typical 4000 series CMOS IC with four independent two-input OR gates 7400 IC showing in figure 3.7. The 7432 is the TTL device. The original 7432 OR gate has numerous offshoots, all with the same pinout but differing internal design, enabling them to function in different voltage levels and/or at faster speeds. There are 3- and 4-input OR gates available in addition to the basic 2-input OR gate. It's these CMOS series.

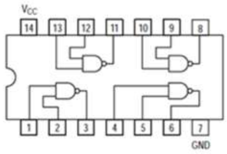

Figure 3.7. 7400 Series Digital Logic Family

Isolator DC to DC converter: A direct current (DC) to direct current (DC) converter is an electrical circuit or electromechanical device that transforms a direct current (DC) source from one voltage step to the next. It is a sort of power converter. Power levels range from extremely low (tiny batteries) to extremely high (high-voltage power transmission). The DC to DC converter utilized in the power board is the RB-0515D, which converts 5 volts to 15 volts. We can see the equivalent circuit of it in figure 3.8.

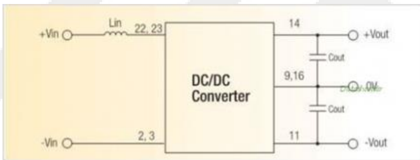

Figure 3.8. RB-0515D Isolator DC to DC converter

Resistor: The resistor that is used here (4.7 ohms for the input of IGBTs gate),(200 ohms for the input of optocoupleres)…..

Capacitor: the 0.1 uF 50 V used for filtering voltage of optocouplers.

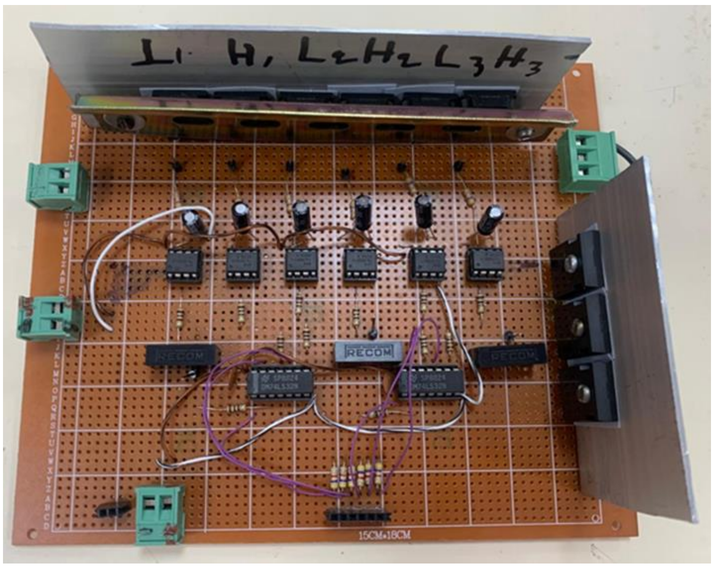

Figure 3.9. Inverter Board (Power Board)

In figure3.9 the final design of Inverter Board (Power Board) showed.

- Component for designing three phases rectifier

Three phases full-wave diode bridge rectifier: In a manner comparable to the single-phase bridge rectifier, the full-wave three-phase Six diodes are used in the uncontrolled bridge rectifier circuit. Two each phase. Two half-wave rectifier circuits are used to create a three-phase full-wave rectifier. The benefit of this circuit is that it provides less ripple output than the preceding half-wave 3-phase rectifier since its frequency is six times the input AC waveform. In addition, because there is no need for a fourth neutral (N) wire, the full-wave rectifier may be powered by a balanced three-phase three-wire delta-linked supply. Consider the following full-wave 3-phase rectifier circuit as showing if figure 3.10. SQLF 50 A 1200 V three-phase full-wave diode bridge rectifier is utilized here.[40]

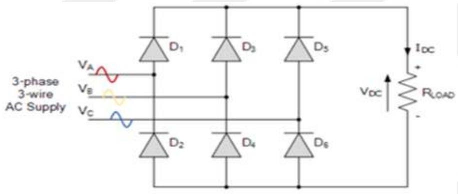

Figure 3.10. Three phase full-wave diode bridge rectifier

Capacitor: Capacitors are used in power supplies to smooth (filter) the pulsating DC output after rectification, resulting in a nearly constant DC voltage being provided to the load. The rectifiers' pulsing output has an average DC value and an AC part known as a ripple voltage. Filter capacitors lower the quantity of ripple voltage to a tolerable level. This must be noticed that resistors and inductors may be used in conjunction with capacitors to create filter networks. We will just look at sensitive filters in this section. Throughout the positive portion of the input, the capacitor in a filter circuit is loaded to the top of the rectified input voltage. When the input deteriorates, the capacitor begins to discharge into the load. The discharge rate is governed by the RC time constant generated by the capacitor and the resistance of the load. The capacitor is necessary for filling the voltage 1200 uF 400 V utilized for this purpose.Figure 3.11 show the design of Three-phase rectifier.

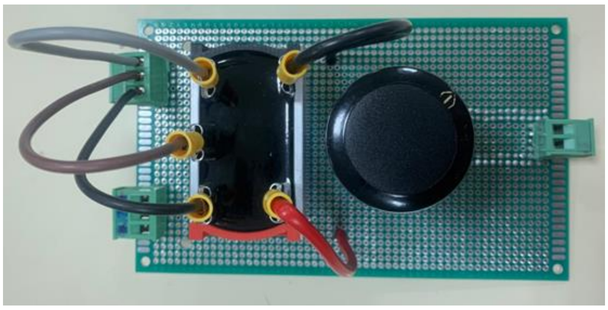

Figure 3.11. Three phase AC to DC board (Three-phase rectifier)

- Component for designing Sensors board

A current sensor is a device that monitors the electric current in a wire and outputs a signal proportional to the observed current. The produced signal might be an analog voltage or current, or it could be a digital output. The produced signal could then be utilized to show the observed current in an ammeter, saved for future analysis in a data collecting system, or employed for control. The output signal and the measured current could be:

Alternating current input consists of (analog output that mimics the wave pattern of the detected current) (bipolar output, which duplicates the wave shape of the sensed current.) in addition (The output is unipolar and proportionate to the mean or RMS value of the detected current. .) .

It includes (unipolar, having a unipolar output that mimics the waveform of the detected current) (When the measured current reaches a specific threshold, the digital output changes). ACS712 5A is the current sensor utilized in this investigation.

A shaft encoder, sometimes referred to as a rotary encoder, is an electromechanical device that transforms the exact displacement or motion of a shaft or axle to an analog or digital output signals. Rotary encoders are classified into two types: absolute and progressive. An absolute encoder's output specifies the current shaft position, rendering it an angle transducer. An incremental encoder's output gives information on the movement of the shaft, which is generally converted into information like position, speed, and distance. Rotary encoders are employed in various applications that need mechanical system monitoring, control, or both, like robotics, industrial controls, photographic lenses, optomechanical mice, and trackballs as examples of computer input devices, rotating radar platforms, and controlled stress rheometers. In this study, an incremental rotary encoder (OVW-2) was employed.

Isolator DC to DC converter: the Isolator DC to Dc converter used in the sensor board is RFM-0505S which converts 5 V to 5 V.

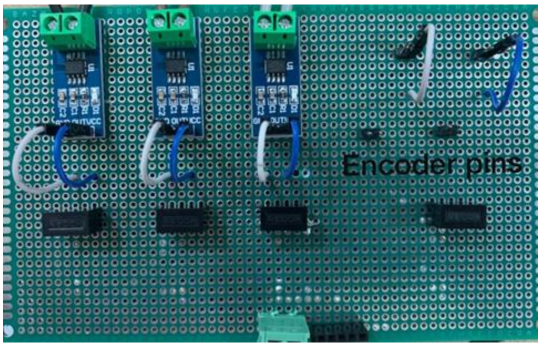

Figure 3.12. Sensor Board (Current Sensor and Encoder)

In figure 3.12 we can see design of sensors in Sensor Board.

- Three-phase voltage transformer
- Measuring and testing devices like (Oscilloscope and Voltmeter)

The details of all of the components are in Appendix

3.2. Software of Work

The modeling and simulation in chapter 4 is done by

- **MATLAB / SIMULINK**: Math Works' (an acronym for "matrix laboratory") is a private multi-paradigm programming language and mathematical computing environment. Matrix manipulation, charting of operations and data execution of algorithms, construction of user interfaces, and connecting with programs developed in other languages are all possible with MATLAB. Although MATLAB is principally designed for numerical computation, an alternative toolbox that employs the MuPAD symbolic engine provides accessibility to symbolic computing capabilities. Simulink, an add-on program, provides graphical multi-domain simulation and model-based design for dynamic and integrated systems. [36]

All of the practical work in chapter 5 is done by

- **STM32CUBEMX**: STM32CubeMX is a graphical method that enables for the very simple setup of STM32 microcontrollers and microprocessors, and also the creation of the correlating initialization C code for the Arm® Cortex®-M core or a partial Linux® Device Tree for the Arm® Cortex®-A core, via a step-by-step procedure. The first stage is to choose either an STM32 microcontroller, microprocessor, or development platform that has the appropriate set of peripherals or an instance operating on a particular development system. For microprocessors, the second phase enables you to define the GPIOs and clock settings for the entire system, as well as allocate peripherals dynamically to the Arm® Cortex®-M or Cortex®A world. DDR configuration and tuning utilities, for example, enable it simply, to begin with, STM32 microprocessors. The configuration for the Cortex®-M core comprises extra procedures that are identical to those outlined for microcontrollers. The second stage for microcontrollers and Arm® Cortex®-M microprocessors is to customize each necessary inserted software using a pinout-conflict solver, a clock-tree setting helper, a power-consumption calculator, and a convenience that configures peripherals (such as GPIO or USART) and middleware stacks (including USB or TCP/IP). Enhanced STM32Cube Expansion Packages allow for the extension of the basic software and middleware stacks. STMicroelectronics or

STMicrolectronics' partner packages may be downloaded immediately via a specialized package manager within STM32CubeMX, but the other packages must be installed from a local disc. Furthermore, STM32PackCreator, a one-of-a-kind application in STM32CubeMX delivery, will assist developers in creating their own improved STM32Cube Expansion Packages. Eventually, the user initiates the production that corresponds to the configuration options specified. This stage delivers the Arm® Cortex®-M initialization C code, suitable for use in a variety of development environments, or a partial Linux® device tree for the Arm® Cortex®-A. STM32CubeMX is included with STM32Cube [41].

- **Keil µ vision**: In a single powerful environment, the µ Vision IDE integrates project management, build tools, run-time framework, source code editing, and program debugging. µ Vision is modest to usage and accelerates embedded program development. µ Vision supports many screens and lets you construct custom window configurations everywhere on the visual surface. The µ Vision Debugger offers a unified environment for testing, verifying, and optimizing your application code. The debugger contains standard capabilities such as basic and complicated thresholds, watch windows, execution control, and a complete view of device peripherals [41].
- **ST Link Utility**: The STM32 ST-LINK Utility (STSW-LINK004) is a comprehensive software interface for programming STM32 microcontrollers. It offers a simple and fast environment for reading, writing, and validating a memory device. The tool includes various capabilities for programming STM32 internal memories (Flash, RAM, OTP, and others), external memories, verifying programming content (checksum, check during and after programming, comparing with the file), and automating STM32 programming. The STM32 ST-LINK Utility comes with a graphical user interface (GUI) and a command-line interface (CLI) [41].
- **STM Studio**: STMicroelectronics STM Studio debugs and analyzes STM32 programs in real-time by accessing and showing their variables. STM Studio, which runs on a PC, communicates with STM32 MCUs using the standard ST-LINK development tools. STM Studio is a non-intrusive tool that preserves applications' real-time functionality. STM Studio is an excellent supplement to standard debugging tools for fine-tuning programs. It is ideally adapted for debugging non-stop applications, including motor control applications. There are several visual views accessible to meet the demands of debugging and diagnostics, as well as to show application behavior [41].

The design of the Inverter, three-phase rectifier, and sensor board and are done by

- Proteus: Proteus Design Package is a patented software tool suite mostly utilized in electrical design automation. Electronic design professionals and technicians primarily use the application to create diagrams and electronic prints to produce printed circuit boards [40].

3.3. Basic of Field Oriented Control

Hasse and Blaschke established the concept of field orientation in 1969 and 1972, respectively, which is widely regarded as the most significant model in theory and practice of induction motor (IM) control. The aim of field orientation is for the IM to function as an independently stimulated dc machine as a variable torque generator. As a result, we'll start with the rudiments of torque creation and control in a dc motor. A dc motor is seen schematically in Figure 3.13 [34,28].

The magnetic poles N and S denote the stator's magnetic field, the machine's field component. As a result, when the field winding is static and parallel to the d axis of the stator, the space vector λ_f flux (flux linkage) is generated. The armature current arrangement in the rotor winding appears to be, which the space vector, i_a This current is often linked with the q axis, while the rotor is spinning, owing to the commutator's operation and strategically placed brushes. Auxiliary windings are used in practical dc motors to counteract the so-called armature response, reducing the main magnetic field caused by the armature current's MMF. The generated torque, T_M, is thus equivalent to the vector invention of i_a and λ_f, or the sine of the angle among these vectors. As illustrated in Figure 3.13 [34,37].

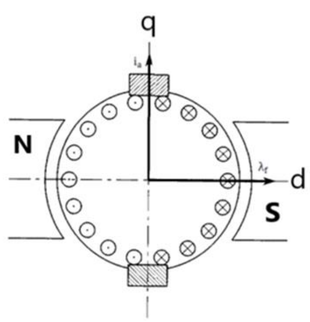

Figure 3.13. DC Motor diagram

This is frequently a perpendicular, which guarantees the greatest torque-per-ampere ratio. As a result, the torque is generated within ideal circumstances, with the armature current being as low as feasible, resulting in defects in the motor and supplying chain are kept to a minimum. In the dc machine that is stimulated independently, the field current, i_f, creating λ_f and the armature current, i_a, flow occurs in different windings. As a result, they may be managed separately. Typically, especially under high-load situations, the flux is remained constant at the specified level inside the speed scope from zero to the desired voltage[35].At speeds greater than rated, field weakening, or flux decrease inversely proportional to speed, is utilized. Motor performance might be improved at low loads by decreasing the flux to a trade-off value where the reduction in core wastes offsets the rise in copper wastage. Such performance optimization techniques can result in considerable energy savings in drives often running at or near full load. The arguments presented illustrate why independently excited dc motors were the preferred actuator in motion control systems for several decades. Whenever the flux and current vectors are orthogonal, the dc motor not only creates torque, but it also enables totally independent ("decoupled") magnetic field and torque control The torque equation that is employed as a basis for the field-oriented IM is as follows [36,39].

Vector control is performed in an IM by autonomously managing the torque and field elements of the stator current by a synchronized adjustment in the frequency, power supply amplitude, and phase. An IM with vector control has the same efficiency as a dc machine. According to the field orientations control idea, the machine's current components must be divided into flux and torque parts. The current flux is aligned with the rotor flux vector in quadrature, and the torque constituent is aligned with it as well. The IM's vector control model is examined in a continuously rotating d-q reference frame; In a steady state, sinusoidal values operate as dc quantities [37]. The torque of the IM T_e the corresponding space phasor amounts may be acquired :

$$T_e = K_T \lambda_r i_{qs} \tag{3.1}$$

The stator current phasor in an IM i_s generates the rotor flux λ_r and the torque. The flux is generated by a component of stator current that is in sync with the rotor flux λ_r or i_{ds}. The field current of a dc machine is comparable to the stator current. The current i_{qs} is in charge of torque production. Only dc machine-like performances is feasible if i_{ds} is in charge of producing total flux and is oriented in the path of the flux vector. The vector control method can be implemented in various ways depending on the reference frames for the space vectors used. There have been three different flux space phases in an IM: rotor flux, stator flux, and air gap flux.. The rotor flux spins at slip speed relative to the rotor, while the air gap flux circles at synchronized speeds . By linking the reference system's d-axis to the relevant flux space phase orientation, Vector control might be applied to all these flux space phases. The reference frame linked to the space vector expressing the overall flux linkage λ_r. of The rotor is the most simple and common datum for vector control of an IM. Because the basis set is the field frame, this technique to speed control is another name for "field-oriented control" Figure 3.14 depicts a basic system [27].

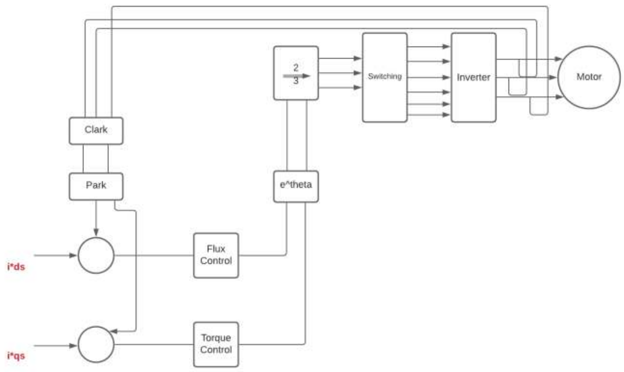

Figure 3.14. Field oriented control scheme

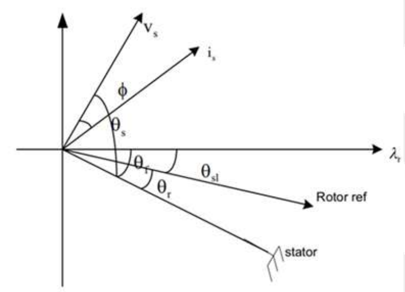

Figure 3.15. Vector diagram of field oriented control

A vector controller and two commanding current input are exposed on the inverter i_{ds}^{*} and i_{qs}^{*}. In a simultaneously rotating reference frame, these currents represent stator current's d axis and q axis mechanisms. The three stator currents i_{as}, i_{bs} and i_{cs} These are changed into d-q constituents in the stator reference frame. The vector rotator block then converts them into field reference frames. The field reference frame is considered to be at an angle, θ_f with regard to the stationary (stator) reference frame. Fig. 3.15 shows a formalized paraphrase. As the rotor flow connection space vector alters, so will this angle λ_r spins and is alluded to as the field angle. If, θ_r denotes the angle among the stator current space vector and the given angular frame fig. 3.3 and, θ_{sl} denotes the slip angle among therefore the rotor axis and the rotor field frame [39].

$$\theta_f = \theta_r + \theta_{sl} \tag{3.2}$$

In terms of speeds

$$\theta_f = \int (\omega_r + \omega_{sl}) dt = \int \omega_s dt \tag{3.3}$$

The converted currents are then matched to the commanding current inputs. i^*_{ds} and i^*_{qs} The acquired error indicators are magnified and utilised to regulate the flux and torque. Inverse transformation is used to transfer these currents from field frames to stator. When the d-q elements of current in the stator frame are determined, the 2/3 transformation may be used to convert them to a-b-c components. These currents are checked to the real motor currents and utilized to regulate the inverter shifting. The inverter is a 3-phase inverter with current regulation. The switching control modifies the current values so that they are consistent with the reference values. The decoupled management of these currents yields a significant degree of reactivity in the face of change, comparable to that of a dc motor. Although the current, I^s_{sd} can be oriented with the air gap flux axis stator flux axis, or rotor flux axis, for vector control. On the other hand, the rotor flux direction provides natural decoupled control, but the stator flux of the direction of the air gap flux causes coupling and needs correction for decoupling.

Vector control is classified as either direct or feedback control or indirect or feed-forward control. In the basic comparison, the flux linkage signal is gathered straight, either by deploying specially built sensors to feel the fields on the machine or through explicitly deriving the flux linkage space vector using the flux model. The indirect approach calculates the comparative speed of the flux link space vector with regard to the rotor and concatenates it to get the field's angle of part assigned to the rotor. To get, multiply this angle by the angle calculated of displacement caused by the rotor. θ_r Because the position of the flux linkage space vector is calculated implicitly, this technique is characterized as indirect vector control or feed forward control [39].

3.4. Rotor Field Oriented Scheme

The rotor field-oriented (RFO) approach is preferred since the algorithm produces a natural breakdown of the d and q axis current responsibilities. The rotor flux is coordinated with the reference frame's d-axis, as the name implies. As a result of this, in $\lambda^e_{qr} = 0$ automatically. By regulating, the axis alignment effort is achieved λ^e_{qr} in the reference frame, a PI controller sets the value to zero. It should be emphasised that the rotor flux circulates at synchronized instead of shaft (mechanical) speed $\frac{p}{2}\omega_r$ [33].

$$v^e_{ds} = (r_s + pL_s\sigma)i^e_{ds} + \frac{L_m}{L_r}p\lambda^e_{dr} - \omega_e\left(L_s\sigma i^e_{qs} + \frac{L_m}{L_r}\lambda^e_{qr}\right) \tag{3.4}$$

$$v^e_{qs} = (r_s + pL_s\sigma)i^e_{qs} + \frac{L_m}{L_r}p\lambda^e_{qr} - \omega_e\left(L_s\sigma i^e_{ds} + \frac{L_m}{L_r}\lambda^e_{dr}\right) \tag{3.5}$$

Stator equation

By letting λ_{qr}^{e}=0 , we gain from (3.4) and (3.5)

$$v_{ds}^{e} = (r_s + pL_s\sigma)i_{ds}^{e} - \omega_e L_s \sigma i_{qs}^{e} + p\frac{L_m}{L_r}\lambda_{dr}^{e} \tag{3.6}$$

$$v_{qs}^{e} = (r_s + pL_s\sigma)i_{qs}^{e} + \omega_e L_s \sigma i_{ds}^{e} + \omega_e\frac{L_m}{L_r}\lambda_{dr}^{e} \tag{3.7}$$

Note that $-\omega_e L_s \sigma i_{qs}^{e}$ and $\omega_e L_s \sigma i_{ds}^{e}$ are the words that connect the d and q axes, and that $\omega_e \frac{L_m}{L_r}\lambda_{dr}^{e}$ is the back Emf.

Rotor equation

$$0 = r_r i_{dr}^{e} + p\lambda_{dr}^{e} = (r_r + L_r p)i_{dr}^{e} + pL_m i_{ds}^{e} \tag{3.8}$$

$$0 = r_r i_{qr}^{e} + (\omega_e - \omega_r)\lambda_{dr}^{e} \tag{3.9}$$

Therefore, we have from (3.8) that

$$i_{dr}^{e} = -\frac{L_m p i_{ds}^{e}}{r_r + pL_r} \tag{3.10}$$

Utilising (3.10), the d-axis rotor flux is discovered to be

$$\lambda_{dr}^{e} = L_m i_{ds}^{e} + L_r i_{dr}^{e} = L_m i_{ds}^{e} - \frac{L_r L_m p i_{ds}^{e}}{r_r + pL_r} = \frac{L_m}{1 + p\tau_r} i_{ds}^{e} \tag{3.11}$$

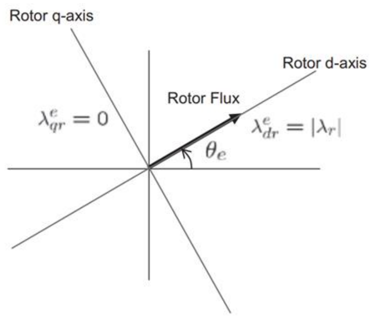

Figure 3.16. Orianting the d-axis frame in relation to the rotor flux

In figure. 3.16 we can see the Orianting the d-axis frame in relation to the flux of rotor.

Where $\tau_r = \frac{L_r}{r_r}$ is the rotor's timing constant . In a stable state, (3.11) reduces to

$$\lambda_{dr}^{e} = L_m i_{ds}^{e} \tag{3.12}$$

Since $\lambda_{qr}^{e} = 0$ it emerges from the rotor field orientated design that

$$0 = L_m i_{qs}^e + L_r i_{qr}^e \tag{3.13}$$

The slip equation then results from (3.9) and (3.13):

$$\omega_{sl} \equiv \omega_e - \frac{p}{2}\omega_r = s\omega_e = -r_r \frac{i_{qr}^e}{\lambda_{dr}} = \frac{1}{\tau_r}\frac{L_m}{\lambda_{dr}} i_{qs}^e \tag{3.14}$$

The slip is often written as $\omega_{sl} = \frac{1}{\tau_r}\frac{i_{qs}^e}{i_{ds}^e}$ in the steady-state.

Comparing $\lambda_{dr}^e = L_m i_{ds}^e$ with $\lambda_{dr}^e = L_m i_{ds}^e + L_r i_{dr}^e$, it has been discovered that $i_{dr}^e = 0$. with $\lambda_{qr}^e = 0$, the torque equation will be

$$T = \frac{3p}{4}\frac{L_m}{L_r}\lambda_{dr}^e i_{qs}^e \tag{3.15}$$

This equation is analogous to the torque equation of a direct current motor. The following are some commonalities between the DC motors:

λ_{dr}^e : relates to the field.

i_{ds}^e : relates to the current in the field

i_{qs}^e : relates to the armature current

The functions of the d and q axis stator currents are now clear:

The rotor has no d-axis current passing through it. Only the stator current moves in the d-direction, therefore it is essential for the gap field to be created. In other terms, the d-axis current of the stator, i_{ds}^e is only utilized to produce λ_{dr}^e .

The q-axis stator current, on the other hand , i_{qs}^e flows are used to create torque. Nevertheless, no flux is created along the q-axis, despite a massive q-axis stator current. i_{qs}^e moves. It is due to the fact that the rotor current is almost the equivalent i_{qs}^e moves in the inverse direction , i.e., $i_{qr}^e = -\frac{L_m}{L_r} i_{qs}^e$ as a consequence, there is a possibility of λ_{qr}^e is repressed. It might indeed be seen as a counter-reaction to the armature response caused by the distortions of the gap field caused by the armature current [33].

The following summarises the responsibilities of currents:

1. i_{ds}^e is only utilised to produce rotor flux (3.11) it functions similarly to the field current of a DC motor.
2. $i_{dr}^e = 0$ in a stable condition only the q-axis current, i_{qr}^e, moves in the rotor to exclude the possibility of a q-axis rotor field production induced by i_{qs}^e.
3. i_{qs}^e is employed in order to create torque (3.14). The q-axis current represents the armature current of an AC motor.

In the steady-state, $p\lambda_{dr} = 0$ and $pi^e_{ds} = pi^e_{qs} = 0$. (3.6) and (3.7) are rearranged using complex variables as [33].

$$V^e_{dqs} = r_s i^e_{dqs} + j\omega_e \sigma L_s i^e_{dqs} + j\omega_e \frac{L_m}{L_r} \lambda^e_{dr} \tag{3.16}$$

(3.12), as illustrated in Figure 3.17, may be used to create a vector diagram for the rotor field orientated control. It is worth noting that the voltage vector is slightly ahead of the current vector by $\emptyset$.

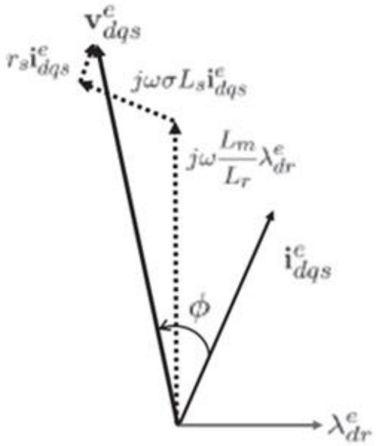

Figure 3.17. Diagram of the voltage vectors for the rotor field-oriented control.

3.5. Stator Field Oriented Scheme

The stator field-oriented (SFO) framework is the control mechanism for linking the d-axis with the stator flux. It provides more torque and is less responsive to machine settings than the rotor field oriented system [44]. The torque-flux decoupling, on the contrary, is more challenging. The q-axis stator flux is zero in the stator field-oriented scheme, i.e., $\lambda^e_{qs} = 0$. Consequently, it derives from (2.40),(2.41),(2.59) and (2.60) that [33].

$$\lambda^e_{dr} = \frac{L_r}{L_m}(\lambda^e_{ds} - \sigma L_s i^e_{ds}) \tag{3.17}$$

$$\lambda^e_{qr} = -\frac{L_r}{L_m}(\sigma L_s i^e_{ds}) \tag{3.18}$$

$$i^e_{dr} = \frac{1}{L_m}\lambda^e_{ds} - \frac{L_s}{L_m} i^e_{ds} \tag{3.19}$$

$$i^e_{qr} = -\frac{L_s}{L_m} i^e_{qs} \tag{3.20}$$

Substituting (3.4)-(3.7) into (2.59) and (2.60) yields the stator flow and slip equations: The rotor d-axis equation yields

$$0 = r_r i_{dr}^e + p\lambda_{dr}^e - \omega_{sl}\lambda_{qr}^e$$

$$= \frac{r_r}{L_m}(\lambda_{ds}^e - L_s i_{ds}^e) + p\frac{L_r}{L_m}(\lambda_{ds}^e - \sigma L_s i_{ds}^e) + \frac{L_r}{L_m}\omega_{sl}\sigma L_s i_{qs}^e$$

$$= \frac{1}{\tau_r}(\lambda_{ds}^e - L_s i_{ds}^e) + p(\lambda_{ds}^e - \sigma L_s i_{ds}^e) + \omega_{sl}\sigma L_s i_{qs}^e$$

$$= \left(\frac{1}{\tau_r} + p\right)\lambda_{ds}^e - L_s\left(\frac{1}{\tau_r} + p\sigma\right)i_{ds}^e + \omega_{sl}\sigma L_s i_{qs}^e$$

We obtain

$$\lambda_{ds}^e = \frac{\left(\sigma p + \frac{1}{\tau_r}\right)L_s}{p + \frac{1}{\tau_r}} i_{ds}^e - \frac{\sigma L_s i_{qs}^e}{p + \frac{1}{\tau_r}}\omega_{sl} \tag{3.21}$$

From the rotor q-axis equation,

$$0 = r_r i_{qr}^e + p\lambda_{qr}^e - \omega_{sl}\lambda_{dr}^e$$

$$= -\frac{r_r L_s}{L_m} i_{qs}^e - p\frac{L_r}{L_m}\sigma L_s i_{qs}^e + \frac{L_r}{L_m}\omega_{sl}(\lambda_{ds}^e - \sigma L_s i_{ds}^e)$$

$$= -L_s i_{qs}^e - p\tau_r\sigma L_s i_{qs}^e + \tau_r\omega_{sl}(\lambda_{ds}^e - \sigma L_s i_{ds}^e)$$

We obtain

$$\omega_{sl} = \frac{\left(\frac{1}{\tau_r} + p\sigma\right)L_s i_{qs}^e}{\lambda_{ds}^e - \sigma L_s i_{ds}^e} = \frac{\left(p + \frac{1}{\sigma\tau_r}\right)i_{qs}^e}{\frac{\lambda_{ds}^e}{\sigma L_s} - i_{ds}^e} \tag{3.29}$$

It should be observed that in the stator field oriented system, the flux and slip formula are not separated. Explicitly, ω_{sl} is included in the flow scheming (3.8). In turn, λ_{ds}^e is used to calculate slip, (3.9). Furthermore, the differential operator, p, is present in the slip equation (3.9). As a result, it necessitates the distinction of, i_{qs}^e, which is unfavourable when compared to (3.14). As a result, the rotor field orientated technique is widely employed in real settings. The torque equation for the stator reference frame is[38]

$$T_e = \frac{3}{2}\frac{p}{2}\lambda_{ds}^e i_{qs}^e \tag{3.30}$$

3.6. Direct FOC Method

We've seen that the direct vector control approach identifies direct flux monitoring or terminal condition calculations to determine the size and location of the rotor flux vector. It is also known as flux feedback control because it obtains the needed information about the rotor flux by direct flux measurements or estimate. Sensors such as the Hall Effect sensor and the search coil detect the flux. Because repairing a large number of sensors is a time-consuming task, the cost factor rises. The values produced by flux sensors are employed in the drive control structure's outer loop. Alternately, flux models could be utilized to replace flux sensors, with stator currents and voltages serving as feedback signals and the rotor flux angle providing an anticipated output. A modified block design of a field control method is shown in Fig. 3.14. the currents on the two axes, i_{qs}^* and i_{ds}^*. The outer control loops manage the required torque and flux elements of stator current, accordingly. Currents, i_{qs}^* and i_{ds}^* to produce stator reference currents, perform a system dynamics to two-phase stator-based values based on a two to 3-phase transformation. i_{as}^* , i_{bs}^* , i_{cs}^* the current-controlled PWM inverter reproduces these reference currents in the stator phases.

As a result, the external reference currents i_{qs}^* and i_{ds}^* are replicated by the IM. These straight and quadrature axis current sources are used to control the system and enable control of flux and torque that is separated, as in a dc machine.

Disadvantages

1. Fixing a large number of sensors is a time-consuming task.
2. The sensors raise the machine's expense.
3. Temperature causes the drift problem.
4. At lower temperatures, flux sensing is weak.

Because of these drawbacks, another approach known as indirect vector control (IFOC) is used [34].

3.7. Indirect FOC Method

The fundamental system architecture of an IM using the indirect vector control approach, Figure 3.18. depicts this. In the controller, the motor speed is employed as a feedback signal. In the SRRF, the controller generates reference values for the two dissociated constituents of the stator current space vector. Which are, i_{qs}^* and i_{ds}^*. for torque and flux control, correspondingly. The two current components are transformed into 3-phase currents in the stationary reference frame of reference. i_{as}^* , i_{bs}^* , i_{cs}^*. Two of the phase currents are experienced as a consequence of the balancing load and the third is calculated from the two perceived currents. The current controller in the stationary reference frame controls the reference currents near the detected 3-phase currents and runs the voltage source inverter to power the 3-phase IM [39]. This ensures that the vector controlled IM operates admirably (VCIMD). VCIMDs are rapidly being utilized in a wide range of drive applications due to their smooth, efficient, and maintenance-free operation, including electric automobiles, air conditioning, refrigeration, wastewater treatment facilities, blowers, fans, pumps, elevators, traction motors, lifts, and so on. the field-weakening controller takes the speed signal, ω_r as an input signal and returns the excitation current's reference amount, i^*_{mrd}. As a result, the two signals serve as the vector controller's reference signals. The d-axis element in the vector controller i^*_{ds} and the q- axis component i^*_{qs} The stator current signals that are essential for flux and torque control are calculated. The slip frequency signal ω^*_2 in vector controller, it also calculated to assess the flow angle. Slip frequency is used to calculate the slip angle ω^*_2. rotor speed ω_r and sampling period ΔT. The vector controller evaluates the slip frequency signal in addition to the flux angle, ω^*_2. The slip frequency is used to calculate the slip angle . ω^*_2, the rotor speed, ω_r, as well as the sample interval ΔT. These signals of flux i^*_{ds} and torque i^*_{qs} are in a continuously revolving reference frame and are converted into stationary reference 3-phase currents (i^*_{as} , i^*_{bs} , i^*_{cs}). The reference currents for a current-controlled VSI-fed vector-controlled IM i^*_{as} , i^*_{bs} , i^*_{cs} and sensed currents i_{as} , i_{bs} , i_{cs} are routed by the pulse width modulated (PWM) current controller At the appropriate switching frequency (fs), a triangle carrier wave is created. The point of phase transition for the resultant PWM signals is the convergence of the triangular carrier wave and altered signals, which is sent into the VSI driver circuit, which drives an IM. The graphic shows the indirect vector controlled IM once more [14].

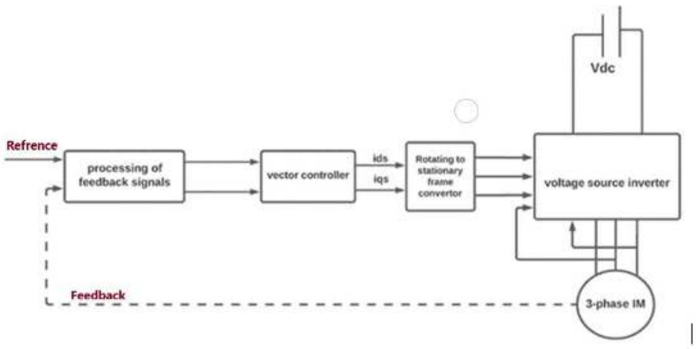

Figure 3.18. The fundamental block diagram of the indirect vector control mode

3.8. Control of a Three-phase IM Using an Indirect Rotor Field-Oriented Control

In this thesis,indirect rotor field oriented control (IRFO) method will use for controlling 3-phase IM. The IRFOC system is designed based on a speed-controlled IM drive operating at speeds in the region below base speed (i.e. the constant flux region). Two inputs are fed to the IRFOC system: The reference speed, the reference toque command, and the rotor reference flux. In its most basic form, an IRFOC system for an IM permits decoupling of the torque and flux controls and assures optimal torque output in the motor. A generic block diagram of an IRFOC system for an IM is shown in Figure 3.19. And in figure 3.20 we can see the diagram of Indirect rotor field oriented Controller.

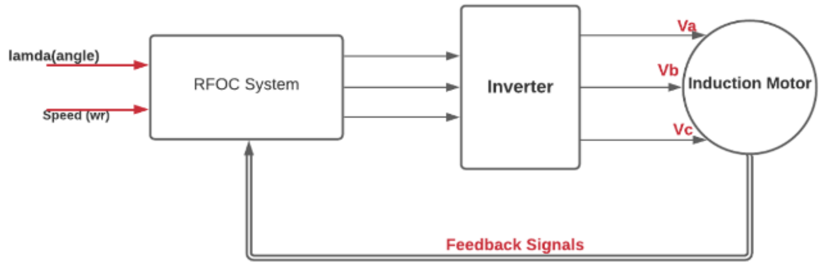

Figure 3.19. General block diagram for IRFOC

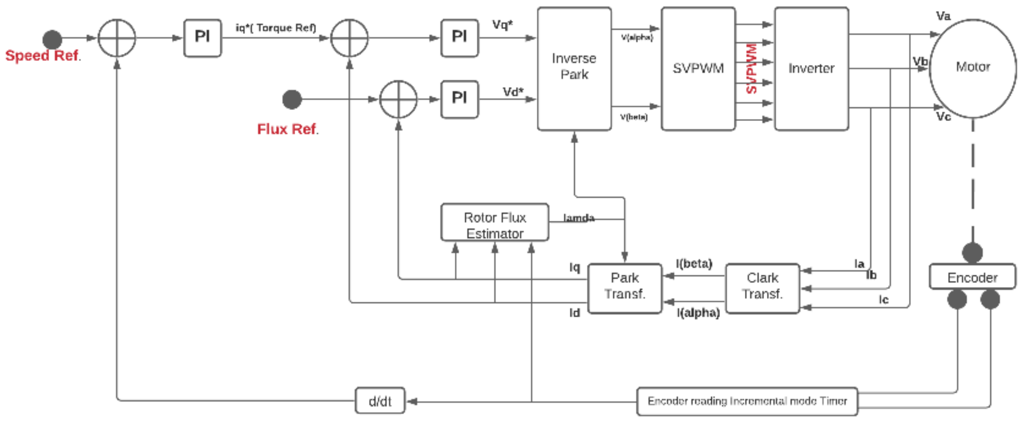

Figure 3.20. Indirect rotor field oriented Controller

The necessary stages for IRFOC are listed below. :

Step1: The 3-phase stator currents i_a, i_b and i_c are monitored, as well as the rotor velocity ω_r. The measurements are described in detail in Chapter 5.

Step2: The Clark transform is used to transform 3-phase currents to a two-axis system. The parameters i_α and i_β calculated from the observed i_a, i_b and i_c values. As illustrated in figure 3.21 i_α and i_β are time changing quadrature current values as seen from the stator's viewpoint[46].

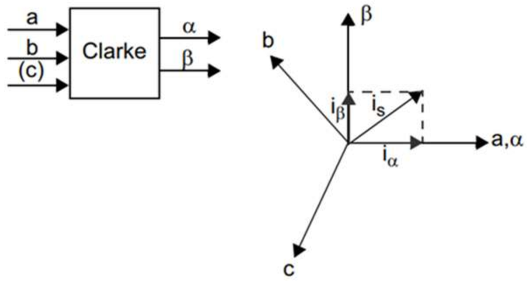

Figure 3.21. Clark transformation vector diagram

The following equation is for Clark transformation

$$i_a + i_b + i_c = 0 \tag{3.31}$$

$$i_\alpha = i_a \tag{3.32}$$

$$i_\beta = \frac{i_a + 2i_b}{\sqrt{3}} \tag{3.33}$$

Step3: The aforementioned 2-axis platform of coordinates is subsequently switched to correspond with the rotor flow employing angle of conversion data generated during the controlling loop's last iteration. This transformation yields the i_d and i_q (I_{sd} and I_{sq}), and the procedure is known as the Park convert variables from i_α and i_β. The quadrature currents are I_{sd} and I_{sq} in the rotating coordinate system. i_d and i_q could be consistent under steady-state circumstances. As seen in figure 3.22 [46].

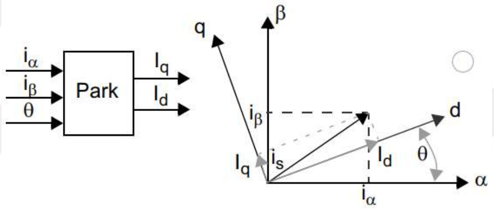

Figure 3.22. Park transformation vector diagram

$$i_d = i_\alpha \cos\theta + i_\beta \sin\theta \tag{3.34}$$

$$i_q = -i_\alpha \cos\theta + i_\beta \sin\theta \tag{3.35}$$

Step4 : Error signals are created by combining i_d and i_q, and their respective reference values. The i_d reference is utilized to adjust the magnetizing flux of the rotor. The i_q reference is utilized to regulate the motor's rotor production. The error signals are the PI controller's inputs. The controller's output gives V_{sd} and V_{sq}, and those are the voltage vectors that would be delivered to the engine , as seen in figure 3.20 [46].

Step5: Design of PI Controller for current, flux and speed loop. The detail is in the next section.

Step6 : A new angle of coordinate transformation is computed. The inputs to this transformation are the motor speed, the rotor electrical time constant and i_d and i_q.

Step7. Utilizing the new angle, the V_{sd} and V_{sq} output values of the PI controller are converted to the stationary reference frame. This computation yields quadrature voltages. V_α and

V_β the process is called the inv-park transform as shown in figure 3.23. Applying the new angle, the PI controller's V_{sd} and V_{sq} output values are returned to the stationary reference frame. This computation yields the quadrature voltage values V_α and V_β.

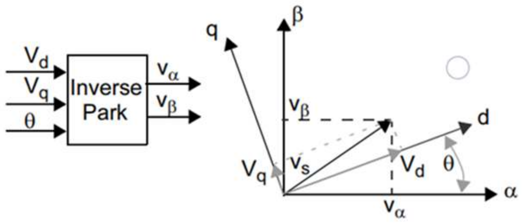

Figure 3.23. Inv-Park transformation vector diagram

$$v_\alpha = v_d \cos\theta - v_q \sin\theta \tag{3.36}$$

$$v_\beta = v_d \sin\theta + v_q \cos\theta \tag{3.37}$$

Step8. The V_α and V_β values are converted back to the 3-phase voltage the process is called the inv-Clark transform as shown in figure 3.24 values, which are then utilized to produce the necessary voltage vector by calculating fresh SVPWM duty cycle values.

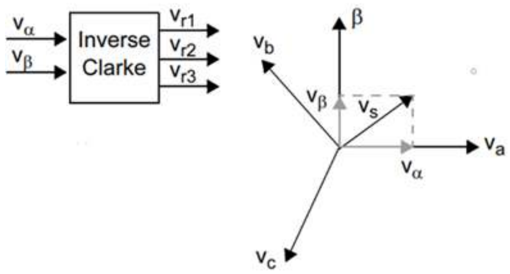

Figure 3.24. Inv-clark transformation vector diagram

$$v_a = v_\beta \tag{3.38}$$

$$v_b = \frac{v_\beta + \sqrt{3}\, v_\alpha}{2} \tag{3.39}$$

$$v_c = \frac{v_\beta - \sqrt{3}\, v_\alpha}{2} \tag{3.40}$$

3.9. Controller Design

Depending on the induction machine parameters and provided requirements, a PI controller would be generated for each loop in this section.

3.9.1. PI Controller for Current Loop

Based on the parameters provided in Table 3.1, a PI controller for the current loop will be built.

Table 3.1. Specifications of Current loop

Specification	Value
Natural frequency(ω_n)	200 Hz , 1256.63 rad/s
Damping factor (ε)	0.7
Stator time constant (τ_s)	0.00645 s
Stator Resistor (R_S)	27.62 Ω
Rated (i_{sd}^*)	0.4993 A
Rated (i_{sq}^*)	0.4762 A

From the parameter of the table, the transfer function (TF) of the system(IM) and PI controller is calculated.

The TF of IM in the current loop is

$$G_p(s) = \frac{5.6}{s+155} \tag{3.41}$$

The PI controller's TF in a current loop

$$G_c(s) = \frac{286.47s+281983.87}{s} \tag{3.42}$$

The calculation is in appendix.

3.9.2. PI Controller for Flux Loop

The requirements provided in Table 3.2 will be used to construct a flux loop PI controller. Specifications of flux loop.

Table 3.2. Will be used to construct a flux loop

Specification	Value
Natural frequency(ω_n)	13.3 Hz , 83.56 rad/s
Damping factor (ε)	0.7
Rotor time constant (τ_r)	0.0536 s
Rated (i_{mrd})	0.4993 A

The TF of IM in the flux loop is

$$G_p(s) = \frac{18.65}{s+18.65} \tag{3.43}$$

The TF of PI controller in flux loop

$$G_c(s) = \frac{5.27s+374.38}{s} \tag{3.44}$$

The calculation is in appendix.

3.9.3. PI controller for Speed Loop

The requirements provided in table 3.3 will be used to construct a speed loop PI controller. Specifications of speed loop

Table 3.3. will be used to construct a speed loop

Specification	Value
Natural frequency(ω_n)	6.3 Hz , 39.58 rad/s
Damping factor (ε)	0.7
Number of pole	2
Stator resistor (R_s)	27.62 Ω
Rated (i_{sd})	0.4993 A
MOI	0.00016 kg.m^2
Rotor inductance (L_r)	1.4866 H
Magnetizing inductance (L_o)	1.402 H

The TF of IM in the speed loop is

$$G_p(s) = \frac{12356.25}{s} \tag{3.45}$$

The TF of PI controller in the speed loop

$$G_c(s) = \frac{0.00448s+0.1267}{s} \tag{3.46}$$

The calculation is in appendix.

3.10. PWM Techniques

Utilizing inversion, alternating current (AC) power may be produced from direct current (DC) power at the required output current or voltage and frequency. Inverter circuits frequently utilize the words voltage-fed and current-fed. The DC input voltage of a voltage source inverter (VSI) is typically constant and is not affected by the load current pulled from it. The inverter determines the load voltage, and the load determines the current waveform. The inverter accepts direct current (DC) input energy from the power supply chain (or) a spinning alternator connected to a converter (or) a battery, fuel cell, solar array, or Magneto Hydro Dynamic (MHD) generator. Voltage source inverters (VSI) and current source inverters (CSI) are the two forms of inverters . The DC voltage source in a voltage source inverter has a low or negligible impedance, indicating as it has a stiff DC voltage source at its terminals. Even when the load is changed, the low internal impedance maintains an almost constant voltage. As a result, it is appropriate for both single and multi-motor drives. Because of its low internal impedance, a short circuit at its terminal allows the current to increase quickly. Because current control does not regulate the fault current, it must be cleared by fast-acting fused connections. Usually, machines do not run smoothly due to a high THD percentage, which produces noise, vibration, and warmth. A substantial amount of study has previously been conducted in this field, with several proposed machine speed control approaches[40].

Inverters function effectively; however, their output waveforms contain harmonics. In high power applications, PWM methods can be utilized to reduce these harmonics. As a result, employing these modulating approaches aims to obtain a better and more regulated output from the inverters, devoid of harmonics and waveform distortion. PWM refers to single pulse width modulation techniques (when only one pulse in a half-cycle is altered), multiple pulse width modulation (where many pulses are amplified in one-half cycle), SPWM, SVPWM, and hysteresis (Delta) PWM[41] based on their modulation output and strategy as showing in figure 3.25.

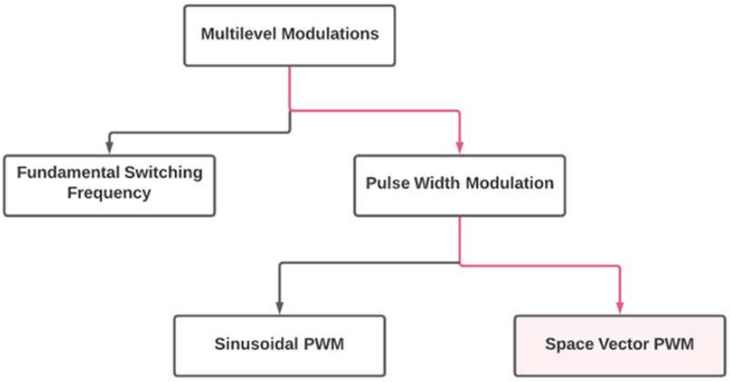

Figure 3.25. PWM techniques classification

The PWM method compares a signal or wave with a high frequency described as the carrier signal (a triangle waveform with frequency) to a low-frequency signal referred to as the reference modulating signal (with frequency f_m). The intended output frequency is decided by the frequency of the reference-modulating signal f_m[32]. Switching devices, such as BJTs, MOSFETs, thermistors, and IGBTs, are utilized as switches in any circuit. The duty cycle of such switches may be used to alter the generated voltage's amplitude and its resonance elements the below are some PWM methods that were used for this investigation to compare inverter performance[30].

3.10.1. Space Vector PWM

SVPWM modulation techniques have a major influence on the voltage balance, in addition to the ripple current rating and the capacitance value of DC bus capacitors. It is critical to select the modulation scheme based on the control requirement since it determines the resulting voltage waveform's harmonic content [45]. The benefit of this SVPWM approach the fact that outputting voltages may be achieved with averaged values by utilizing the closest three vectors, resulting in the greatest spectrum performance. Figure 3.35 depicts the structure of a two-level (3-leg) voltage source inverter[42].

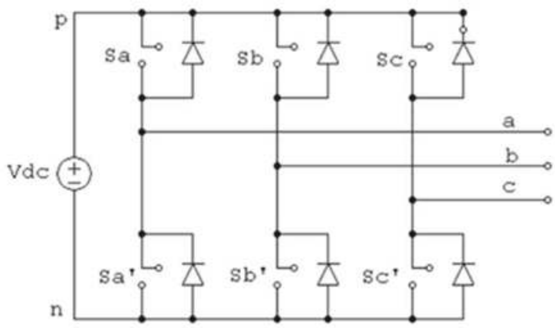

Figure 3.26. The two-level (3-leg) voltage source inverter structure

The upper leg is formed by the switches S_a, S_b and S_c, whereas the lower leg is formed by the switches $S_{a'}, S_{b'}$ and $S_{c'}$.V_{dc} represents the inverter's DC link voltage. The topology requires that no two switches on the same leg be switched on at a similar time, or the DC bus would be shorted. As a result, S_a and $S_{a'}$ ought not be activated at the same time , and so on. As a result, $S_{a'}, S_{b'}$ and $S_{c'}$ are just additions to S_a, S_b and S_c, correspondingly. As a result, just the top half of the leg will be included for examination. The development of a dynamic closed-loop control scheme for a three-phase converter system using the PWM approach entails two steps: The design of a dynamic closed-loop control and the selection of a modulation strategy, each switch will suppose either $+V_{dc}$ when linked to the positive DC rail, i.e. point p, or $-V_{dc}$ when connected to the negative DC rail, i.e. point [31].

A. The following are the essential stages in constructing space vector modulation for a two-level voltage source inverter:

Step1: Convert the a-b-c frame sampled input to the alpha-beta frame.

Step2: In the alpha-beta frame, compute the incoming voltage's magnitude and timing details.

Step3: Determine which sector the vector belongs to using the phase information is in at the time of sampling.

Step4: Using the equation, compute the timings T_1, T_2 and T_0.

Step5: Based on sector and time data, generate switching pulses for devices.

SVPWM (modification of the pulse width of a space vector) for three-leg inverters transforms 3-phase quantities in-plane vectors to two-phase quantities.

B. Benefits of SVPWM Approaches

- Space Vector Modulation for 3-phase inverter systems may familiarize to various switching behaviors like linear load, full-load, non-linear load, half-load, static load, pulsing load, and so on.
- The overall harmonic aberrations in the output voltage are quite minimal.
- The dynamic reaction that is strong.
- For each loading scenario, the inverter efficiency may be improved.
- DC voltage is used efficiently.

C. SVPWM Technique Design Methodology

Determined the architecture shown in Figure 3.27 the line voltages V_{ab}, V_{bc} and V_{ca} are represented by equation.

$$V_{ab} = V_{dc} \tag{3.47}$$

$$V_{bc} = 0 \tag{3.48}$$

$$V_{ca} = -V_{dc} \tag{3.49}$$

V_1 denotes the vector of maximum voltage produced by this architecture (pnn). V_{ab}, V_{bc} and V_{ca} are line voltage vectors that are displaced, 120° in space. The symbol pnn alludes to the three legs or phases a, b, and c that are linked to either the positive dc rail (p) or the negative DC rail (n) (n). Thus, pnn phase matches to a system, which is connected to the positive DC rail, and phases b and c, are linked to a negative DC rail [32]. In figure 3.27 we can see the 3-phase abc frame representation to alpha-beta.

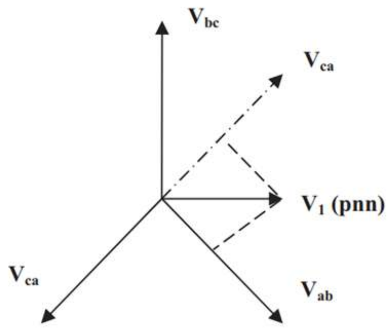

Figure 3.27. 3-phase abc frame representation to alpha-beta plane

Similarly, Clarks transformation may be used to express in the plane the six non-zero voltage vectors ($V_1 - V_6$) and the two zero vectors (V_7, V_8) known as state-space vectors α-β. Suppose T_s is split into three subintervals T_1, T_2 and T_0. The space vector shifting method uses eight space vectors (Vn, n=0...7) to mimic the sinusoidal line modulation signal V_s. The modulating signal, on the other hand, is located among the arbitrary vectors, V_n and V_{n+1}. Then, using the following equations, the two non-zero vectors (V_n and V_{n+1}) and one zero space vector (V_0) must be used to get the highest load line voltage while minimising switching frequency

$$T_1V_1 + T_2V_2 = T_SV_S = mV_{DC} \tag{3.50}$$

$$T_1 + T_2 + T_0 = T_S \tag{3.51}$$

Where T_0, T_1 and T_2 are computed utilizing

$$T_1 = T_S m \sin(\pi/3 - \theta) \tag{3.52}$$

$$T_2 = T_S m \sin\theta \tag{3.53}$$

$$T_0 = T_s - T_1 - T_2 \tag{3.54}$$

And duty phases are provided by

$$d_1 = T_1/T_s \ , d_2 = T_2/T_s \tag{3.55}$$

Defining the modulation index,m $= \frac{|V_S|}{V_{dc}}$

assumptions, a switching table is created, as illustrated in Table 3.4.

- 'The number '100' corresponds to the switch locations 'S_a S_b S_c'.

The values' 1' and '0' $T_S$is the interval of shifting or sampling ,θ is angle between V_s and V_n

- Based on the foregoing indicate the open and closed states of the switch, correspondingly. For instance, if the reference vector is in sector 2, the Sa must be in the ON position for $T_0/4$ and $T_1/2$ period, in OFF position for $T_2/2$ period and so on. As it is showing in table 3.4.

Table 3.4. Switching Table for 2- level inverter

Sector No.	$T_0/4$	$T_1/2$	$T_2/2$	$T_0/4$	$T_0/4$	$T_2/4$	$T_1/4$	$T_0/4$
1	000	100	110	111	111	110	100	000
2	111	110	010	000	000	010	110	111
3	000	010	011	111	111	011	010	000
4	111	011	001	000	000	001	011	111
5	000	001	101	111	111	101	001	000
6	111	101	100	000	000	100	101	111

By adjusting the shifting time of space vectors for each of the six sectors seen in Table. 3.4, the SVM method is employed to produce a reference vector. At each sector, two active vectors and zero vectors combine to form the space voltage vector [43]. Active vector's ($(T_1$ to $T_6)$ is determined by varying the switching time and the related activities and zero vectors to produce an angle produced by the reference vector. (T_0) Table 3.5 shows the calculation for each sector[32].

Table 3.5. Switching Table for 2- level inverter

No. of Sectors	Position	Vectors
Sector 1	$(0 \leq wt \leq \pi/3)$	$T_1 = \sqrt{3}/2\, mT_s\, \cos(wt + \pi/6)$ $T_2 = \sqrt{3}/2\, mT_s \cos(wt + 3\pi/2)$ $T_0 = T_s - T_1 - T_2$
Sector 2	$(\pi/3 \leq wt \leq 2\pi/3)$	$T_2 = \sqrt{3}/2\, mT_s\, \cos(wt + 11\,\pi/6)$ $T_3 = \sqrt{3}/2\, mT_s \cos(wt + 7\pi/6)$ $T_0 = T_s - T_3 - T_2$
Sector 3	$(2\pi/3\ \leq wt\ \leq \pi)$	$T_3 = \sqrt{3}/2\, mT_s\, \cos(wt + 3\,\pi/2)$ $T_4 = \sqrt{3}/2\, mT_s \cos(wt + 5\pi/6)$ $T_0 = T_s - T_3 - T_4$
Sector 4	$(\pi \leq wt \leq 4\pi/3)$	$T_4 = \sqrt{3}/2\, mT_s\, \cos(wt + 7\,\pi/6)$ $T_5 = \sqrt{3}/2\, mT_s \cos(wt + \pi/2)$ $T_0 = T_s - T_4 - T_5$
Sector 5	$(4\pi/3 \leq wt \leq 5\pi/3)$	$T_5 = \sqrt{3}/2\, mT_s\, \cos(wt + 5\,\pi/6)$ $T_6 = \sqrt{3}/2\, mT_s \cos(wt + \pi/6)$ $T_0 = T_s - T_5 - T_6$
Sector 6	$(5\pi/3 \leq wt \leq 2\pi)$	$T_6 = \sqrt{3}/2\, mT_s\, \cos(wt + \pi/2)$ $T_1 = \sqrt{3}/2\, mT_s \cos(wt + 11\,\pi/6)$ $T_0 = T_s - T_1 - T_6$

During each sample interval, space-vector modulation generates the pulse width for dynamic vectors depending on the aforementioned active vectors line voltages are increased by adding critical elements in the line. Inside the sample interval, the optimal switching sequences result in enhanced space-vector modulation performance [32].

4. MODELING OF THREE-PHASE IM

There are many ways to running three phase IM, as described in chapter two, relying on the load acceleration, starting current, and torque needed. The diagram below depicts a 0.25 kilowatt, 50Hz three-phase IM in an alpha-beta system. In this part, the DOL technique will be modeled and simulated with various load torque values (no-load, half load and full-load).

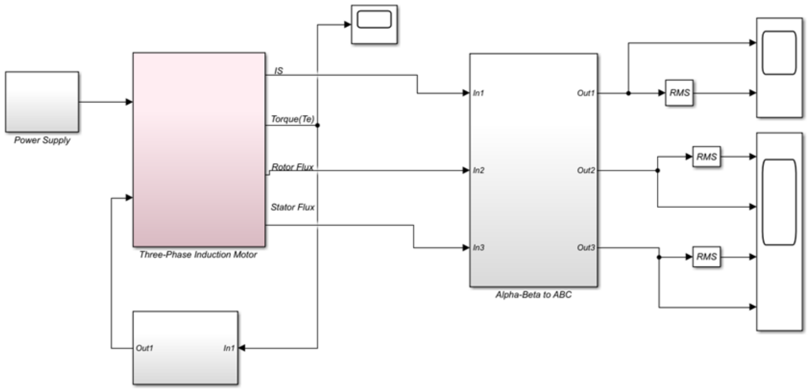

Figure 4.1. DOL model of three-phase Induction Motor

By using Equation (3.6) and (3.7) three-phase IM model is design. Direct quadrature current, torque, rotor and stator flux may be modeled using these equations, as shown in figure 4.1. the electrical and mechanical parameter of motor is calculated in theoretical and practical and the detail of them is in appendix.

The motor is connected by delta and it is supplied by 220 three phase voltage. Because of the voltage source is in abc coordinate by changing it to alpha-beta coordinate it will good for the motor model by the following equation.

$$\begin{bmatrix} i\alpha \\ i\beta \end{bmatrix} = \begin{bmatrix} 3/2 & 0 & 0 \\ 0 & \sqrt{3}/2 & -\sqrt{3}/2 \end{bmatrix} * \begin{bmatrix} ia \\ ib \\ ic \end{bmatrix} \tag{4.1}$$

And result is showing in alpha-beta coordinate by using the following equation we can see the result in abc coordinate.

$$\begin{bmatrix} ia \\ ib \\ ic \end{bmatrix} = \begin{bmatrix} 2/3 & 0 \\ -1/3 & 1/\sqrt{3} \\ -1/3 & 1/\sqrt{3} \end{bmatrix} * \begin{bmatrix} i\alpha \\ i\beta \end{bmatrix} \tag{4.2}$$

In figure 4.2, a schematic design of a three phase to alpha-beta and alpha-beta to three phase conversion is presented based on the aforementioned formule.

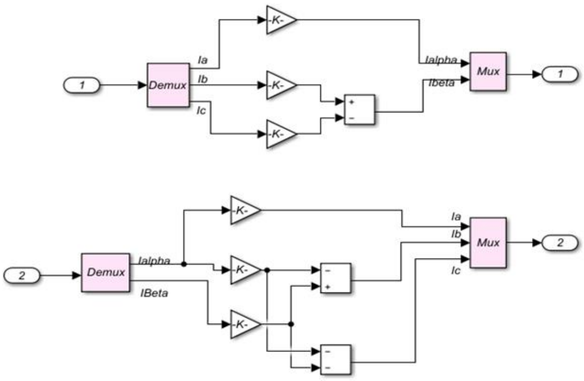

Figure 4.2. ABC to alpha-beta and alpha-beta to ABC conversion

4.1. Modeling of Controller

As discussed in Chapter 3, in order to regulate IM using the IRFOC technique, a controller for the current loop, flux loop, and speed loop must be designed. To every loop, a PI controller is designed based on IM parameters and specified specifications in this section. Figure 4.3 showing the general block diagram of PI controller with system.

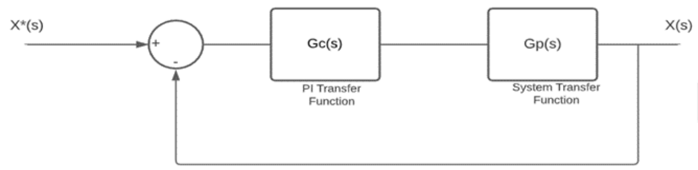

Figure 4.3. General block diagram of PI controller with system

$Gc_{(s)}$ is the transfer function of the PI controller, and $Gp_{(s)}$ is the transfer function of the system in our study, which is a 0.25 kw three phase induction motor. X*(s) is the system's reference input, and X(s) is the system's output.

$$Gc(s) = \frac{k(s+a)}{s} \tag{4.3}$$

$$Gp(s) = \frac{k}{s+p} \tag{4.4}$$

4.1.1. D-Q Current Loop PI Controller

The current loop must always be much faster than the speed loop in a control philosophy as show in figure 4.4. The calculation of both PI controller and system transfer function is on appendix

.

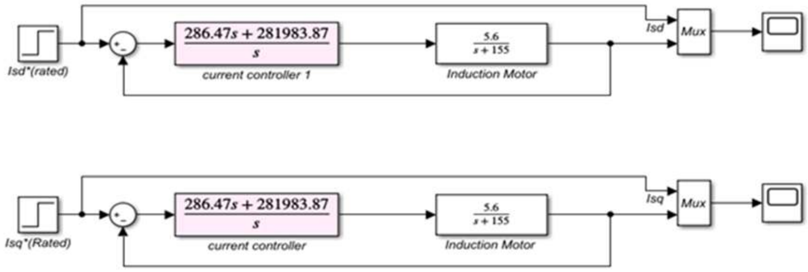

Figure 4.4. Controller for dq current loop

4.1.2. Flux Loop PI Controller

The Flux loop PI controller must be slower by (20-15) times according to current loop PI controller. Figure 4.5 show the model of testing flux loop PI controller. The calculation of PI controller and system transfer function is on Appendix.

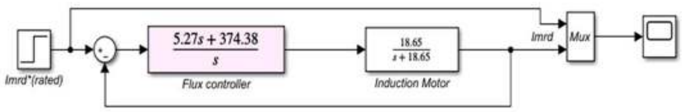

Figure 4.5. Controller for flux loop

4.1.3. Speed Loop PI Controller

For speed, loop PI controller the mechanical parameter of motor is nessecry. Figure 4.6 show the model of testing speed loop PI controller. The calculation of PI controller and system transfer function is on Appendix.

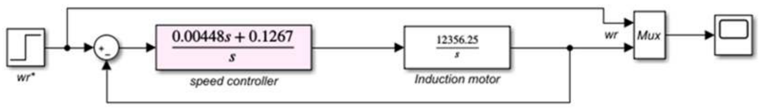

Figure 4.6. Controller for speed loop

4.2. Examine Current Loop Controller with IM Model

As mentioned before for using PI controller to controlling current, flux and speed. The three-phase induction motor must be transformed to DC motor. The model in this work it is in alpha-beta coordinate for showing the output in dq coordinate we should design a block to converting alpha-beta to dq and for input also block for converting dq to alpha- beta coordinate is done as showing in figure 4.7.and one of the required parameter in both converting is known as Lamda which is the rotor flux angle and for designing it the following equations is use.

$$\omega_e(t) = \frac{d}{dt}\lambda(t) \tag{4.5}$$

$$\lambda = \int \omega_e dt \tag{4.6}$$

$$\lambda = \int(\omega_r + \omega_{sl})dt \tag{4.7}$$

$$\omega_{sl} = \frac{R_r}{L_r * i_{mrd}} * i_{sq} \tag{4.8}$$

$$\omega_{sl} = \frac{i_{sq}}{\tau_r * i_{mrd}} \tag{4.9}$$

Subsituting in the above equation

$$\lambda = \int\left(\omega_r + \frac{i_{sq}}{\tau_r * i_{mrd}}\right)dt \tag{4.10}$$

Here λ = Rotor Flux Angle

when (i_{sq}^*) is utilized for batter results

As indicated in the equations above, (I_{mrd}) is required and may be obtained as described below.

$$I_{mrd} = \frac{I_{sd}}{\tau_r s+1} \tag{4.11}$$

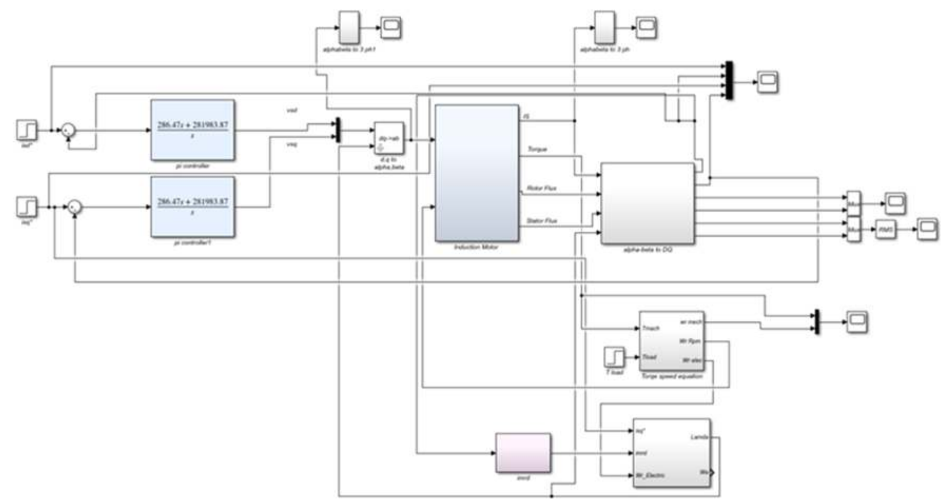

Figure 4.7. Current loop control for IM

4.2.1. Exmaine Current Loop Controller and Compensation Term with IM Model

As previously stated in Chapter 3, by altering the load, the PI controller delivers a desirable value of voltage to decrease or raise the current of the motor, therefore affecting the flux and back-emf. A voltage compensator or decoupling term is employed to solve fluctuating flux and back-emf. For designing of the block diagram equations(3.4) and (3.5) in chapter three is used figure 4.8 show the voltage compensation model. Figure 4.9 depicts the current loop architecture with voltage compensation phrase.

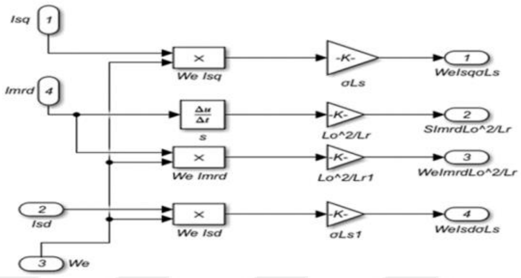

Figure 4.8. Compensation term model

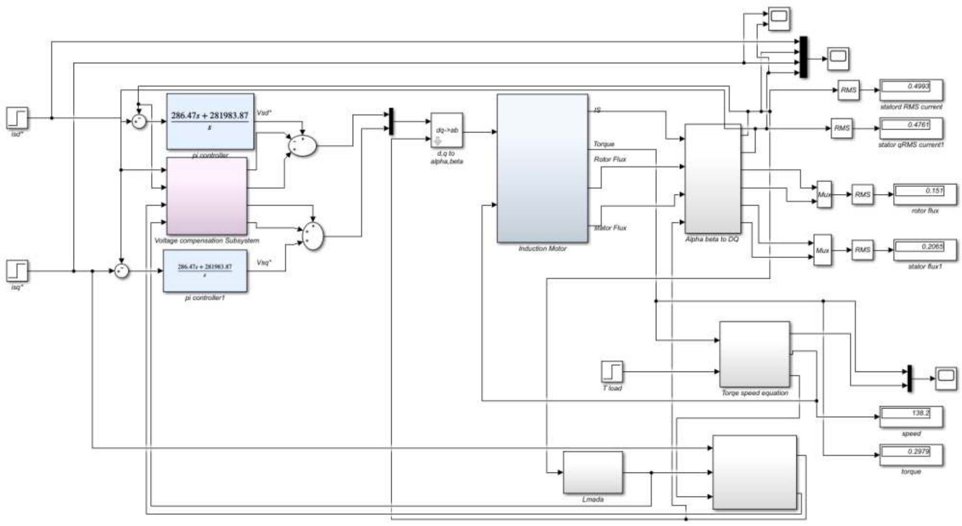

Figure 4.9. The current loop design with voltage compensation term

4.3. Examine Speed Loop Controller with IM Model

In this section control of speed loop will be showing, time of controlling is less than current controller. Speed loop is outer loop in the IRFOC. Figure 4.10 show that controlling of Induction motor that designed in section 4.1

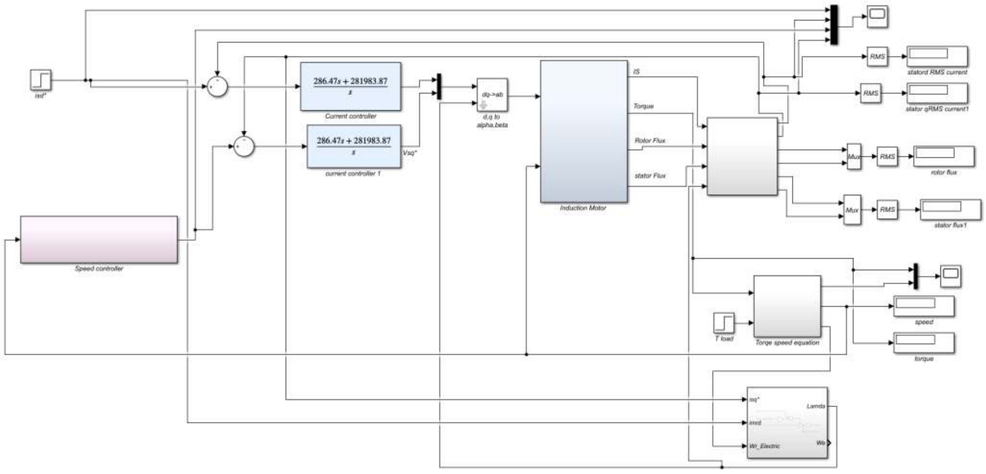

Figure 4.10. Current and speed control for IM

After testing the model in different load torque we saw that when the load torque is 0 Nm speed is nearly 2990 rpm and it is normal for no load condition. After that by increasing load torque to 0.8 Nm that is full load torque in the motor that controlling the speed is directly decreasing to nearly 2800 rpm. By giving it over 0.8 Nm it is still controlling the speed but in practical it is not safe for motor because the winding of stator will be damage. Because of that the block of look up table is done. Figure 4.11 show the speed controller.

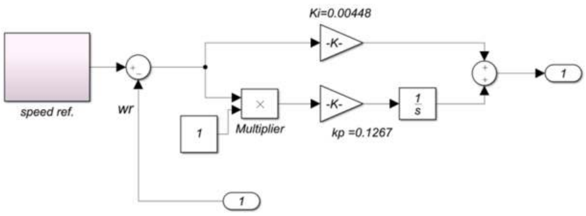

Figure 4.11. PI controller for speed

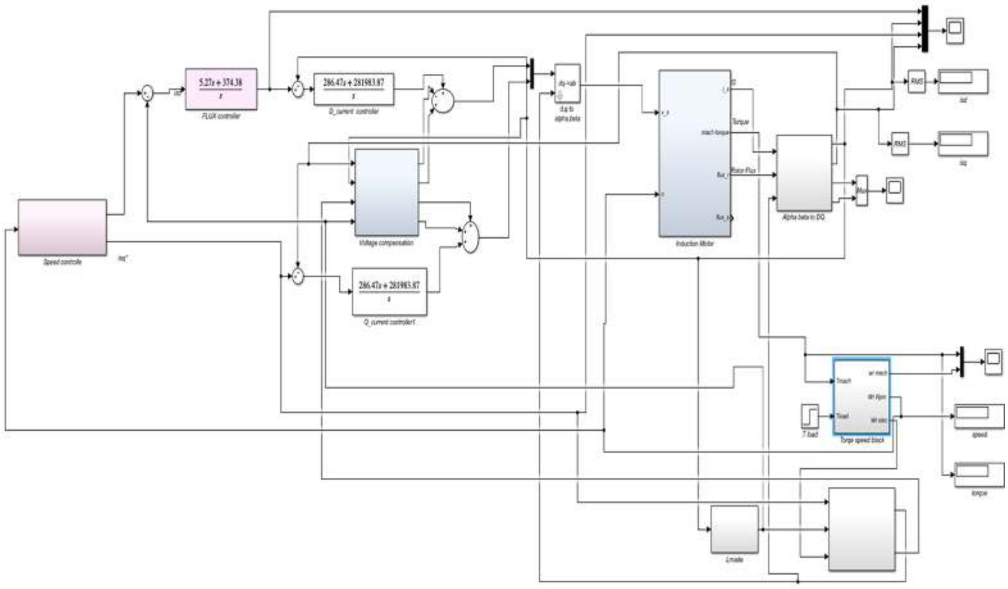

Figure 4.12. Current and speed controller with lookup table and composition term

In figure 4.12 we can see the model of all of system with adding speed controller

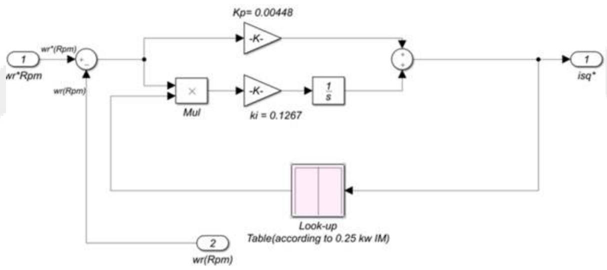

Figure 4.13. PI controller with look up table

In figure 4.13 model of speed controller explained.

According to value of I_{sq} in practical work the look up table block is done for avoiding damaging the motor as showing in table 4.1 and in figure 4.14 we can see the design page in MATLAB.

Table 4.1. Look up Table

Break Point	Isq(Amp)	Value
1	-0.47 A	0
2	-0.46 A	1
3	0	1
4	0.46 A	1
5	0.47 A	0

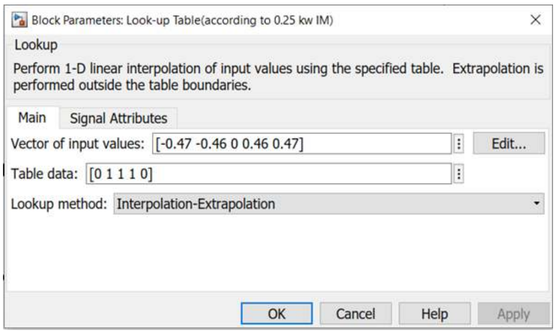

Figure 4.14 . Look up table block diagram

By using this block, we can see that after giving the motor more than 0.8 Nm the motor will stop working.

4.4. Field Weakening Design

As is well understood, increasing the speed necessitates the application of additional voltage, and increasing the speed will result in a voltage violation. An essential and successful approach known as field weakening is utilized to remove the stator voltage, violation of the induction machine at high speed. As is evident, the speed and flux are related to the induction machine's back induced emf, which must be smaller than the stator voltage; hence, lowering the flux will result in a faster speed. When the speed exceeds the specified value, the produced torque is influenced by additional torque elements including friction and windage torque, which fluctuate at high speeds. As a result, the torque form will grow nonlinear and dependent on the induction motor's capability. The field weakening approach, that is dependent on the equation, could be used to enhance the speed. ($T \propto \frac{1}{\omega_r}$) When using constant power, the speed improves as the torque decreases. Torque is reduced by lowering flux, and flux reduction ensures that the applied voltage is not violated. Depending on the description above, the lookup table for field weakening may be constructed, and thus the machine's flux is dependent on I_{sd}. As a result, the I_{sd} and speed are utilized to prepare the lookup table. $I_{sd} = \frac{\omega_r^*}{\omega_r} \times I_{sd}^*$. Figure 4.15 showing model of field weakening with flux controller.

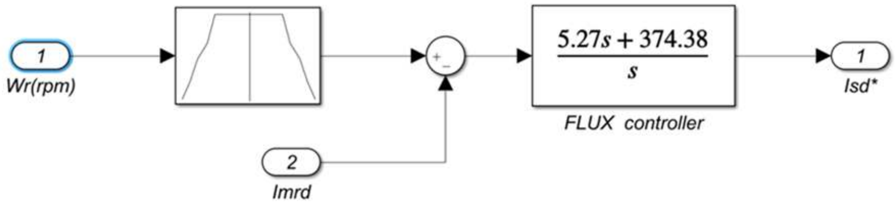

Figure 4.15. Field weakening

In table 4.2 showing the design of field weakning parameter and in figure 4.16 we can see the MATLAB page for values of field weakening.

Table 4.2. Field weakening parameters

Break Point	Speed (rpm)	Isd (A)
1	-5950	-0.25
2	-5500	-0.3
3	-4500	-0.35
4	-4000	-0.4
5	-3000	-0.4993
6	3000	0.4993
7	4000	0.4
8	4500	0.35
9	5500	0.3
10	5950	0.25

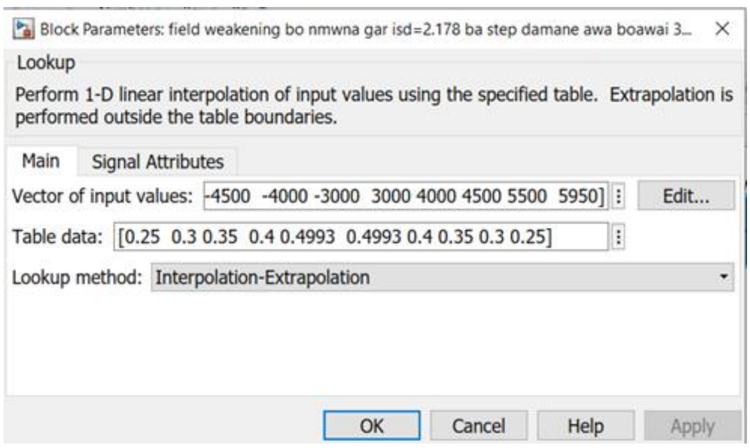

Figure 4.16. Design of field weakening in MAT LAB

4.5. Control of IM by IRFO Method (Alpha-Beta System)

By adding all of the block models that designed, we can see the final model of control of IM by IRFOC In the figure 4.17.

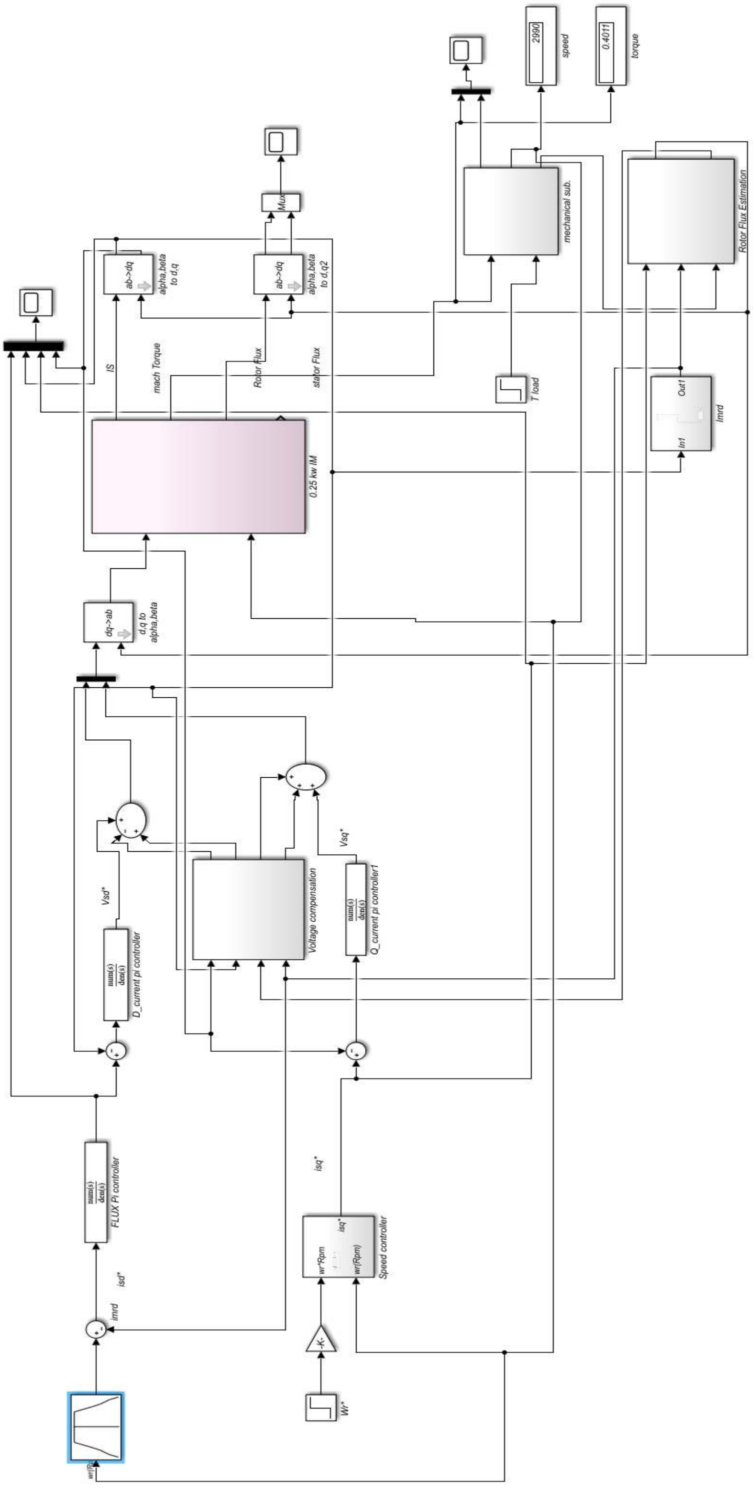

Figure 4.17. Control of IM by IRFOC by SIMULINK/MATLAB

4.6. Control of IM by IRFO Method (ABC System)

In figure 4.18 we can see the modelling of control of IM by IRFO method in ABC System using the IM in MATLAB library and using the PI Controllers that designed before.

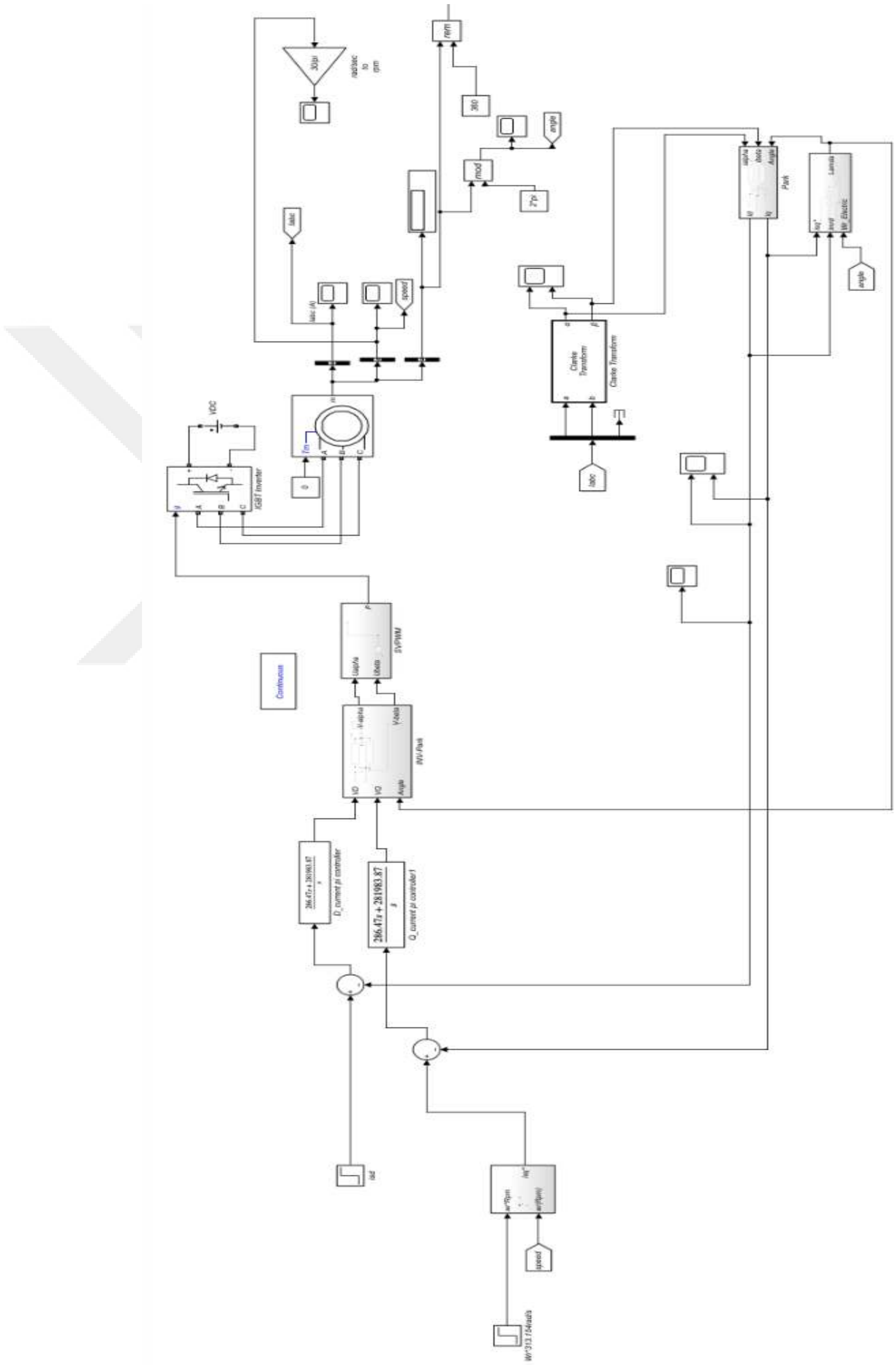

Figure 4.18. Control of IM by IRFOC (ABC System) by SIMULINK/MATLAB

5. EXPERIMENTAL WORK

The implementation of IRFOC for IM will be introducing using STM32F103C8 micro controller systematically. In addition, some experiment should be done in a laboratory.

5.1. Experiments for Three-Phase IM

To determine values for the multiple aspects of the equivalent circuit, testing should be performed on the machine that the equivalent circuit will describe.

DC Test of three-phase IM : This exam was created by myself. To determine the value of the 3-phase IM stator resistance, a DC voltage is supplied to the stator windings of a three-phase IM. As its current is direct current, there really is no generated voltage and hence no rotor current. In addition, at direct current, the motor's reactance is zero. As a result, the only quantity restricting current in the motor is the stator resistance, which can be measured. To transform its value from DC to AC, the determined resistance of 3-phase IM should be increased by a factor (Skin effect) spanning from (1.05-1.25). The temperature of the motor determines the skin impact factor before test and the temperature of the motor at the time of the DC test. After supplying DC voltage to the endpoints of the stator winding and obtaining voltage and current readings, the connection ship amongst them must be charted. Figure 5.1 showing practical work for DC test.

$$R_{dc} = \frac{V_{dc}}{I_{dc}} \tag{5.1}$$

$$R_1 = R_{1dc} * \text{Skin effect} \tag{5.2}$$

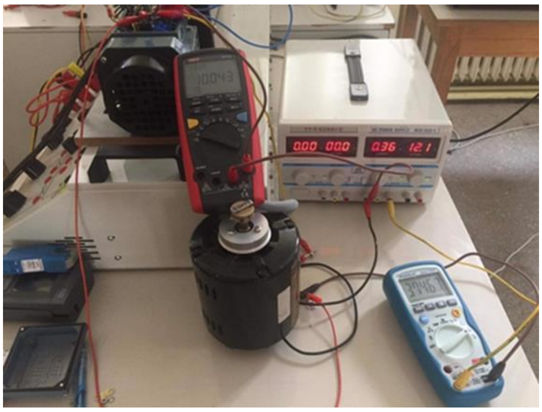

Figure 5.1. DC Test of 0.25 kW three-phase IM

No load Test of Three-phase IM : The no-load test is analogous to an open circuit test on a transformer. It is used to calculate the magnetizing branching parameters (shunt parameters) in the synchronous generator of an induction machine. In this check, the motor is permitted to operate with no load through its terminals at the specified voltage and frequency. The machine will revolve at nearly synchronous speed, resulting in near-zero slip. As a result, the equivalent rotor resistance is quite high (theoretically infinite, neglecting the frictional and rotational losses). As a result, the rotor equivalent impedance might be considered open. The findings in this study will reveal information about the stator and the magnetizing branch. In this test we can find (I_m, X_m, R_c, I_c and L_m). Figure 5.2 showing practical work for no-load test.

$$I_c = I_1 * \cos\theta \tag{5.3}$$

$$I_m = I_1 * \sin\theta \tag{5.4}$$

$$R_c = \frac{V_{ph}}{I_c} \tag{5.5}$$

$$X_m = \frac{V_{ph}}{I_m} \tag{5.6}$$

$$L_m = \frac{X_m}{2*\pi*f} \tag{5.7}$$

Figure 5.2. No load Test 0.25 kW three-phase IM

Blocked Rotor Test of Three-phase IM: The motor shaft is secured, so it could even turn during this test. The motor connections are linked to a three-phase power supply. The rotor is transformed into the auxiliary of a transformer that operates at the supplied frequency. As a result, the blocked rotor test is analogous to the short circuit test on a transformer. It is used to compute the induction machine's series components or leaking impedances. To inhibit spinning, the rotor is obstructed, and balancing voltages are delivered to the stator terminals until the rated current is attained. Core loss and the magnetizing portion of the current are very tiny percentages of the overall current when the voltage is lowered, and the current is regulated.

$$R_{1e} = \frac{P_{sc}}{3(I_{sc})^2} \tag{5.8}$$

$$R_2' = R_{1e} - R_1 \tag{5.9}$$

$$X_{1e} = \sqrt{Z_{1e}^2 - R_{1e}^2} \tag{5.10}$$

$$X_{1e} = X_1 + X_2' \tag{5.11}$$

Load test of Three-phase IM : The load test on an induction motor is used to calculate its overall efficiency such as torque, slip, effectiveness, power factor, and so on. Throughout this test, the motor is run at its specified voltage and frequency and is practically loaded properly. A DC motor is utilized as a mechanical load. Figure 5.3 showing practical work for load test.

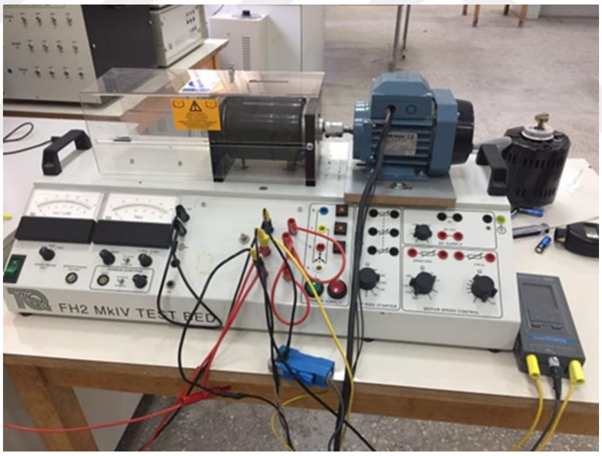

Figure 5.3. Load test of 0.25 kW three-phase IM

Calculation By Hand: On usual, manufacturers give motor characteristics whether on the motor nameplate or in a datasheet, and this information is rated value.Using equivalent circuit and phasor diagram we can calculate motor parameters.
In figure 5.4 can see the flow chart of expermental work for finding motor’s parameter.

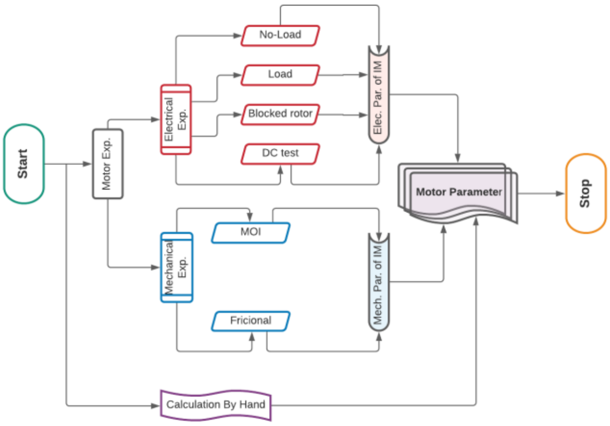

Figure 5.4. Flow chart for finding IM's parameter

5.2. Open Loop Test

Generally, in this section, the detail of designing the inverter board (power board) and the process for generating SVPWM by STM32F103 will be discussed. This test aims to see how the SVPWM technique works and how it can rotate the three-phase IM by SVPWM.

5.2.1. Hardware Setup

The component that needs for the open loop test is (0.25kw three-phase induction motor, STM32F103 as a microcontroller, Inverter board or power board, three-phase rectifier). The main component for the inverter board that designed in this work is IGBTs 6 IGBTs is used for this purpose as mentioned before, the type of IGBT that used in this work is starting working from 7.5 volts in figure 5.5: we can see that the IGBT will be starting working from 7.5 V. And the LED start working.

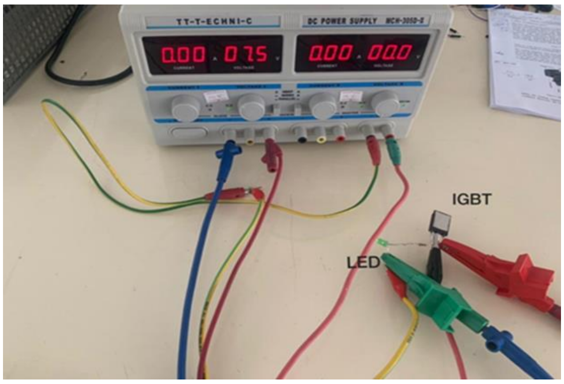

Figure 5.5. Test for IGBT

Due to the IGBTs working from 7.5 V and the maximum output voltage of STM32F103 is 3.3 v, and for protecting the lower side voltage from higher side voltage, the optocouplers used. In figure 5.6 ; below, we can see that the first leg is connected and the optocouplers are working. We can notice that the output signal is 13.2 V due to we gained 13.2 v to optocouplers, and input signals are smaller than the output.

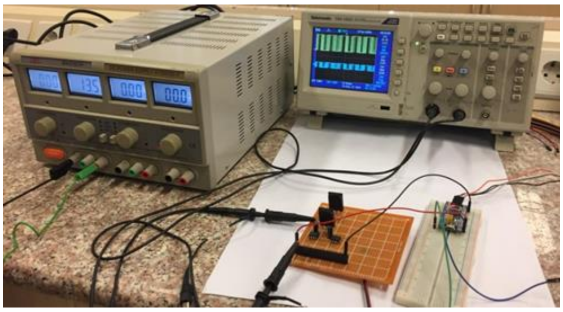

Figure 5.6. IGBTs (first leg) with optocoupler

For giving each optocoupler the voltage that it needed the isolator DC to DC converter is used for the 3 higher Optocoupleres each of them needs one supply voltage, but the lowers need just one due to the V_{EE} that connected to the emitter of the IGBTs.in figure below, we can see the design of inverter board by proteus program in figure 5.7. And in figure 5.8 we can see Hardware setup for open loop test with SVPWM

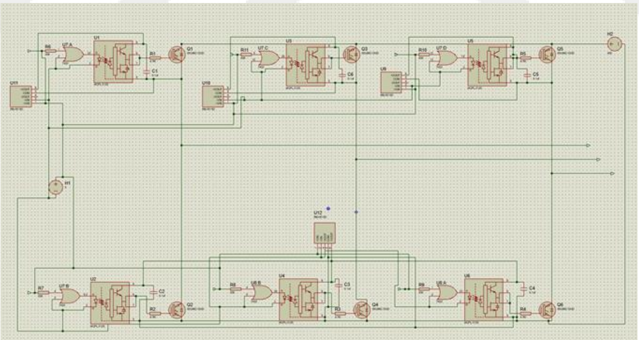

Figure 5.7. Inverter board designed by Proteus

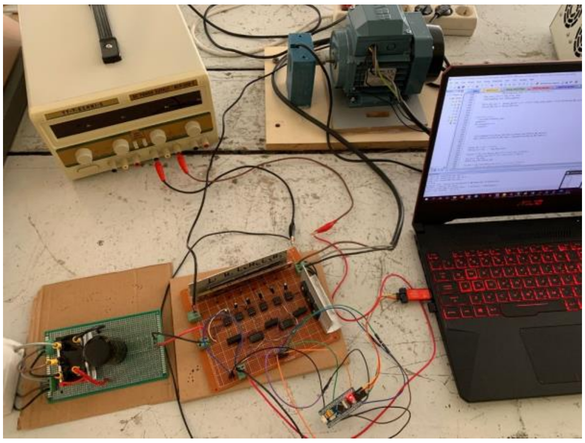

Figure 5.8. Hardware setup for open loop test with SVPWM

5.2.2. Software Setup (Generating SVPWM Signals)

The following steps describe the process of generating SVPWM signals:

To generating SVPWM signals is to producing three sine waves that the phase shift between them is 120 degrees, but as shown in the detail of STM32F103, there are not any digital to analog converter (DAC) due to this reason, these three sine waves generated by PWM technique. In STM32 microcontrollers, the PWM peripheral may be utilized as a DAC to produce analog voltage according to the duty cycle of the PWM signal. As a result, creating analog waveforms is just a matter of copying waveform data points from anywhere in memory to the PWM duty cycle control register (CCRx). This procedure may be broken down into two key steps:

Step1: Generating the lookup table

The lookup table is an array of integer value data that reflect the data samples of a given waveform throughout a whole cycle (from 0 to 2π). Ns, or the number of sample points per full cycle, denotes the length of the lookup table. The higher the number of sample points each cycle, the greater the output waveform.

As we will see in the following part, we will generate the sample points lookup table for different waveforms employing a MATLAB script. After that, we'll copy it to our code, and the wave LUT[NS] array will be ready to be transmitted to the DAC output.

Step2: Moving the data to the DAC Output (PWM Duty Cycle)

There are several methods for transferring data points from memory to the PWM duty cycle control register. The first is by utilizing the CPU's own power. We may cycle over the lookup table and transmit the waveform sample points to the CCRx register one at a time. However, this approach is extremely inefficient in loading the CPU and requiring 100% of its time. Furthermore, any CPU interruptions or leaving to perform other duties will disrupt the timing of the PWM-To-DAC system's output signal. Regardless of the fact that it operates, this is clearly not a good idea (in extremely restricted circumstances). In this example, the output waveform frequency is adjusted by varying the delay period (x).

```
while(1)
{
 TIMx->CCRx = Wave_LUT[i++];
DWT_Delay_us(x);      }
```

Another approach is to employ timer interruptions to emit an interrupt signal on a regular basis, allowing the CPU to transmit data points to the CCRx on a regular basis. It is, nevertheless, a more efficient method than the prior one. However, it still needs a significant amount of CPU involvement, particularly when a high sampling rate is needed. Sometimes it can be impossible to achieve at all, and other times it's possible, but the CPU is overloaded by 60% or more, which is also a bad concept. Aside from the fact that it works and is superior to the prior technique.

Finally, we can utilize the DMA & Timer to regularly activate the DMA unit, causing it to transport a sample data point from the memory-stored lookup table to the PWM duty cycle control register (CCRx). When a timer triggering event occurs, the DMA transfers a data point from the table to the CCRx and advances the memory pointer in preparation for the next triggering event. This is the most effective method for doing the task without utilizing the CPU.

The DMA may also be set to run in circular mode, which causes it to loop around the lookup table whenever it hits the end of the table. As a result, the CPU is not obligated to take any action as show in figure 5.9. Moreover, this is what we intend to do in this project.

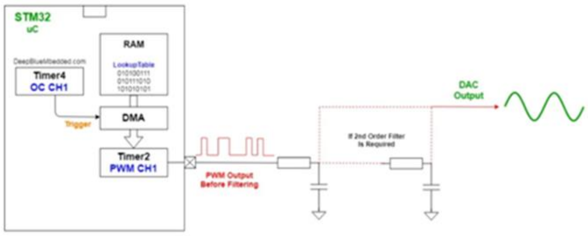

Figure 5.9. Process of designing Sine wave

The MATLAB script that produces the lookup table is provided below.

```
clear; clc;   % Clear the Previous Points
Ns     = 128; % Set The Number of Sample Points
RES    = 10;  % Set The DAC Resolution
OFFSET = 0;   % Set An Offset Value For The DAC Output
%------------[ Calculate The Sample Points ]-------------
T = 0:((2*pi/(Ns-1))):(2*pi);
Y = sin(T);
Y = Y + 1;
Y = Y*((2^RES-1)-2*OFFSET)/(2+OFFSET);
Y = round(Y);
plot(T, Y);
grid
%--------------[ Print The Sample Points ]---------------
fprintf('%d, %d, %d, %d, %d, %d, %d, %d, %d, %d, %d, %d, %d, %d, %d, \n', Y);
%-------------------[ Other Examples To Try ]-------------------
%  Y = diric(T, 13);      % Periodic Sinc
```

We created a sine wave lookup table with 128 sample points (Ns) and set Timer2 to initiate the DMA transition to the PWM duty cycle. Then the output sine wave frequency can be found by

$$\text{Trigger Frequency} = \frac{F_{clk}}{(PSC+1)*(ARR+1)} \tag{5.12}$$

$$\text{OutWaveFrequency} = \frac{\text{Trigger Frequency}}{Ns} \tag{5.13}$$

Using the PWM-to-DAC technique implies the following fact “PWM’s resolution dictates the resulting DAC’s resolution”. In other words, the final DAC’s resolution is defined by the PWM’s resolution it’s the same value. Therefore, we’ve to decide on the required resolution for the final DAC so that we can pick the PWM's frequency that guarantees to achieve the required resolution.

In this project, we'll stick to a 10-bit resolution. This means the resulting DAC we'll be building using the PWM technique will also be 10-bit in resolution.

A rule of thumb is to choose the f_{PWM} to be some order of magnitudes larger than the desired output signal's frequency f_{BW}. The larger the factor k the better.

$$f_{PWM} = K \times f_{BW} \tag{5.14}$$

And as we can see from the formula down below. This indicates that raising the f_{PWM} will decrease its resolution at any value for timer clock f_{CLK}, and therefore the DAC's resolution decreases as well.

$$\mathrm{Resolation}_{PWM} = \frac{\log(\frac{f_{clk}}{f_{pwm}})}{\log(2)}\,[\mathrm{Bit}] \tag{5.15}$$

The formula to be used in configuring the timer module in PWM mode to control the PWM output frequency.

Designing RC low pass filter (LPF) design this step is the most critical step in the design process as it defines the dynamic characteristics of the resulting DAC system at the end. The LPF filter introduces some delay due to the time constant that can limit the DAC's ability to swing very quickly to follow a specific waveform pattern. We need to filter out all the PWM signal frequency components and leave out the f_{BW} of the signal to be generated. As shown in the diagram below, we want to eliminate the high-frequency components and leave only the low-frequency sine wave.In figure 5.10 we can see how sine wave will be generate by PWM.

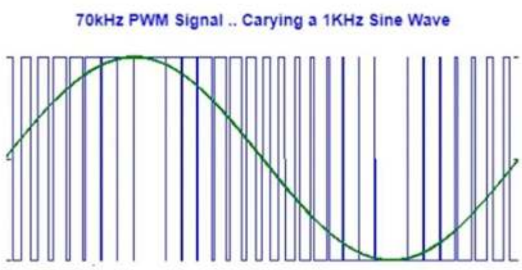

Figure 5.10. PWM signal in time-domain

Figure 5.11 showing the response of PWM signal in frequency-domain.

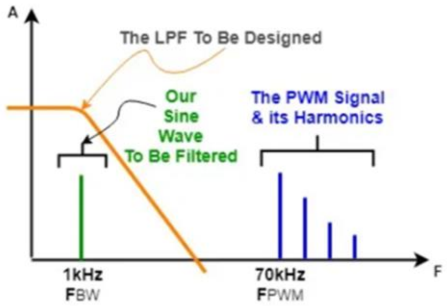

Figure 5.11. PWM signal in frequency-domain

The LPF should be designed so as to pass the frequency of the desired signal f_{BW} while blocking the f_{PWM} harmonics. And the following formula is used for this.

$$RC = \frac{1}{2\pi \times f_{BW}} \tag{5.16}$$

Hoose the resistor R depending on the GPIO pin output driving capability and solve for C to find the capacitor value. Moreover, you can calculate the attenuation using the following formula. And if the attenuation is not sufficient, you'll have to increase the k factor.

$$\text{Attenuation(dB)} = -10 \times \log[1 + (2\pi \times f_{pwm} \times RC)^2] \tag{5.17}$$

Now by applying all these steps, we can generate a sine wave for producing SVPWM signals; as mentioned before, 50 Hz 3 sine wave is necessary that they have phase shift by 120 degrees and 5KHz rectangular wave. The figure below showing the pin configuration by STM32CubeMX. Figure 5.12 show the clock configuration that desined for open loop test by STM32CubeMX.

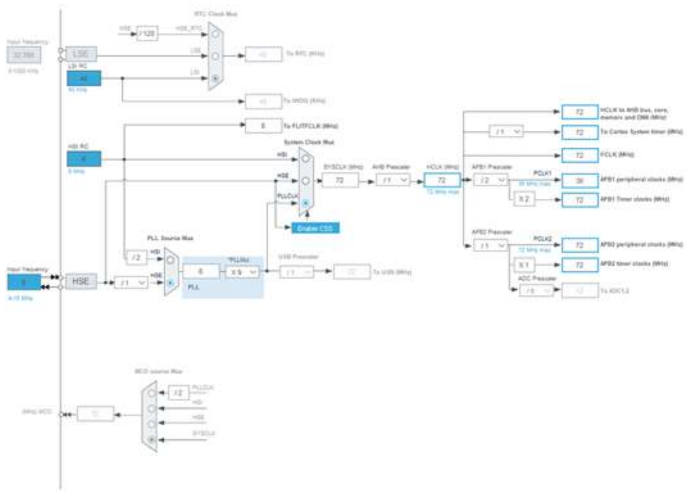

Figure 5.12. Open-loop test clock configuration

At the same time, all the process is done by MATLAB/SIMULINK to comparing each step in STM32F103C8 as show in figure 5.13.

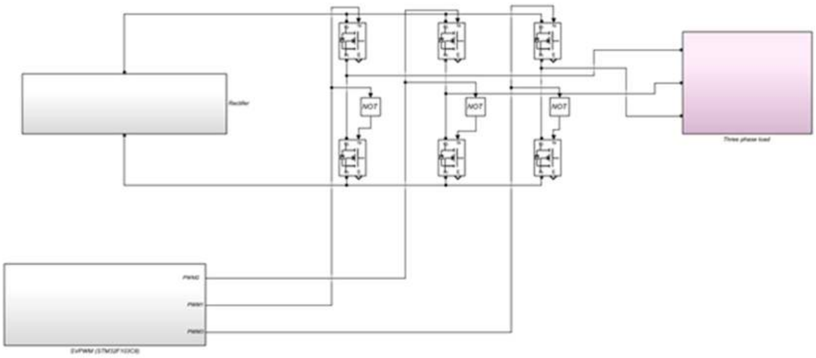

Figure 5.13. Modeling of open-loop test

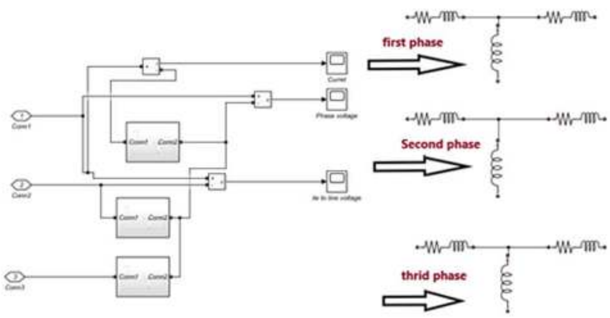

Figure 5.14. Modeling of load

In figure 5.14 we can see the model of three phase load

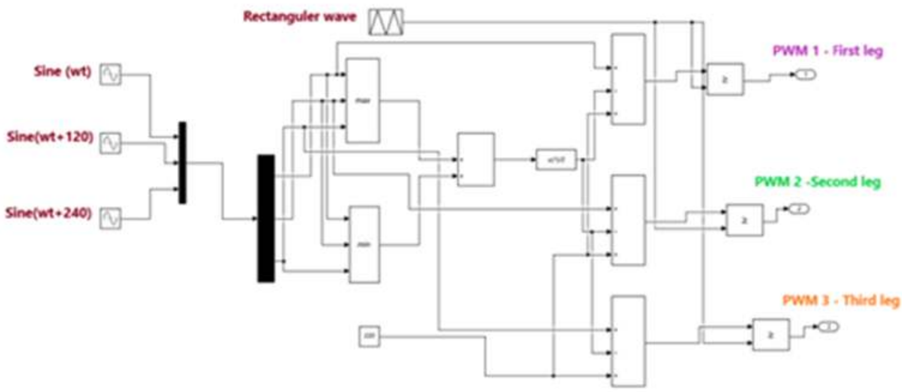

Figure 5.15. Modeling of SVPWM

In figure 5.15 showed the model of generating SVPWM signals

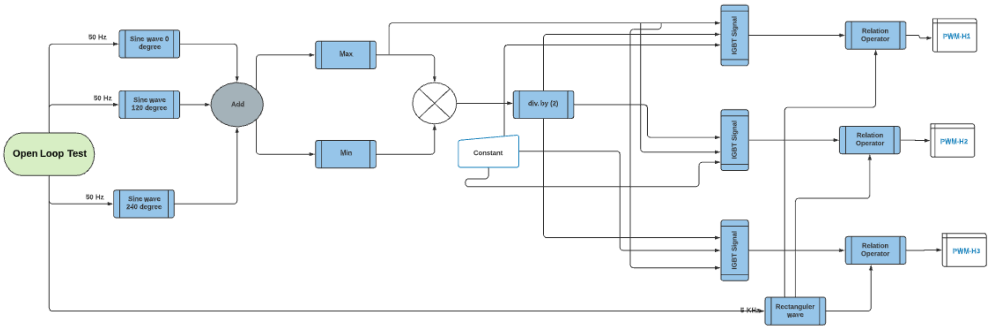

Figure 5.16. Flow chart for open-loop Test

In figure 5.16 showed the flow chart of open loop test and generating SVPWM signals.

5.3. Close Loop Control

In order to validate FOC of induction motor using STM32, all equation in Matlab Simulink is discretized, and the stator currents of the induction motor will be measured using current sensors. Later on, the speed of the motor will be recorded using a rotary encoder. In this step, the inverter board, rectifier board, sensor board, STM32F103C8, 0.25KW three-phase IM will be used. As mentioned before in chapter 3 there is some step for controlling IM by FOC method here in this section all the steps will be discussed according to the programming. The processer is working under 72 MHz.

First: Sensing current and speed

For sensing a three-phase current, as mentioned before, ACS712 is used that is AC/DC current sensor. After connecting each current sensor with each phase in IM the output of the current sensor connected in ADC channels in STM32F103C8 the frequency that used for reading analog signal and converting to digital is 12 MHz and the sampling time 55.5 cycle. The time of converting is 5.6 us by using the equation below.

$$T_{conv} = \frac{\text{Sampling time+cycles}}{\text{ADC Clock}} \tag{5.18}$$

Due to there are just two ADC channels in STM32F103C8, and for increasing the work performance, DMA is used for converting.

After testing the output of the current sensor, we noticed that the output voltage is 2.5 V while there is not any load in the input.

For finding the digital data, the following code was used.

HAL_ADC_Start_DMA(&hadc1,data,3);

After finding the digital data by using the following equation, we can find the voltage that is sensed.

$$\text{volt} = \left(\frac{3.3}{4096}\right) * \text{data} \tag{5.19}$$

The voltage that was calculated in the previous equation was given 2.5 volt so,2.5 volt will be the offset value for our calculation. The following code is showing the process.

```
Volt1=(3.3/4096)*data[0];
Volt2=(3.3/4096)*data[1];
Volt3=(3.3/4096)*data[2];
Main_volt1=volt1-2.5+0.15;
Main_volt2=volt2-2.5+0.15;
Main_volt3=volt3-2.5+0.15;
```

The (0.15) equation is the error found while testing the values of volt1,volt2, and volt3. Moreover, as mentioned in the datasheet of the ACS712 current sensor, the sensitivity of the particular module is 0.185. Moreover, for finding the current, we divided the main_volt to the sensitivity of the current sensor.

I_a=Main_volt1/0.185;

I_b=Main_volt/0.185;

I_c=Main_volt/0.185;

For sensing the speed directly, 72 MHz was used in the timers, and the encoder mode was used in the program for sensing the pulses of the encoder.

In the following code, we can sensing the pulses

```
HAL_TIM_Encoder_Start(&htim1,TIM_CHANNEL_ALL);
```

Sensing the pulses well can give the angle of the shaft of the motor while it is rotating by this equation that is used in the code.

```
encoder = htim1.Instance->CNT;
angle_mech= (CountS)*0.36;
angle_electrical=(P/2)*angle_mech;
```

After sensing the pulses well, the rising edge in each channel of the encoder was measured by using the interrupt mode between the TIM1 that from there we sensed the pulses and TIM3 that from there we would measure the time as shown below.

```
HAL_TIM_IC_Start_IT(&htim3,TIM_CHANNEL_1);
rise = htim3.Instance->CCR1;
```

from rising, we can find the speed of the motor.

Second: From this step, we can say that the algorithm of FOC will start as mentioned before. The first step is transforming the three-phase current to a two-phase current using the Clark and Park Transformation.Figure 5.17 showing the hardware setup for sensing current and speed.

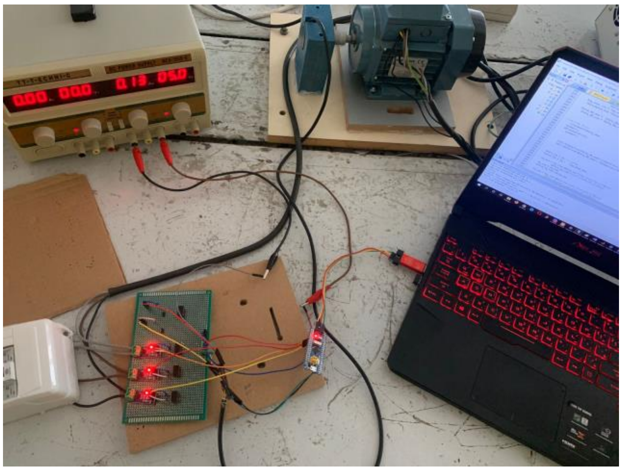

Figure 5.17. Hardware setup for sensing current and speed

- Clark Transformation :

From Clark Transformation, we can see that the three-phase current can be changed to a two-phase current (Alpha) and (Beta). The Clark equations give as a two sine wave that there is a 90-degree phase shift between them. The following code shows the transformation by code.

I_{alpha}=(3/2)*I_a;

I_{beta}=(0.866*I_b)-(0.866*I_c);

- Park Transformation:

From Park Transformation, we can see that the 2 sine waves from the Clark step can change to two DC values of current, that is (Q) and (D), and they are in the reference frame as mentioned before. For finding I_q and I_d, we need (I_{alpha}, I_{beta}, and rotor flux angle) for finding the angle the angle_electrical will use that found in the first step with angle_ω_{sl} the following equation

$$\omega_{sl} = \frac{1}{\tau_r * i_{mrd}} * i_{sq} \tag{5.20}$$

When i_{mrd} is equal to i_{sd} in stady state condition

$$\omega_{sl} = \frac{1}{\tau_r * i_{sd}} * i_{sq} \tag{5.21}$$

Now we should transfer the (5.21) equation to frequency domain

$$\theta_{(s)} = (\omega_{rs}) + \frac{isq}{\tau_r * i_{sd}} * \frac{1}{s} \tag{5.22}$$

then

$$\theta_{rk+1} = \omega_{mk} T_S + \frac{1}{\tau_r} \frac{iq}{id} T_s + \theta_{rk} \tag{5.23}$$

the equation of I_q and I_d it will be

$$i_d = i_\alpha * \cos(\theta) + i_\beta * \sin(\theta) \quad (5.24)$$

$$i_q = -i_\alpha * \sin(\theta) + i_\beta * \cos(\theta) \quad (5.25)$$

The result of the second step was the DC value, and we can control this DC value.

Third: as mentioned in chapter three, for controlling IM by IFOC PI controller will be using the design of the PI controllers that have done in chapter three (Transfer function of PI) will transfer from the time domain to frequency domain.

For current controller

$$V_{sd}(k) = V_{sd}(k-1) + (I_{sd}^* - I_{sd}) * \left(286.47 + 281983.87 * \frac{T}{2}\right) + (I_{sd}^* - I_{sd})(k-1) * (-286.47 + 281983.87 * \frac{T}{2}) \quad (5.26)$$

$$V_{sq}(k) = V_{sq}(k-1) + \left(I_{sq}^* - I_{sq}\right) * \left(286.47 + 281983.87 * \frac{T}{2}\right) + \left(I_{sq}^* - I_{sq}\right)(k-1) * (-286.47 + 281983.87 * \frac{T}{2}) \quad (5.27)$$

For flux controller

$$I_{sd}^*(k) = I_{sd}^*(k-1) + (I_{mrd}^* - I_{mrd}) * \left(5.27 + 374.38 * \frac{T}{2}\right) + (I_{mrd}^* - I_{mrd})(k-1) * (-5.27 + 374.38 * \frac{T}{2}) \quad (5.28)$$

For Speed controller

$$I_{sq}^*(k) = I_{sq}^*(k-1) + (\omega_r^* - \omega_r) * \left(0.00448 + 0.1267 * \frac{T}{2}\right) + (\omega_r^* - \omega_r)(k-1) * (-0.00448 + 0.1267 * \frac{T}{2}) \quad (5.29)$$

Fourth: After controlling the signal in the third step, the signal will be changed again to a two sine wave with a 90-degree phase shift between them. For this reason, the inverse park method will be used as follow.

$$V_\alpha = V_d * \cos(\theta) - V_q * \sin(\theta) \quad (5.30)$$

$$V_\beta = V_d * \sin(\theta) + V_q * \cos(\theta) \quad (5.31)$$

In this step, the updated angle should be select, which means the same angle can not be chosen as the second step.

Fifth: In this step, we will transfer the signals in step fourth to a three sine wave with 120 degrees between them.

$$V_a = \frac{2}{3} V_\alpha \tag{33.5}$$

$$V_b = -\frac{1}{3} V_\alpha + \frac{1}{\sqrt{3}} V_\beta \tag{5.32}$$

$$V_c = -\frac{1}{3} V_\alpha - \frac{1}{\sqrt{3}} V_\beta \tag{5.33}$$

Sixth: In the result of the fifth step, we had a three sine wave for doing the final step was working on SVPWM we need a triangular wave so, the same processer for building the triangular in open-loop will be used with 10 kHz frequency.Figure 5.18 showing the final hardware setup for closed loop control. And in figure 5.19 we can see the flow chart of close loop control.

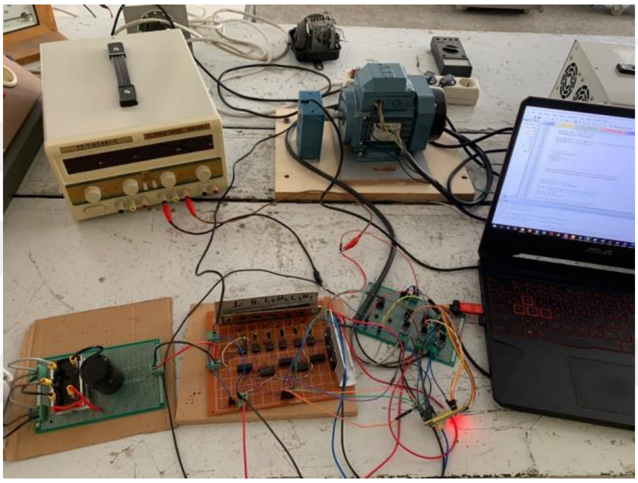

Figure 5.18. Hardware setup for closed loop control

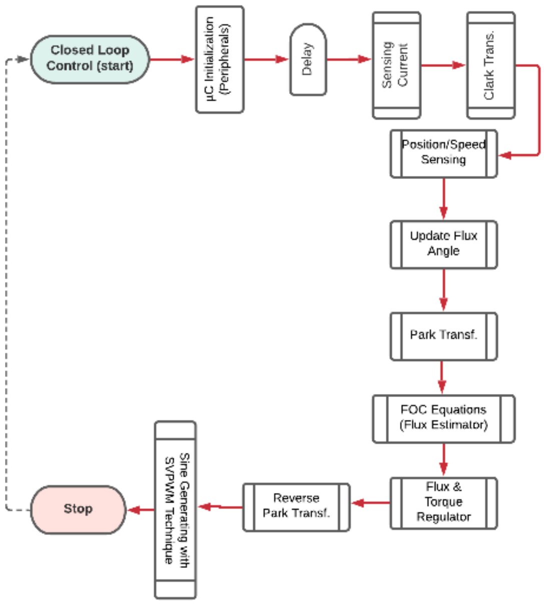

Figure 5.19. Flow chart of close-loop-test

6. RESULTS AND DISCUSSION

In this section, the results of the chapter four that was about modeling of three phase IM and control of three phase IM will be present and the results of practical works will discuss that done in chapter five.

6.1. Experimental tests for three phase IM

For finding the 0.25 kW three phase IM two ways used first one the experimental tests (no-load, load, DC, blocked rotor tests) is done the second one is hand calculation way using the name plat information and vector diagram and equivalent circuit of the three phase IM.

DC Test of three-phase IM: Table 6.1 shwoing the valuse from DC test.

Table 6.1. Reading of DC test of 3-phase IM

Voltage (V)	**Current(A)**
5.09	0.190
10	0.375
15	0.553
19.2	0.702

The DC resistance may be calculated as follows:

$$R_{dc} = \frac{V_{dc}}{I_{dc}} = \frac{19.2}{0.702} = 27.35\ \Omega$$

$\text{Skin effect} = 1.01 \text{ or } 1.15$

$R_1 = 27.35 * 1.01 = 27.62\ \Omega$ for one phase. Line to nutral.

No load Test of Three-phase IM: Table 6.2 shwoing the valuse from no-load test.

Table 6.2. Reading some data from the no-load test-delta connection

Parameter	Value
Voltage (V)	220
Current (A)	0.772
Power (W)	65
Power Factor	0.22
Starting Rotating (v)	47

$\theta = \cos^{-1} 0.22 = 77.29$ $\sin 77.29 = 0.975$

$$I_c = I_1 * \cos\theta = \frac{0.772}{\sqrt{3}} * 0.22 = 0.098 \text{ A}$$

$$I_m = I_1 * \sin\theta = \frac{0.772}{\sqrt{3}} * 0.975 = 0.434 \text{ A}$$

$$X_m = \frac{V_{ph}}{I_m} = \frac{220}{0.434} = 506.9\Omega$$

$$L_m = \frac{X_m}{2 * \pi * f} = \frac{506.9}{314} = 1.614 \text{ H}$$

Blocked Rotor Test of Three-phase IM : Table 6.3 shwoing the valuse from blocked rotor test.

Table 6.3. Reading some data from blocked rotor test-delta connection

Parameter	Value
Voltage (V)	57.2
Current (A)	1.20
Power (W)	85.3
Power Factor	0.72

$$R_{1e} = \frac{P_{sc}}{3(I_{sc})^2} = \frac{85.3}{3 * (1.2/\sqrt{3})^2} = \frac{85.3}{3 * 0.479} = 59.359\ \Omega$$

$$R_2' = R_{1e} - R_1 = 59.359 - 27.62 = 31.73\ \Omega$$

$$Z_{1e} = \frac{57.2}{0.6928} = 82.56\ \Omega$$

$$X_{1e} = \sqrt{Z_{1e}^2 - R_{1e}^2} = \sqrt{6816.15 - 3523.49} = 57.38\ \Omega$$

$$X_{1e} = X_1 + X_2' = 57.38\ \Omega$$

Load test of Three-phase IM: Table 6.4 shwoing the valuse from load test.

Table 6.4. Result of load test

Parameter	Value				
Torque(N/m)	0	0.1	0.2	0.3	0.4
Voltage(V)	400	400	400	400	400
Current(mA)	558	608	658	701	744
Power(W)	110	224	286	330	372
Power Factor	0.28	0.52	0.62	0.65	0.67
Speed(rpm)	2980	2900	2868	2833	2810

Calculation By Hand: In table 6.5 we can see all the IM parameter calculated by hand

Table 6.5. Parameter of 0.25 kw IM

Parameter of Motor	Value
Phase Voltage (V)	220
Phase Current (A)	0.69
Electrical input power(W)	314.226
Rated Torque (Nm)	0.8526
Effincey	0.795
Slip	0.06
I_r (A)	0.4761
I_o (A)	0.4993
L_s (H)	1.4864
L_r (H)	1.4866
L_o (H)	1.402
Stator leakage factor	0.06
Rotor leakage factor	0.06
R_r (ohm)	27.72
l_r (Stator leakage inductance)(H)	0.0844
l_r (Rotor leakage inductance)(H)	0.0846
Starting Current(A)	4.14

The calculation in detail is in appendix.

6.2. Simulation of IM Without Control

As mentioned in chapter two according to load- torque characteristic the speed will be decreasing when we increase load torque. the motor is connected in DOL without controlling. the following figures show that the decreasing of speed when the load torque is increasing.

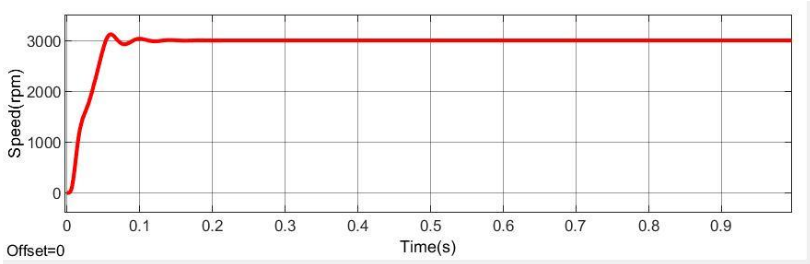

(a)

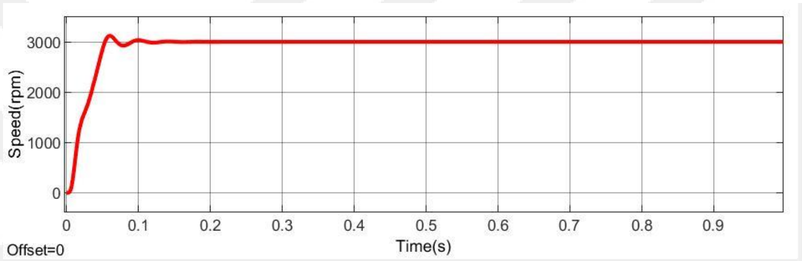

(b)

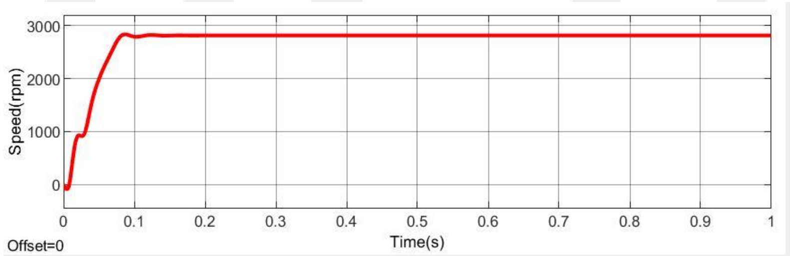

(c)

Figure 6.1. Speed of motor when load torque is (a) zero (b) 0.4 Nm (c) 0.8 Nm

As shown in the figure 6.1, a- the speed in no-load mode or once the load torque is zero is almost 2990 rpm. b- When we increased load torque at 0.1 s to 0.4 Nm that is half of rated torque the speed decreased directly.c- By increased load torque at 0.1 s to 0.8 Nm that is rated torque the speed decreased directly to nearly 2800 rpm.

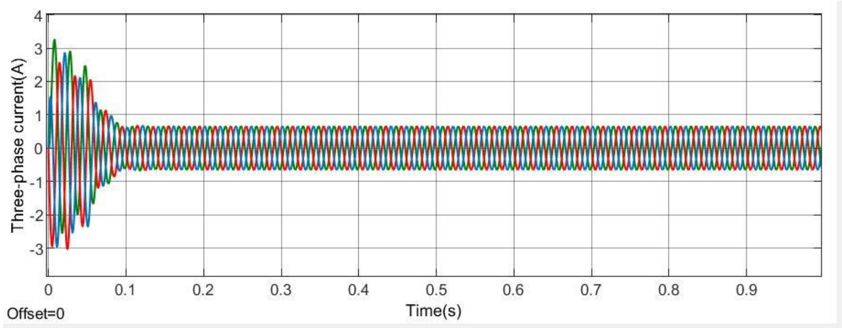

(a)

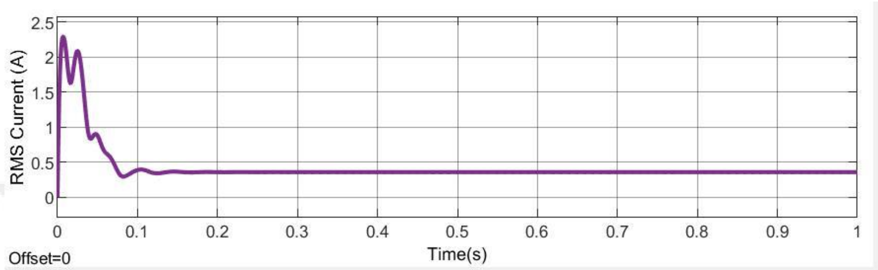

(b)

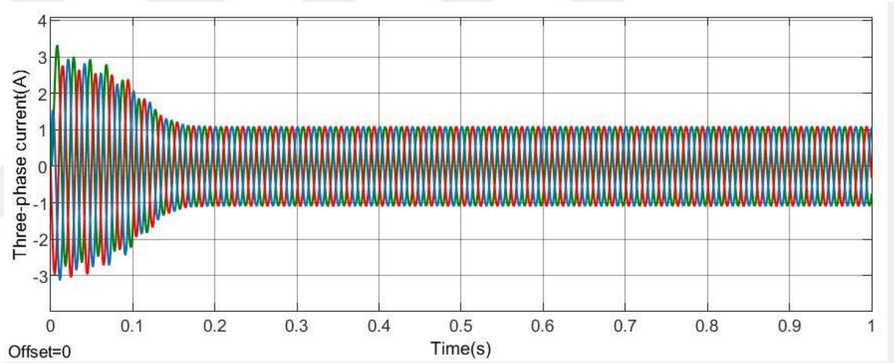

(c)

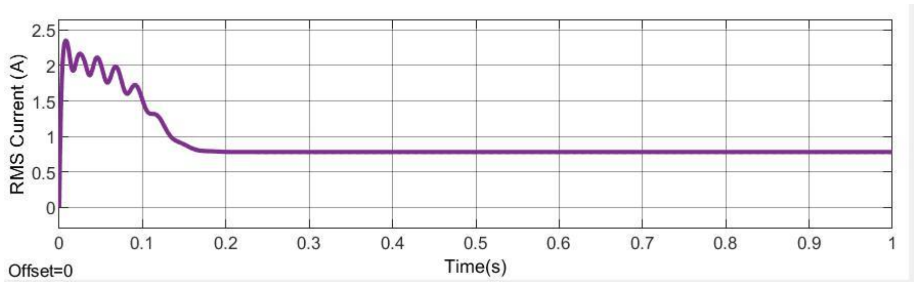

(d)

Figure 6.2. (a) Current in abc coordinate(No-load) (b) RMS current (no-load) (c) current in abc coordinate(Full-load) (da) RMS current (Full-load)

From figure 6.2 we can see that in no load condition (when load torque is equal to 0) the current is equal nearly 0.4 A and we can see that in full-load condition (when load torque is equal to 0.8) the phase current is equal to 1.2 A and the line to line current is equal to 0.69 A. By comparing simulation result to no-load test and load test of 0.25 kW three-phase IM. We can see that the modeling of IM in DOL operation is right. An essential point to note is that all of the numbers in this section show that this high current will impact the electric motor but might destroy the windings during a sudden start current (6 than rated), resulting in a longer transient duration. This is one reason why it is not preferable to use the direct operation method when good transient performance is needed. As shown by other operating methods, this high starting current must be controlled.

6.3. Simulation of Controllers

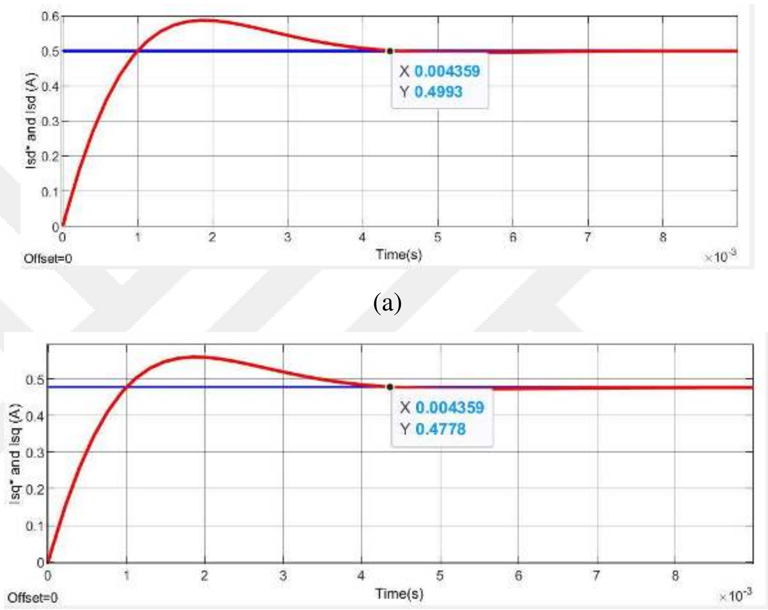

(b)

Figure 6.3. (a) Closed loop current response for I_{sd} (b) Closed loop current response for I_{sq}

In figure 6.3 we can see that the red one is response of PI controller in both d axise and q axise and blue is a refrense value for a- d is equal to 0.4993 A for b- q is equal to 0.4778 A

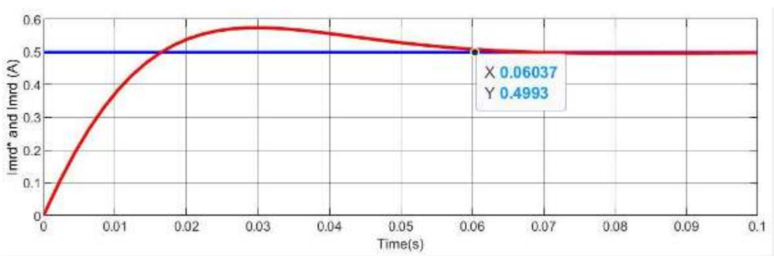

Figure 6.4. Response of flux loop control

In figure 6.4 we can see that the red one is respose of i_{mrd} while the blue is refrense value that is equal to i_d.

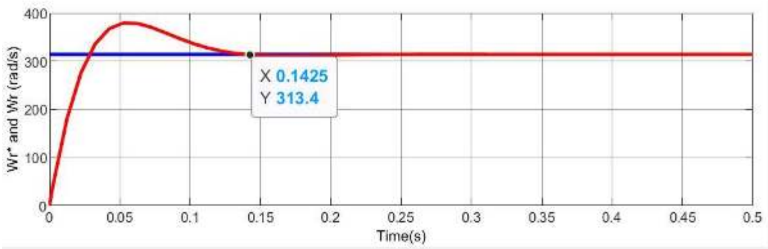

Figure 6.5. Response of speed loop

In figure 6.5 we can see the response of speed PI controller while we give 313 rad/s as a refrense value.

6.4. Simulation of Current Loop Controller with IM

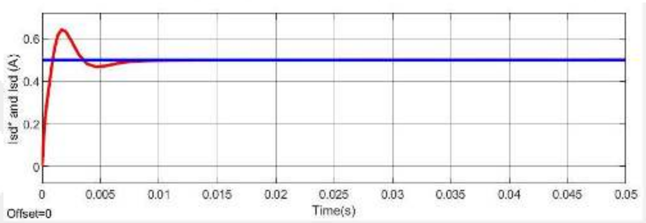

(a)

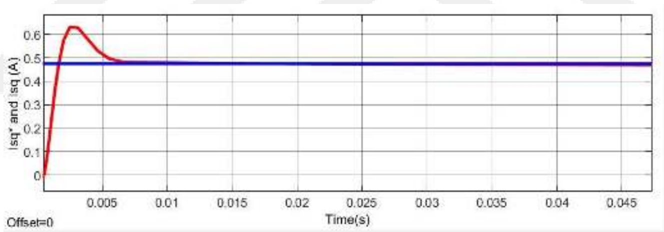

(b)

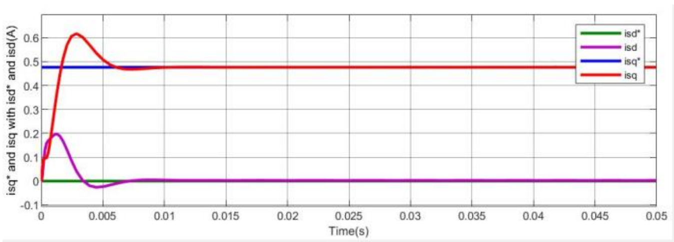

(c)

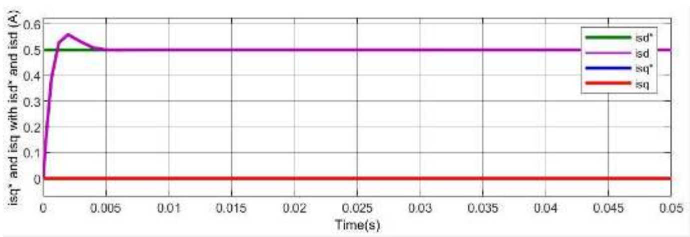

(d)

Figure 6.6. Response of current controller in different condition

In figure 6.6 a and b the rated value of i_{sd} and i_{sq} (0.4993 A and 0.4762 A) when the load torque is zero, and in c show that when isd is zero and i_{sq} in the rated value that is 0.4762 A and in d the graph of zero i_{sq} and rated isd is showed both of them is done when load torque is zero.

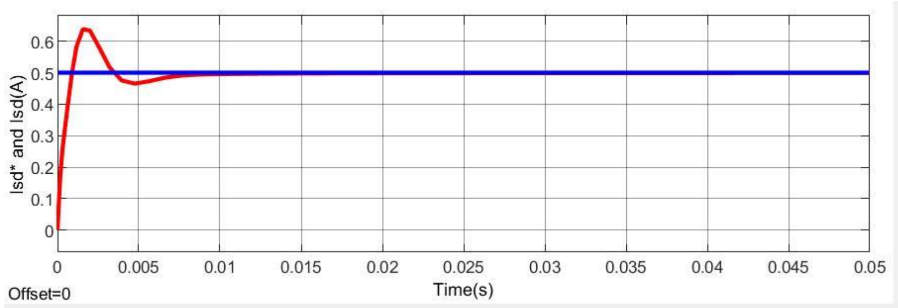

(a)

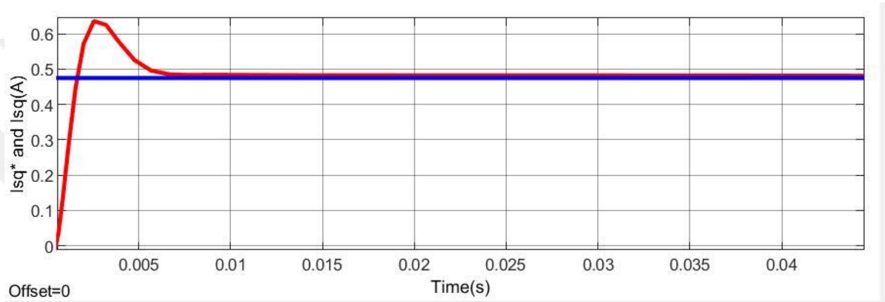

(b)

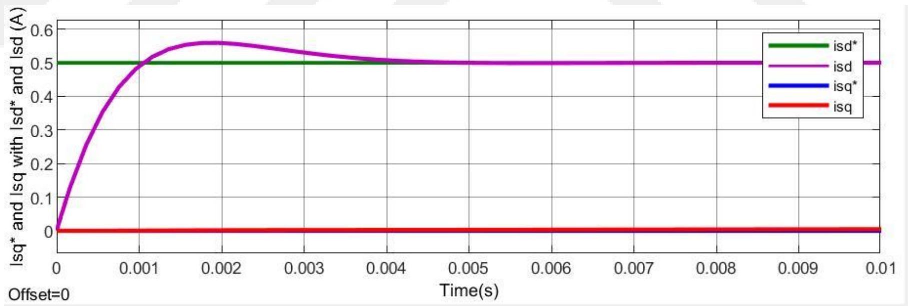

(c)

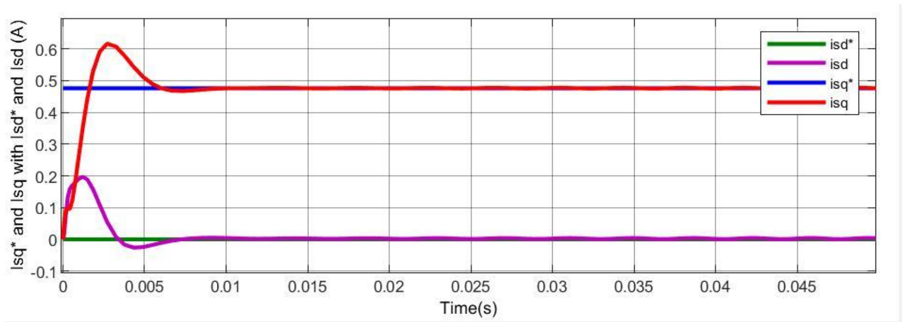

(d)

Figure 6.7. Response of current controller in different condition (full Load)

In figure 6.7 (a and b) the rated value of i_{sd} and i_{sq} (0.4993 A and 0.4762 A) when the load torque is maximum (0.8 Nm) , and in d show that when i_{sd} is zero and i_{sq} in the rated value that is

0.4762 A and in c the graph of zero i_{sq} and rated i_{sd} is showed both of them is done when load torque is (0.8 Nm).

6.4.1. Simulation Current Loop Controller and Compensention Term with IM Model

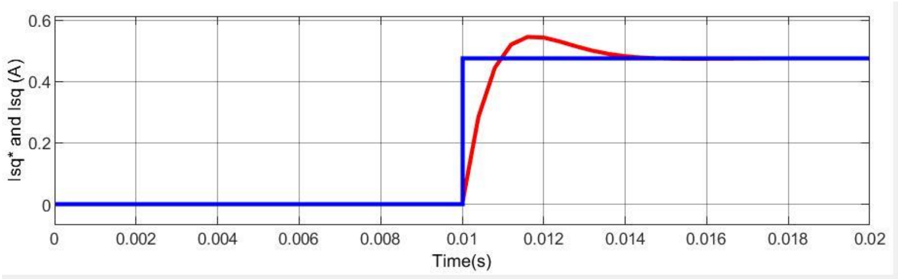

(a)

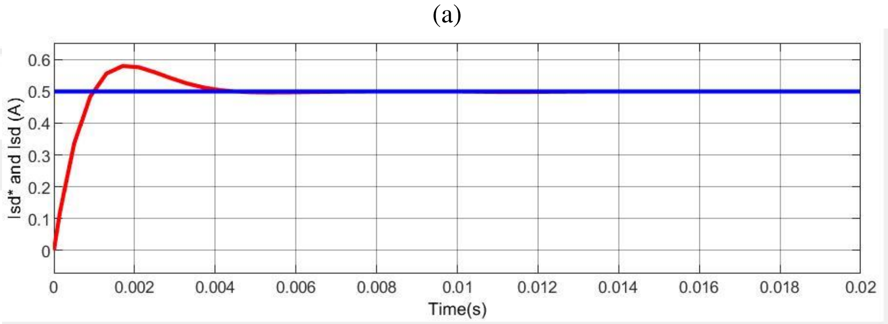

(b)

Figure 6.8. Controller response with voltage compensation a- is i_{sq} response while b is isd response (no-load)

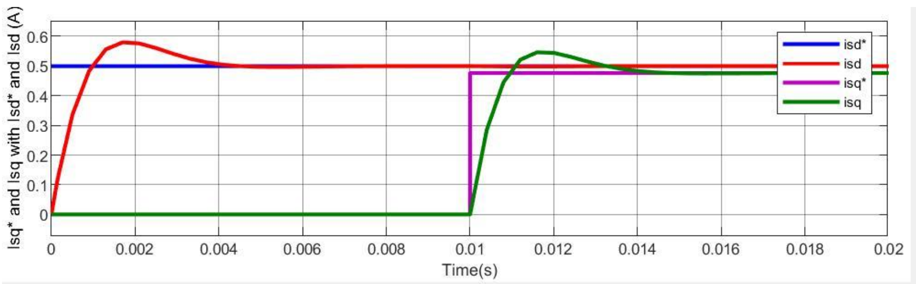

Figure 6.9. Controller response with voltage compensation (full-load)

As seen in figure 6.8 and 6.9, with a voltage compensation term, the i_{sd} takes less time to achieve a steady state value and has a very tiny overshoot. and it is due to i_{sq} affects the Isd when we do not using voltage compensation term. Another essential consideration when utilizing the phrase voltage compensator is feed forwards. It reduces sensitivity to bad controllers and attempts to reduce the system's reliance on feedback.

6.5. Simulation of IM Controlled by IRFOC

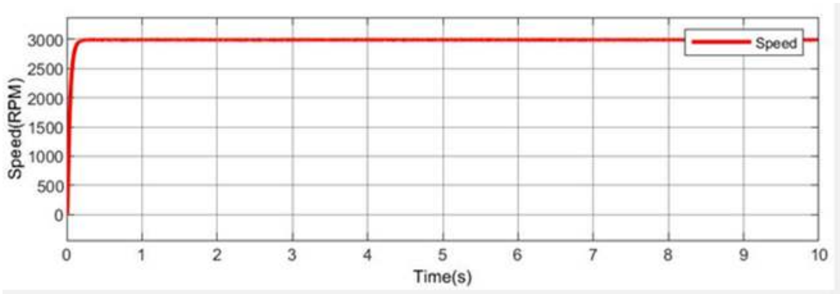

(a)

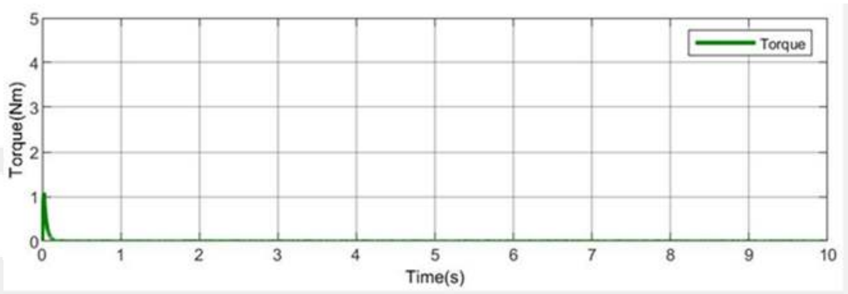

(b)

Figure 6.10. We can see the behavior of the system in different load torque is zero.

In figure 6.10 we can see the response of speed when load torque is zero.

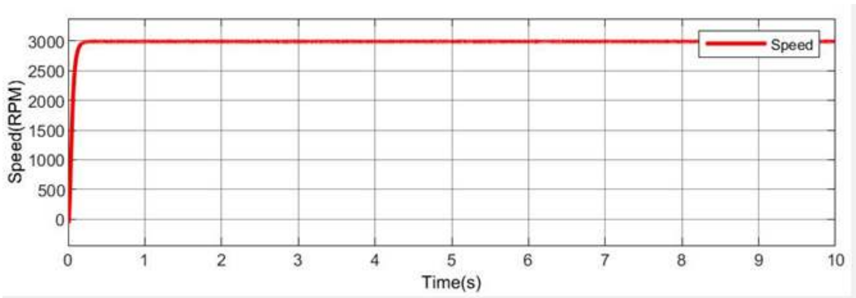

(a)

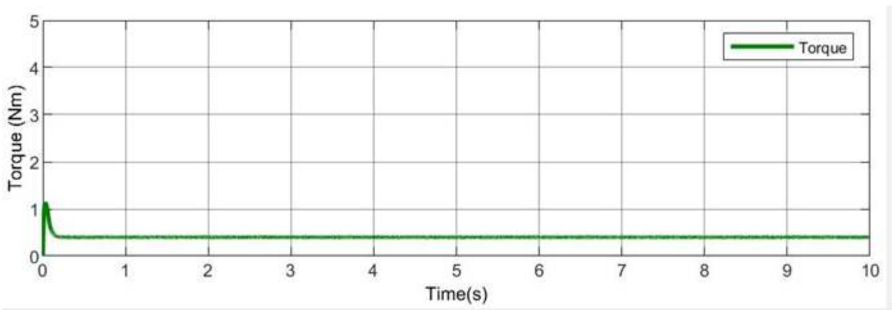

(b)

Figure 6.11. We can see the response of the system when we give the motor 0.4 Nm.

As we can see in figure 6.11 by increasing the load torque to 0.4Nm the speed still nearly 3000 rpm.

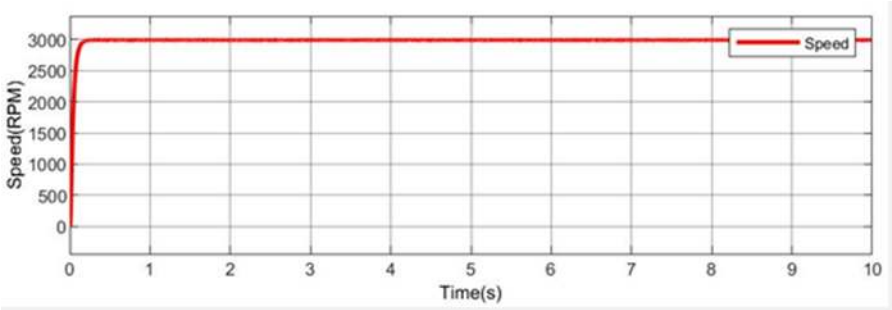

(a)

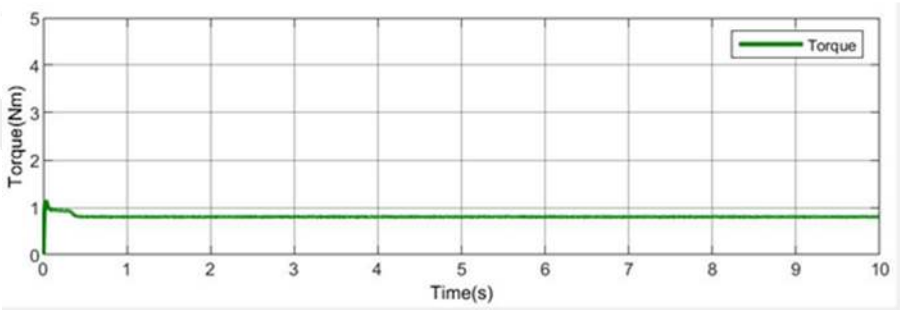

(b)

Figure 6.12. We can see the response of the system when we give IM 0.8 Nm that is maximum load torque.

As showed in the figure 6.12 by increasing the load torque to maximum that is 0.8 Nm the speed is still in nearly 3000 rpm.

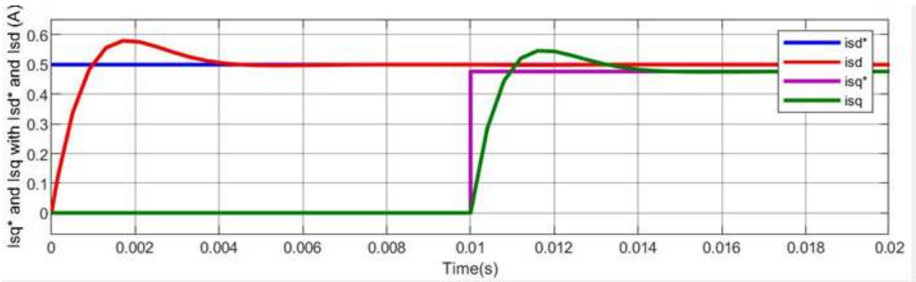

Figure 6.13. q and d axis current control

In figure 6.13 we can see the response of current controlled by Appling IRFOC.

6.6. Result of Open Loop Test

In this section the result of open loop test will be introduce in MATLAB and Practical by STM32F103C8 Micro controller.

6.6.1. Simulation of Open loop test

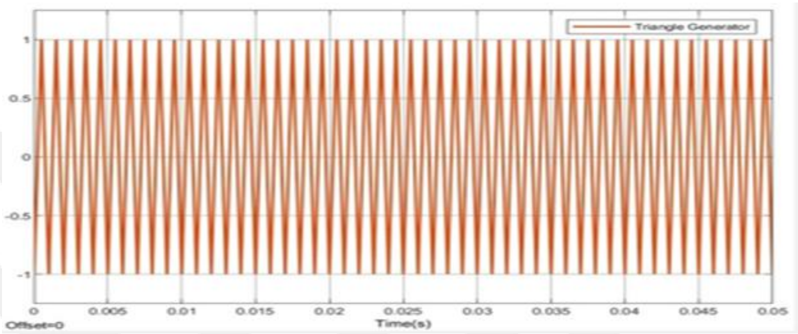

Figure 6.14. Triangular wave 5 KHz(simulation)

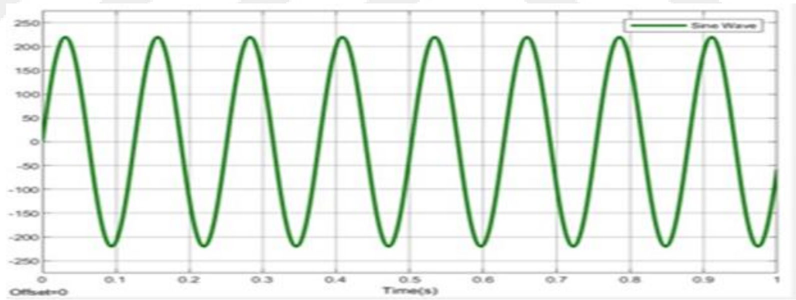

Figure 6.15. sine wave 50 Hz (simulation)

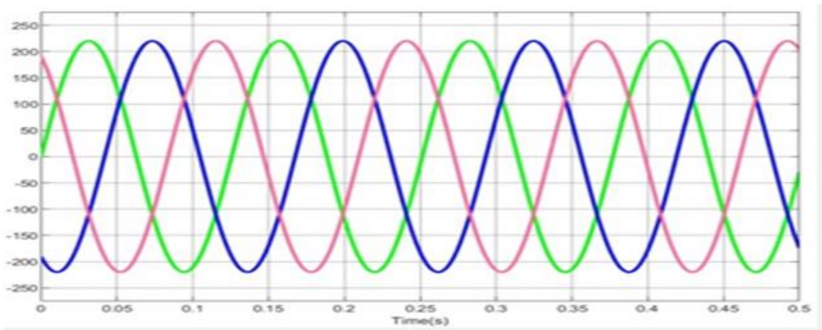

Figure 6.16. Three sine waves with a 120-degree phase shift (simulation)

In figure 6.14, 6.15 and 6.16 we can see the result of generating sine waves that they have phase shift between them by 120 degrees with 50 Hz. And also generating 5 KHz Triangular wave.

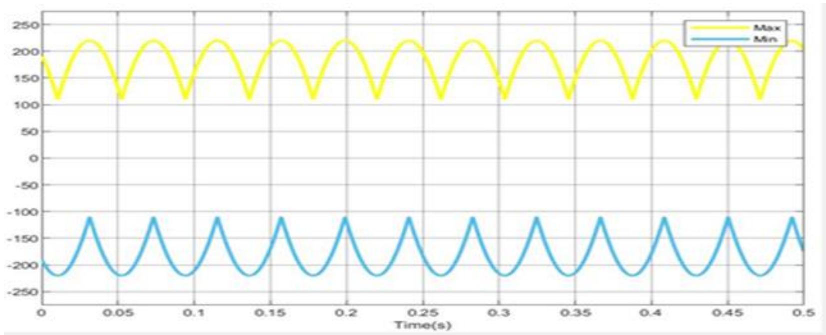

Figure 6.17. Result of Max and Min block (simulation)

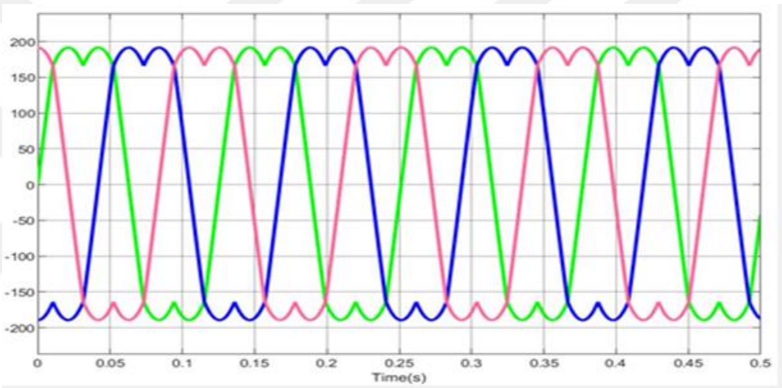

Figure 6.18. The result of harmonics before comparing with triangular wave (simulation)

In figure 6.18 we can see the three phase harmonices that produse due to the stepes of generating SVPWM signals.

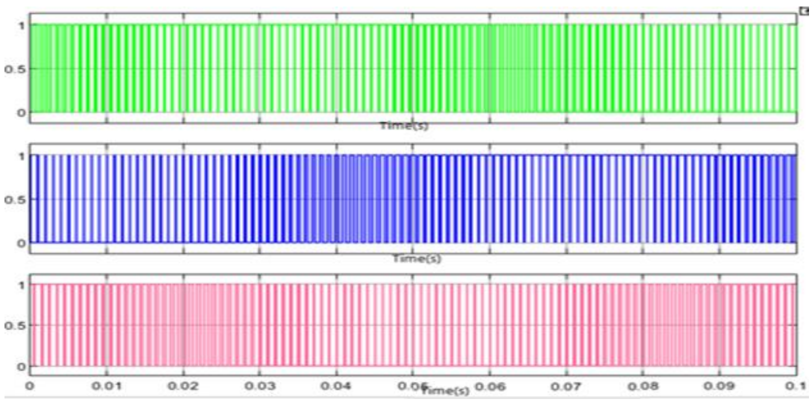

Figure 6.19. SVPWMH1, SVPWMH2 and SVPWMH3(simulation)

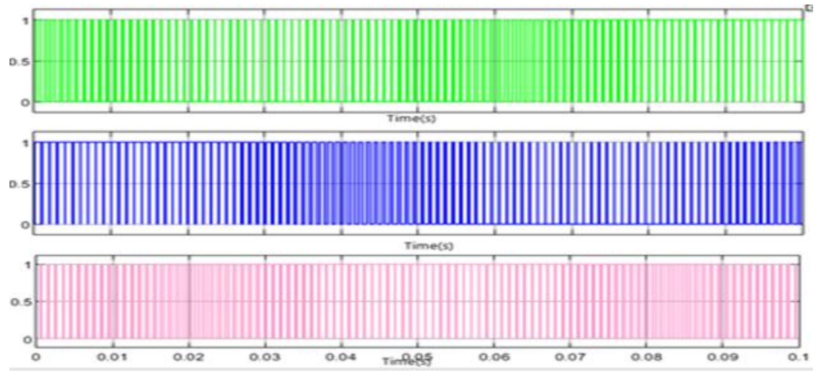

Figure 6.20. SVPWML1, SVPWML2 and SVPWML3 (Simulation)

In figure 6.19 we can see the result of SVPWMs for higher side IGBTs while figure 6.20 showing the result of SVPWMs for lower side IGBTs.

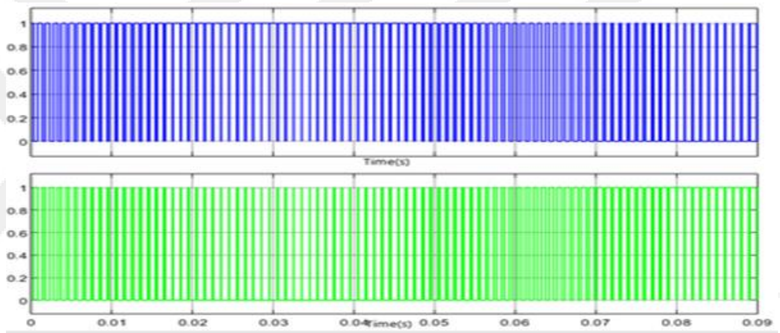

Figure 6.21. SVPWMH1 and SVPWML1 (simulation)

In figure 6.21 we can see the signals for first leg of inverter.

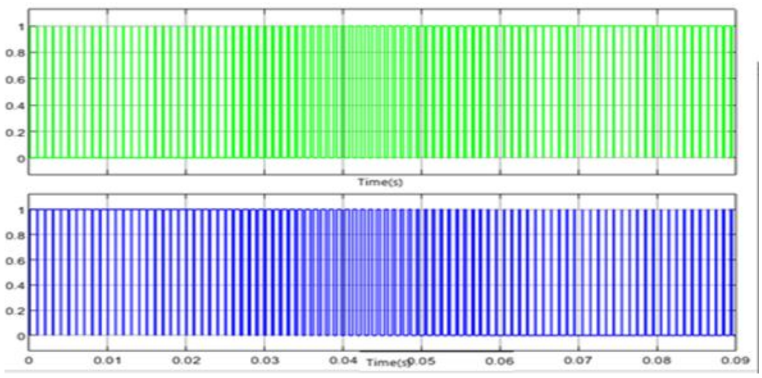

Figure 6.22. SVPWMH2 and SVPWML2 (simulation)

In figure 6.22 we can see the signals for second leg of inverter.

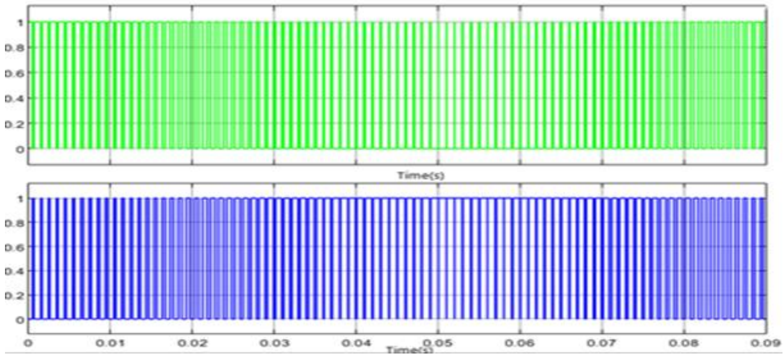

Figure 6.23. SVPWMH3 and SVPWML3 (simulation)

In figure 6.23 we can see the signals for third leg of inverter.

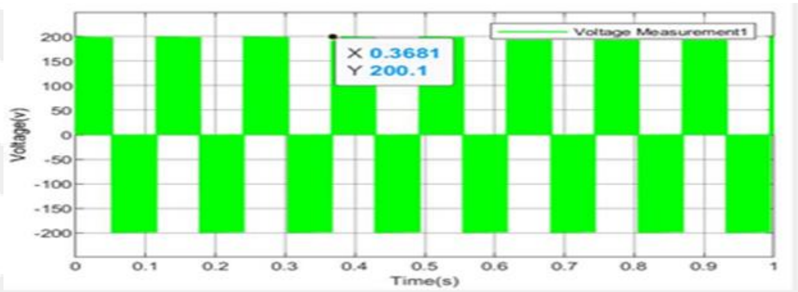

Figure 6.24. Line to line voltage 220 V (simulation)

In figure 6.24 finall result that is line to line voltage when we put 220 V as DC voltage to the inverter.

6.6.2. Practical Result of Open Loop Test

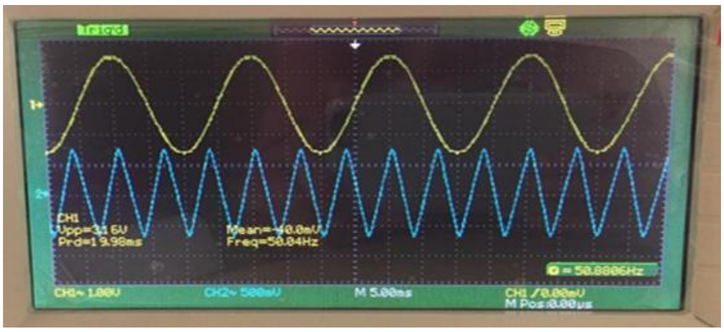

Figure 6.25. One of the sine waves with rectangular wave (practical)

Figure 6.25 showing as the result of sine wave and trainguler wave that generated by PWM in STM32F103C8.

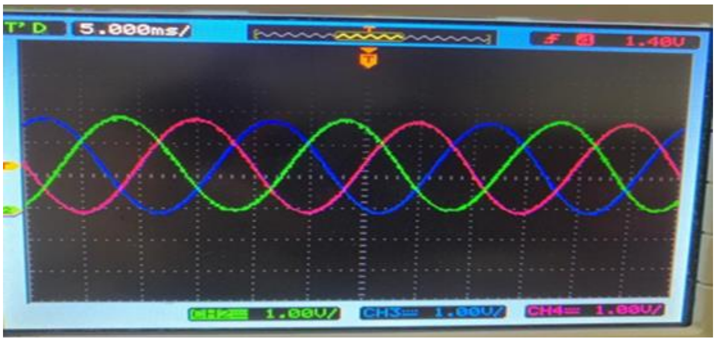

Figure 6.26. Three sine waves with a 120-degree phase shift (practical)

Figure 6.26 shwoing the result of generating three sine wave that they have phase shift between them by 120 degree.

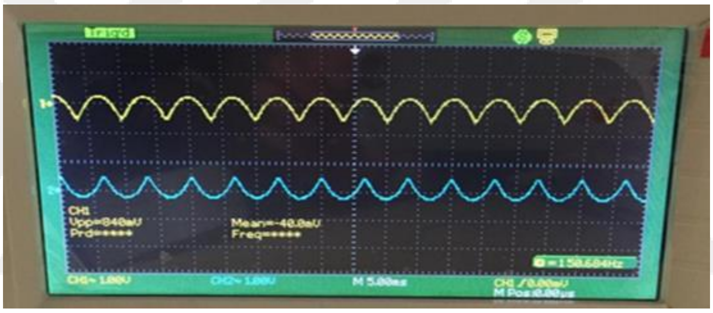

Figure 6.27. The result of the Max and Min equation (practical)

In figure 6.27 we can see the maximum and minimum of three sine waves that generated in figure 6.26.

Figure 6.28. The result of harmonics before comparing with triangular wave (practical)

In figure 6.28 we can see the three phase harmonices that produse due to the stepes of generating SVPWM signals.

Figure 6.29. SVPWMH1, SVPWMH2 and SVPWMH3(practical)

Figure 6.30. SVPWML1, SVPWML2 and SVPWML3(practical)

In figure 6.29 we can see the result of SVPWMs for higher side IGBTs while figure 6.30 showing the result of SVPWMs for lower side IGBTs.

Figure 6.31. SVPWMH1 and SVPWML1 (practical)

In figure 6.31 we can see the signals for first leg of inverter.

Figure 6.32. SVPWMH2 and SVPWML2 (practical)

In figure 6.32 we can see the signals for second leg of inverter.

Figure 6.33. SVPWMH3 and SVPWML3 (practical)

In figure 6.33 we can see the signals for third leg of inverter.

Figure 6.34. Line to line voltage when 10 volt is give to inverter

In figure 6.34 finall result that is line to line voltage when we put 10 V as DC voltage to the inverter.

6.7. Result of Closed Loop Test

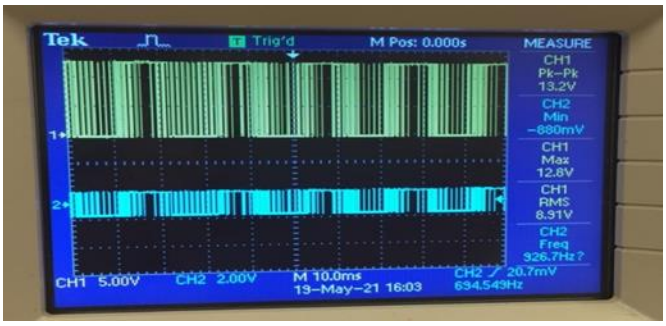

Figure 6.35. SVPWM signal in input and output of optocoupler

Figure 6.35 showing the effect of using the optocoupler for increaseing the signals voltage and also isolating the higher side volatge to lower side voltage.

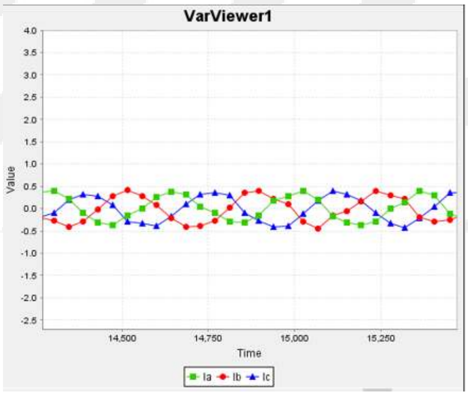

Figure 6.36. The output of the current sensor while the motor is running

In figure 6.36 we can see the result of sensing the motor's current by using current sensor and STM32F103C8 microcontroller and seeing the result by STM Studio.

Figure 6.37. The pulses of the encoder in practical

In figure 6.37 the pulses from the incremental rotary encoder is showed. Green one is channel A while the pink one is channel B.

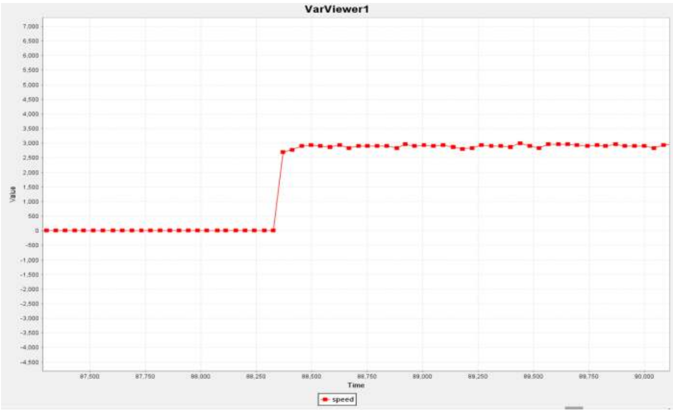

Figure 6.38. The result of Incremental rotary encoder

In figure 6.38 we can see the working of incremental rotary encoder from stop and run mode of motor in no-load condition.

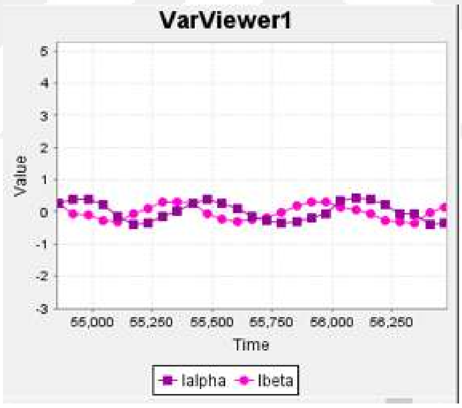

Figure 6.39. Clark transformation (practical)

In figure 6.39. we can see the result of appling clark transformation to a three phase current that we found in figure 6.36 we can notice that the have phase shift between them by 90 degree.

7. CONCLUSION

A three-phase IM modeled and worked in DOL condition according it is simulation we saw that when we increase the load torque, the speed is decreasing, so an IRFOC used to control the motor in every situation, for this reason, a three PI controller designed and for designing this controller the (Load, No-load, Blocked rotor, and DC test) done. After testing the PI controller with a three-phase IM, we saw that by increasing the load torque, the speed is constant (do not decrease) for increasing the control system performance a lookup table designed to stop working when we give more than the rated torque to the motor that is 0.8 Nm. In practice, it will protect the motor due to, as we understand, by increasing the load, the value of i_q will be increase, and by increasing the value of i_q also I_q will be increased and this makes the motor damage practical if we give the motor extra voltage. In addition, a voltage compensator was created to decouple the d-axis and q-axis. When tested, it was discovered that the shifting flux and back emf are overcome. In addition, a field weakening approach was developed and included in the system. When investigated, it was discovered that the motor works faster while producing less torque, with no severe oscillation of the stator supplied voltage. Based on the results of both approaches, it can be proposed that for motors that do not necessitate excellent transient answers, the direct online method is preferable, however when it comes to good performance, constancy, and good transient reactions are required vector control method must be employed.

One of the peculiarities of this study is that the practical work provided in this thesis sought to interpret and understand the design and practical execution of the IFOC of induction motor and governed employing an STM32 platform. At In the first stage, a sensor board were designed and implemented where three current transducers are used to sense the current of each phase. Additionally, an encoder is used to measure the speed of the motor. Moreover, the inverter board and rectifier board designed for testing them with three-phase IM and SVPWM Signals designed by STM32F103C8 next step the IRFOC implemented in STM32F103C8 and motor control.

RECOMMENDATIONS

1. As we saw it while the motor is working the temperature will increase and the parameter will be change specially rotor time constant solving this problem will increase the performance of the system.

2. Apply DFOC on IM using STM32 Serise.

3. Apply IRFOC on PMSM motor using STM32 Serise.

REFERENCES

[1] Liu, H., Zhou, Y., Jiang, Y., Liu, L., Wang, T., & Zhong, B. (2005, September). Induction motor drive based on vector control for electric vehicles,*International Conference on Electrical Machines and Systems* ,Vol.1,861-865. doi: 10.1109/ICEMS.2005.202661.

[2] Hashemnia, N., & Asaei, B. (2008, September). Comparative study of using different electric motors in the electric vehicles.*18th International Conference on Electrical Machines* ,1-5. doi: 10.1109/ICELMACH.2008.4800157.

[3] Herwald, M. A. (1999). *Control Design and analysis of an advanced induction motor electric vehicle drive* Doctoral dissertation, Virginia Tech.

[4] Patra, N. (2013). *Study of Induction motor drive with Direct Torque Control scheme and Indirect Field Oriented control scheme with Space Vector Modulation* ,Doctoral dissertation.National institute of technology.

[5] Şimşek, G. (2004). *Sensorless direct field oriented control of induction machine by flux and speed estimation using model reference adaptive system* ,Master's thesis, Middle East Technical University.

[6] Srilad, S., Tunyasrirut, S., & Suksri, T. (2006, October). Implementation of a scalar controlled induction motor drives.*SICE-ICASE International Joint Conference* ,3605-3610, doi: 10.1109/SICE.2006.314749.

[7] Sbita, L., & Hamed, M. B. (2007). Regular paper Internal Model Controller for Scalar Controlled Induction Motor Drive: Design and Experiments. *J. Electrical Systems*, Vol.*3*(2), 73-87,

[8] Bojoi, R., Guglielmi, P., & Pellegrino, G. M. (2008). Sensorless direct field-oriented control of three-phase induction motor drives for low-cost applications. *IEEE Transactions on Industry Applications*, Vol.*44*(2), 475-481, doi: 10.1109/IAS.2006.256627.

[9] Vaghela, D. J., Chaudhari, H. N., & Bardoli, G. I. (2015, January). Investigation of design, analysis and performance of hysteresis current control PMSM drive. In *Electrical, Electronics, Signals, Communication and Optimization (EESCO),* 1-6.doi: 10.1109/EESCO.2015.7254050.

[10] Shang, Z. (2011). Simulation and Experiment for Induction Motor Control. *Master of of Applied Science, University of Windsor, Windsor, Ontario*.

[11] Alnasir, Z. A., & Almarhoon, A. H. (2012). Design of direct torque controller of induction motor (DTC). *International Journal of Engineering and Technology (IJET)*,Vol. *4*(2), 54-70.

[12] Bitar, Z., & Al Jabi, S. (2014). Studying the performances of induction motor used in electric car. *Energy Procedia*, Vol.*50*, 342-351.

[13] Hussin, A. M. (2014). *Direct torque control induction motor drives* ,Doctoral dissertation, Universiti Tun Hussein Onn Malaysia.

[14] BT, V. G. (2017). Comparison Between Direct and Indirect Field Oriented Control of Induction Motor. *Int. J. Eng. Trends Technol*, Vol,*43*(6), 364-369.

[15] Kumar, A., & Ramesh, T. (2015, May). Direct field oriented control of induction motor drive. In *2015 Second International Conference on Advances in Computing and Communication Engineering* ,219-223, doi: 10.1109/ICACCE.2015.55.

[16] Liu, H., Tian, J., Gai, Y., & Huang, S. (2010, August). Design of controlling system about the high-power PMSM based on STM32,*International Conference on Computer, Mechatronics, Control and Electronic Engineering* ,Vol. 4,374-377, doi: 10.1109/CMCE.2010.5610141.

[17] Guo, Z., Zhang, J., Sun, Z., & Zheng, C. (2017). Indirect field oriented control of three-phase induction motor based on current-source inverter. *Procedia engineering*, Vol.*174*, 588-594.

[18] Zhang, C., & Wang, N. (2017, May). Research on asynchronous motor control of electric vehicle. In *2017 International Conference on Mechanical, System and Control Engineering (ICMSC)* ,165-169, doi: 10.1109/ICMSC.2017.7959464.

[19] Agrawal, A., Nema, P., & Lodhi, R. S. (2018). Comparison between Scalar & Vector Control Technique for Induction Motor Drive. *International Research Journal of Engineering and Technology*,Vol. *5*(6), 2504-2509.

[20] Begh, M. A. W., & Herzog, H. G. (2018). Comparison of field oriented control and direct torque control. *Technical University of Munich, Germany*.

[21] Annuar, K. A. M., Sapiee, M. R. M., Nor, R. M., Azali, M. S. M., Shah, M. B. N., & Rozali, S. M. (2019). Squirrel cage induction motor scalar control constant V/F analysis. *TELKOMNIKA (Telecommunication Computing Electronics and Control)*, Vol.*17*(1), 417-424.

[22] Suresh, S., & Rajeevan, P. P. (2020). Virtual space vector-based direct torque control schemes for Induction Motor Drives. *IEEE Transactions on Industry Applications*, Vol.*56*(3), 2719-2728.

[23] Qinglong, W., Changzhou, Y., & Shuying, Y. (2020, July). Indirect Field Oriented Control Technology for Asynchronous Motor of Electric Vehicle. In *2020 IEEE International Conference on Power, Intelligent Computing and Systems (ICPICS)* ,673-677.,doi: 10.1109/ICPICS50287.2020.9201983.

[24] Yadav, S., & Mishra, A. K. (2020, February). Performance Evaluation in IFOC Induction Motor Drive with various PWM Techniques. In *2020 International Conference on Electrical and Electronics Engineering (ICE3)*,65-70,doi: 10.1109/ICE348803.2020.9122877.

[25] Kakodia, S. K., & Dynamina, G. (2020, June). A Comparative Study of DFOC and IFOC for IM Drive. In *2020 First IEEE International Conference on Measurement, Instrumentation, Control and Automation (ICMICA)*,1-5, doi: 10.1109/ICMICA48462.2020.9242909.

[26] Stopa, P. (2009). High speed field oriented control. *Aalborg University Institute of Energy Technology*.

[27] Abdelkarim, E. A. H. (2011). Control and measuring method for three phase induction motor with improved efficiency,PhD Thesis, Darmstadt University.

[28] Farasat, M., & Karaman, E. (2011, August). Speed sensorless electric vehicle propulsion system using hybrid FOC-DTC induction motor drive.*International Conference on Electrical Machines and Systems*,1-5, doi: 10.1109/ICEMS.2011.6073516.

[29] Zhai, L., & Li, H. (2008, September). Modeling and simulating of SVPWM control system of induction motor in electric vehicle.*IEEE International Conference on Automation and Logistics* ,2026-2030,doi: 10.1109/ICAL.2008.4636495.

[30] Singh, S., & Tiwari, A. N. (2017, March). Simulation and Comparison of SPWM and SVPWM Control for Two Level Inverter. In *Conference paper, Madan Mohan Malaviya University of Technology, Gorakhpur (UP) India*.

[31] Sabarad, J., & Kulkarni, G. H. (2015, August). Comparative analysis of SVPWM and SPWM techniques for multilevel inverter.*International Conference on Power and Advanced Control Engineering (ICPACE)*,232-237, doi: 10.1109/ICPACE.2015.7274949.

[32] Abood, S. I., & Raheem, M. S. A. (2014). Performance analysis of SPWM and SVPWM inverters fed induction motor. *International Journal of Computer Applications*, Vol.*86*(5),doi: 10.5120/14984-3191.

[33] Nam, K. H. (2017). *AC motor control and electric vehicle applications*. CRC press.

[34] Trzynadlowski, A. M. (2000). *Control of induction motors*. Elsevier.

[35] Filizadeh, S. (2013). *Electric machines and drives: principles, control, modeling, and simulation*. CRC Press.

[36] Abu-Rub, H., Iqbal, A., & Guzinski, J. (2021). *High Performance Control of AC Drives with Matlab/Simulink*. John Wiley & Sons.

[37] Chapman, S. (2005). *Electric machinery fundamentals*. Tata McGraw-Hill Education.

[38] Quang, N. P., & Dittrich, J. A. (2008). *Vector control of three-phase AC machines* (Vol. 2). Heidelberg: springer.

[39] Ahmad, M. (2010). *High performance AC drives: modelling analysis and control*. Springer Science & Business Media.

[40] Rashid, M. H. (Ed.). (2017). *Power electronics handbook*. Butterworth-Heinemann.

[41] https://en.wikipedia.org/w/index.php?title=STM32&oldid=1021771194 , Access :July 6, 2021.

[42] https://en.wikipedia.org/w/index.php?title=MATLAB&oldid=1025300740 , Access : July 6, 2021

[43] Kumar, R. R., Kumar, S., & Yadav, A. (2013). comparison of PWM techniques and inverter performance. *IOSR Journal of Electrical and Electronics Engineering (IOSR-JEEE)*, Vol.*4*(1), 18-22.

[44] Hughes, A., & Drury, B. (2019). *Electric motors and drives: fundamentals, types and applications*. Newnes.

[45] Ogata, K. (2010). *Modern control engineering*. Prentice hall.

APPENDICES

APPENDIX- 1:

In table A1.1 we can see the parameter of motor in it is name plat

Table A1. 1 Motor rated parameter by name plat

Motor Parameter	Value
Line to Line Voltage (v)	220
Rated Mechanical Power (kw)	0.25
Connection Type	Delta
Frequency (Hz)	50
Full-Load Power Factor	0.69
Line to Line Rated Current (A)	1.2
Rated Speed (rpm)	2800
Moment of Inertia	0.00016 kg.m^2
Line to Line Starting Current (A)	4.14

In induction motor, synchronous speed is faster than rated speed (Nr) which was given therefore, synchronous speed can be calculated and it is equal to 3000 rpm. Before calculating the requirements, certain essentials and fundamental parameters have been found from given parameters as shown.

$$\omega_e = 2 * \pi * f_e = 314.159 \frac{\text{rad}}{\text{s}}$$

$$\omega_e = 314.159 * \frac{60}{2 * \pi} = 3000 \text{ rpm}$$

$$V_{ph} = V_L = 220 \text{ v}$$

$$I_{ph} = \frac{I_L}{\sqrt{3}} = \frac{1.2}{\sqrt{3}} = 0.6928 \text{ Amp}$$

$Electrical\ input\ power = 3 * V_{s-rated} * I_{s-rated} * \cos\theta$ where $V_{s-rated}$ and $I_{s-rated}$ are phase quantity.

$$Electrical\ input\ power = 3 * 220 * 0.6928 * 0.69 = 315.5 \text{ w}$$

$$P_{mechanical-rated} = T_{rated} * \omega_{rated}$$

$$T_{rated} = \frac{250}{2800 * \frac{2 * \pi}{60}} = 0.8526 \text{ Nm}$$

$$\eta = \frac{P_{out}}{P_{in}} = \frac{250}{315.5} = 0.79 = \%79$$

$$S = \frac{n_s - n_r}{n_s} = \frac{3000 - 2800}{3000} = 0.066 \quad \text{So,} \quad S = 0.066$$

$$n_{sl} = 3000 - 2800 = 200 \rightarrow \omega_{sl} = 200 * \frac{2*\pi}{60} = 20 \text{ rad/s}$$

For calculating leakage inductances, at the starting instance, it is assumed that the motor is stationary which means speed is zero and slip is one. Supply voltage 220 V is applied, then RR/S is very small and << $\omega_e * L_r$, therefore, it can be neglected. Since at the starting, starting current is too large and I_o is very small, thus, the magnetizing inductance can also be neglected. Then per phase equivalent circuit can be drawn as shown in figure A1.1.

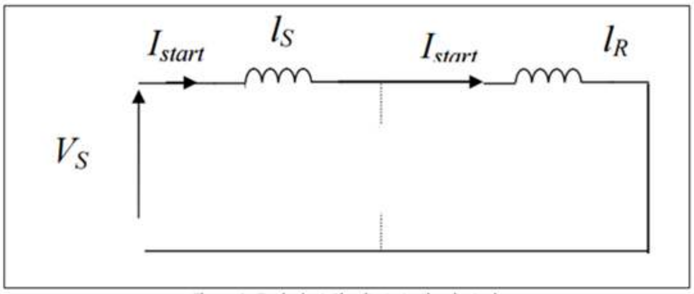

Figure A1.1. Equivalent Circuit at starting

$$I_{start} = 6 * 1.2 = 7.2 \text{ Amp}$$

$$V_s = j * \omega_e * (l_s + l_R) * I_{start}$$

$$(l_s + l_R) = \frac{V_s}{j * \omega_e * I_{start}}$$

$$= \frac{220}{2 * \pi * 50 * 4.14} \qquad (l_s + l_R) = 0.169 \text{ H} \ldots\ldots\ldots \text{equ (1)}$$

Since resistance values are available (R_s given and R_r obtained), their ratio can be obtained (R_s/R_r). Now, same ratio can be assumed for leakage inductances for calculating (l_s , l_r), because the number of turn ratio is direct proportional to both leakage inductances and resistance.

$\frac{l_s}{l_r} = \frac{R_s}{R_r}$ where $R_s = 27.62$ ohm given and $R_r = 27.72$ ohm calculated

$\frac{l_s}{l_r} = \frac{27.62}{31.73}$ $\quad l_s = 0.996\, l_r \ldots\ldots\ldots . . \text{equ}(2)$

By substituting equation 2 in equation 1

$0.996\, l_r + \; l_r = 0.169$ $\quad l_r = \frac{0.169}{1.996} = 0.0846 \text{ H}$

$l_s + 0.0846 = 0.169 \text{ H}$ $\quad l_s = 0.0844 \text{ H}$

Next step, calculating the stator and rotor self-inductances L_S , L_R and the leakage factors (σ)

$L_S = L_m + l_s$, $\quad L_R = L_m + l_R$, $\quad \sigma s = l_s/L_m$, $\quad \sigma r = l_r/L_m$,

$\sigma \approx \sigma s + \sigma r,$

$L_S = 1.402 + 0.0844 = 1.4864 \text{ H}$

$L_R = 1.402 + 0.0844 = 1.4866 \text{ H}$

$\sigma s = \frac{0.0453}{1.614} = 0.06$

$\sigma r = \frac{0.052}{1.614} = 0.06$

$\sigma = \sigma s + \sigma r = 0.028 + 0.032 = 0.120$

Since leakage inductances, resistances and leakage factors have been obtained, the stator and rotor time constants can be calculated as shown below.

$\tau_s = \sigma\, L_S/R_s$ $\quad \tau_s = 0.06 * \frac{1.659}{27.62} = 0.00645 \text{ s}$

$\tau_r = \sigma\, L_R/R_r$ $\quad \tau_r = 0.06 * 1.666/31.73 = 0.0536 \text{ s}$

When applied voltage is changed, the rate of the motor magnetic field variation can be determined by rotor time constant

Final step, for determining i_{sq} which produces torque, i_{sd} which produces field, magnetization current (i_{mrd}) and rotor flux (φ_r) , below equations will be used.

In no-load case: $i_{sd} = i_m = i_{mrd} = 0.4993$ A

From dq-axis $i_s = \sqrt{i_{sq}^2 + i_{sd}^2}$ $\quad i_{sq} = \sqrt{i_s^2 - i_{sd}^2}$

$i_{sq} = \sqrt{(0.6928)^2 - (0.4993)^2}$

$i_{sq} = 0.54$ Amp

$i_{mrd} = i_{sd}$ under steady state codition

$\varphi_r = L_m * i_{mrd}$

$= 1.402 * 0.54 = 0.757$ Wb

d-q Current Loop PI Controller

Stator resistor and stator time constant have been calculated previously. Considering PI controller scheme, the transfer functions of the system are driven as shown below.

$$u_{sd} = R_s i_{sd} + \sigma L_s \frac{d}{dt} i_{sd} - \omega_e \sigma L_s i_{sq} + \frac{L_o}{L_r}\frac{d}{dt}\varphi_{rd}$$

$$u_{sq} = R_s i_{sq} + \sigma L_s \frac{d}{dt} i_{sq} + \omega_e \sigma L_s i_{sd} + \omega_e \frac{L_o}{L_r}\varphi_{rd}$$

$$u_{sd} = R_s i_{sd} + \sigma L_s \frac{d}{dt} i_{sd} \quad \rightarrow \quad u_{sd} = R_s i_{sd} + \sigma L_s s i_{sd} \quad \rightarrow \quad u_{sd} = (\, s\sigma L_s + R_s) i_{sd}$$

$\rightarrow \quad i_{sd} = \frac{1}{(s\sigma L_s + R_s)} u_{sd}$ $\qquad \xrightarrow{u_{sd}} \boxed{\frac{1/R_s}{s\tau_s + 1}} \xrightarrow{i_{sd}}$

$GP(s) = \frac{\frac{1}{R_s * \tau_s}}{s + 1/\tau_s}$ $where\ k = \frac{1}{R_s * \tau_s}\ and\ p = \frac{1}{\tau_s}$ $\qquad GP(s) = \frac{5.6}{s+155}$ by substituting parameters

$Gc(s) = \frac{k_p(s+a)}{s}$

$X^*_{(S)} = I^*_{sdq}(s)$ and $X(s) = I_{sdq}(s)$

Let $G(s) = Gc(s) * Gp(s)$ and based on control theory the closed loop transfer function will be as shown below

$$\frac{I_{sdq}(s)}{I^*_{sdq}(s)} = \frac{G(s)}{1 + G(s)} \quad \rightarrow \quad \frac{I_{sdq}(s)}{I^*_{sdq}(s)} = \frac{5.6 k_p (s + a)}{s^2 + \left(5.6 k_p + 155\right) * s + 10 * k_p * a}$$

Since the closed loop transfer function is second order, the values of K_P *and a* can be found by comparing the denominator of the above equation with the denominator of the general form of the second order transfer function which is shown below.

$s^2 + 2\varepsilon\omega n + \omega_n^2$ Compering with the denominator of $\frac{I_{sdq}(s)}{I_{sdq}^*(s)}$

$$(5.6k_p + 155) = 2\varepsilon\omega_n \;\rightarrow\; (5.6k_p + 155) = 2 * 0.7 * 1256.63 \;\rightarrow\; k_p = 286.47$$

$$5.6 * k_p * a = \omega_n^2 \;\rightarrow\; 5.6 * 286.47 * a = 1256.63^2 \;\rightarrow\; a = 984.34$$

Now, by substituting K_P *and a*, the PI controller can be obtained.

$$Gc_{(s)} = \frac{286.47(s + 984.34)}{s}$$

$$Gc_{(s)} = \frac{286.47s + 281983.87}{s}$$

Flux loop PI Controller

Rotor time constant and i_{mrd} have been obtained previously. Considering PI controller block diagram, the transfer functions of the flux loop can be driven as shown below.

$Gp_{(s)} = \frac{\frac{1}{\tau_r}}{s+1/\tau_r}$ where $k = \frac{1}{\tau_r}$ and $p = \frac{1}{\tau_r}$ $Gp_{(s)} = \frac{18.65}{s+18.65}$ by substituting parameters

$$Gc_{(s)} = \frac{k_p(s+a)}{s}$$

$X_{(S)}^* = I_{mrd}^*(s)$ and $X(s) = I_{mrd}(s)$

Let $G(s) = Gc_{(s)} * Gp_{(s)}$ and based on control theory the closed loop transfer function will be as shown below

$$\frac{I_{mrd}}{I_{mrd}^*} = \frac{G(s)}{1 + G(s)}$$

$$\frac{I_{mrd}(s)}{I_{mrd}^*(s)} = \frac{18.65k_p(s + a)}{s^2 + (18.65k_p + 18.65) * s + 18.65 * k_p * a}$$

Again, by comparing the denominator of the closed loop transfer function with the dominator of the general form of second order transfer, the values of K_P *and a* can be calculated.

$$(18.65k_p + 18.65) = 2\varepsilon\omega_n \rightarrow (18.65k_p + 18.65) = 2 * 0.7 * 83.56 \rightarrow k_p = 5.27$$

$$18.65 * k_p * a = \omega_n^2 \quad \rightarrow \quad 18.65 * 5.27 * a = 83.56^2 \quad \rightarrow \quad a = 71.04$$

By substituting K_P, the flux loop PI controller can be driven as shown below.

$$Gc_{(s)} = \frac{5.27(s + 71.04)}{s}$$

$$Gc_{(s)} = \frac{5.27s + 374.38}{s}$$

Speed Loop PI Controller

I_{sd}, L_r and L_o have been calculated previously and moment of inertia has been assumed (0.00016 kg.m^2). Considering PI controller scheme, the transfer functions of the system are driven as shown below.

$$T_e = T_{Load} + J\frac{d}{dt}\omega_r + B_v\omega_r + B_a\omega_r^2$$

$$T_e = T_{Load} + J\,s\,\omega_r + B_v\omega_r$$

$$\omega_r = \frac{1/J}{s + B_v/J}(T_e - T_{Load})$$

$$Gp_{(s)} = \frac{\frac{kt}{J}}{s + B_v/J} \quad \text{where } k = \frac{kt}{J} \text{ and } p = \frac{B_v}{J}$$

$$T = \left(3 * \frac{P}{2} * \frac{L_o^2}{L_r} * imrd\right) * isq \quad \rightarrow \quad T = kt * isq$$

$$kt = \left(3 * \frac{P}{2} * \frac{L_o^2}{L_r} * imrd\right) \quad \rightarrow \quad kt = 1.977$$

$$Gp_{(s)} = \frac{12356.25}{s}$$

$$Gc_{(s)} = \frac{k_p(s + a)}{s}$$

$$X_{(S)}^* = \omega_r^*(s) \quad \text{and} \quad X(s) = \omega_r(s)$$

Basing on the control theory, the speed closed loop transfer function can be written as shown below.

$$\frac{\omega_r(s)}{\omega_r^*(s)} = \frac{G(s)}{1 + G(s)}$$

$$\frac{\omega_r(s)}{\omega_r^*(s)} = \frac{12356.25k_p(s + a)}{s^2 + (12356.25k_p)s + 12356.25k_p * a}$$

Similar to the previous PI controller, by comparing the denominator of the closed loop transfer function with the dominator of the general form of second order transfer, the values of K_P *and* a can be found.

$$(12356.25k_p) = 2\varepsilon\omega_n \rightarrow (12356.25k_p) = 2 * 0.7 * 39.58 \rightarrow k_p = 0.00448$$

$$12356.25 * k_p * a = \omega_n^2 \rightarrow 12356.25 * (0.00448) * a = 39.58^2$$

$$a = 28.29$$

Now, by substituting K_P *and* a, the PI controller can be obtained.

$$Gc_{(s)} = \frac{0.00448(s + 28.29)}{s}$$

$$Gc_{(s)} = \frac{0.00448s + 0.1267}{s}$$

CURRICULUM VITAE

Lana Majeed MOHAMMED

[redacted]

[redacted]

[redacted]

[redacted]

[redacted]

[redacted].